MIX

ORF-9615

MECHANICAL

TECHNOLOGY

INCORPORATED

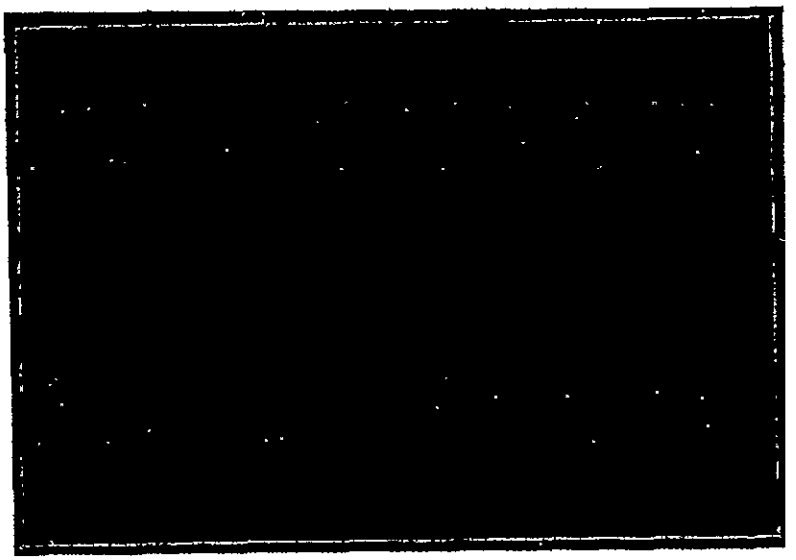

ANALYSIS, DESIGN AND PROTOTYPE DEVELOPMENT OF SQUEEZE-FILM BEARINGS FOR AB-5 GYRO - PHASE V - DEVELOPMENT OF AN INTEGRAL-DESIGN PROTOTYPE SQUEEZE-FILM BEARING SUPPORTING A LIVE AB-5 GYRO FLOAT

L. Hoogenboom, et al.

Mechanical Technology Incorporated
Latham, New York

30 April 1969

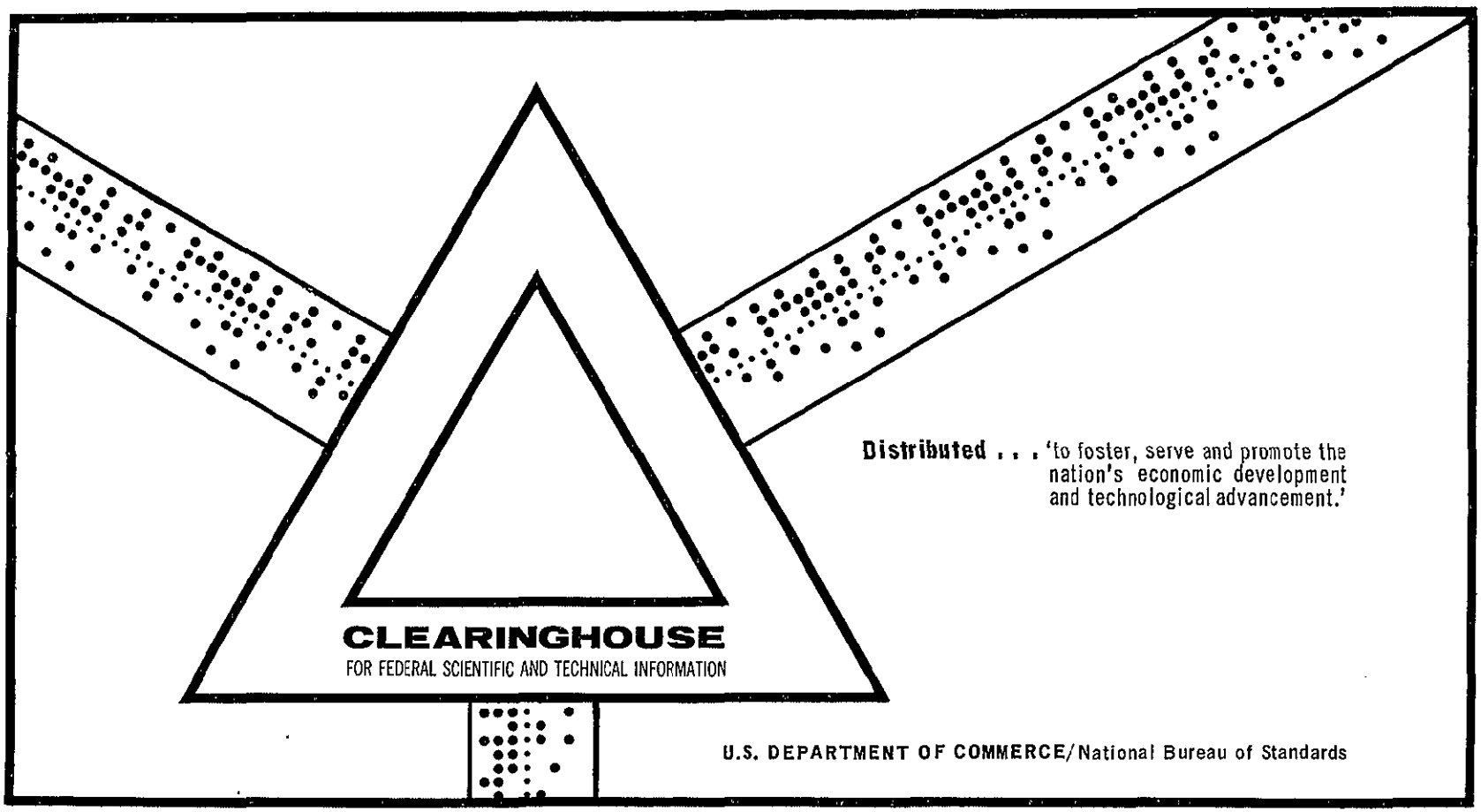

Mechanical Technology Incorporated
968 Albany Shaker Road
Latham, New York 12110

MTI 69TR11

ANALYSIS, DESIGN AND PROTOTYPE DEVELOPMENT OF SQUEEZE-FILM BEARINGS FOR AB-5 GYRO
PHASE V FINAL REPORT
DEVELOPMENT OF AN INTEGRAL-DESIGN PROTOTYPE SQUEEZE-FILM BEARING SUPPORTING A LIVE AB-5 GYRO FLOAT

by

L. Hoogenboom
T. Chiang

April 30, 1969

TECHNICAL REPORT

NO. MTI-69TR11

DATE: April, 1969

ANALYSIS, DESIGN AND PROTOTYPE DEVELOPMENT OF SQUEEZE-FILM BEARINGS FOR AB-5 GYRO

PHASE V FINAL REPORT

DEVELOPMENT OF AN INTEGRAL-DESIGN PROTOTYPE SQUEEZE-FILM BEARING SUPPORTING A LIVE AB-5 GYRO FLOAT

by

L. Hoogenboom
T. Chiang

L. Hoogenboom T. Chiang

Author (s)

Approved

Approved

Prepared for

National Aeronautics and Space Administration
George C. Marshall Space Flight Center
Huntsville, Alabama

Prepared under

Contract: NAS 8-11678

MTI
MECHANICAL TECHNOLOGY INCORPORATED

968 ALBANY - SHAKER ROAD — LATHAM, NEW YORK — PHONE 785-0922

TABLE OF CONTENTS

I. INTRODUCTION

Mechanical Technology Incorporated has been under contract with George C. Marshall Space Flight Center, NASA, to conduct a project entitled, "Analysis, Design, and Prototype Development of Squeeze-Film Bearings for AB-5 Gyro". This report covers Phase V of this Program. The main objective of this phase is to investigate, design, fabricate and test a prototype squeeze-film bearing incorporating a live AB-5 inner cylinder and gyro assembly.

II. REVIEW OF BACKGROUND AND PREVIOUS TRANSDUCER DEVELOPMENT

In a gaseous squeeze-film bearing, one of the bearing surfaces undergoes a transverse vibratory motion. Because of the viscous action and the non-linear nature of squeeze motion, the pressure inside the film becomes higher than the ambient. Thus, load-carrying capacity is developed.

Previous analytical and experimental investigations have demonstrated that in order for a squeeze-film to be effective, it is necessary to have high squeeze frequency and large squeeze amplitude. Therefore, the most critical element in a squeeze-film bearing is the transducer which provides this high frequency, large amplitude squeeze motion.

It has been established [Ref. 1] that piezoelectric drivers are particularly suitable for squeeze-film transducer applications. The advantages are low voltage, low power dissipation and light weight.

The first transducer developed in this Program (Phase II) involves the use of the piezoelectric body as the vibrating bearing element [Ref. 2]. In

this concept, the transducer is a tube of piezoelectric material driven at its hoop mode. The float, representing a gyro, fits inside the piezoceramic tube. The squeeze-film action in the annular gap provides radial load capacity whereas the squeeze-film action in the clearance between thrust plates and the end surfaces of the piezoceramic tube provides the axial load capacity. Although this prototype squeeze-film bearing demonstrated its capability in supporting the float, it had the following disadvantages:

1) Squeeze amplitudes were very small (about 10^{-4} inch peak-to-peak per inch of bearing diameter).

2) The plated surfaces of the piezoceramic tube were subject to material transfer and deterioration due to contact during starts.

3) The squeeze motion was not uniform.

4) Because of limited axial bearing area, the axial load capacity and stiffness are smaller than the radial load capacity and stiffness.

With the above shortcomings of the "first generation" squeeze-film bearing in mind, a modified transducer was developed in Phase IV of the program [Ref. 3], which can be called the "second generation" squeeze-film bearing. The design of this bearing was shown in Fig. 4 of Ref. 3, and is reproduced here as Fig. 1. Note that in this modified design, the piezoelectric material is not directly used as bearing surfaces. The novelty of the modified design is the use of a piezoelectric tube to drive two conical or spherical bearings through the action of a flexure at each end. The

purpose of the flexure is to amplify the axial vibratory motion of piezoelectric tube to render a large squeeze motion at the bearing surfaces. The amplification can be achieved by a proper combination of the piezoelectric tube, the stiffness of the flexure and the bearing mass. (See Ref. 4 and 5). Also, the spherical or conical bearings can be designed to be isoelastic in the axial and radial directions, which is a desirable feature in gyro applications. With all the aforementioned attractive features, this "second generation" squeeze-film bearing still has the following disadvantages:

1) There are many bolted joints between the vibrating sections of the structure and between the piezoelectric tube and the structure. The losses in these bolted joints are very high, so that most of the power put into the piezoelectric driver is consumed by the bolted joints.

2) A long piezoelectric tube is used in the design. The dimensional stability of piezoelectric material has to be considered, because it may appreciably change the bearing gap.

3) Electrical connections made through conductive resin bond or soft solder joint to vibrating surfaces are not very secure.

4) The attachment of the piezoceramic tube to the mounting frame is made by using resin bond, which is again not very secure.

5) Operation of the squeeze-film bearing is limited to the audible frequency range.

Before discussing the next transducer design, it should be remarked that a structure vibrating at ultrasonic frequency with appreciable amplitude (100-1000 inch generally does not permit the direct attachment of parts to it through threaded joints, resin bonds and the like. The point of attachment becomes literally a hot spot and failure of the joint is only a matter of time.

III. EXPERIMENTAL TRANSDUCER DESIGN

To overcome some of the limitations cited in the previous section, a new transducer design was made as shown in Fig. 2. It consists of an aluminum body with six radial holes in the center plane, and a cone shaped section at both ends. The cone sections are connected to the center part through a weakened section similar to the flexure of Fig. 1. The holes in the center plane are filled with tubular ceramic drivers and solid center posts; they are shrink fitted into the holes. The center posts serve as a solid core to the ceramic drivers and as one of the electrodes. The frame is the second electrode. The center posts are also the logical point of attachment for mounting the frame, as will be shown later.

The conical sections can be replaced by spherical sections if spherical bearing geometry is to be used. Both can be designed to be isoelastic for gyro applications.

The piezoelectric tube is slit axially to eliminate hoop stress due to shrink fit. The piezoelectric tube was poled in the radial direction. The slitted piezoelectric tube drives the metallic structure through its thickness expansion. This mode of operation renders axial excursion in the center part of the transducer, which is then transmitted to the conical sections through the flexures. Note that one of the remarkable features of this transducer is that the dimensional stability of the crystals will not affect the bearing gaps, although it may affect the shrink fit. A closer examination indicates that even the shrink fit will not be appreciably affected due to dimensional change of the piezoelectric, because

the tube thickness is typically much smaller than the tube radius.

Before the design concept of the present experimental transducer was conceived, the dimensional stability of piezoelectric tube was considered to be important if configurations such as illustrated in Fig. 1 are to be used. MTI, therefore, requested Clevite to carry out an experimental investigation of the dimensional stability of piezoelectric material under subcontract with MTI. A report submitted by Clevite is included in the appendix.

The piezoceramic material used was PZT4, which has a maximum rated static stress of 12000 psi, and a maximum rated dynamic stress of 12000 psi at 25°C. A shrink fit of 0.003 inch per inch of tube outer radius was used, resulting in an interface compressive stress of less than 10 kpsi approximately (see Section in "Design Calculation"). Since this compressive stress is in a direction parallel to the poling direction, it tends to depole the piezoelectric material. This depoling tendency is further enhanced by the oscillating driving voltage which is also in the poling direction.

The experimental transducers we have assembled so far, using a shrink fit of 0.003 inch per inch of tube outer radius, do not show any appreciable depoling. Any attempt to increase the shrink fit beyond 0.003 in/in should not be made until tests to establish depoling data have been carried out.

The transducer was driven by a power amplifier through a suitable matching transformer. The amplifier was driven by an oscillator.

The lead connections were made to the driver center posts with screws in the center. The screws extended outside the center post and were used to support the unit vertically on three points. They had a jacket of soft thick walled rubber tubing to dampen vibrations. The dissipation in the rubber was larger than in the transducer itself. The rubber heated rapidly and at high amplitudes tests were limited to 5-10 minutes of operation.

The ground lead connection to the transducer body was made with a screw in a threaded hole. This screw and the lead and its insulation became heated due to vibration. Some times connections broke as a result of heat and vibration. Total power dissipation in these tests was 10-30 watt. Most of the power was dissipated in the mechanical joints.

The transducer shown in Fig. 2 has 6 holes in the center plane. Experiments were run either with 3 holes filled or with all six holes filled. In either case, two resonant modes were found at 11 khz and 18 khz. The mode shapes of the transducer with all six holes filled are shown in Fig. 3. Note that there is no nodal line in both modes, indicating that these are the lower modes of the structure vibration.

When the transducer has 3 holes filled, there is one additional mode at about 27 khz. (This mode cannot be excited if all six holes are filled with drivers). A description of this mode is shown in Fig. 4. The motion of the cone is mainly radial and is rotationally symmetric. This radial motion has a nodal line in the conical section at approximately 1/3 way down from the large cone diameter. Another nodal line was found in the

center portion of the transducer (just above the crystal drivers) as shown in Fig. 4. This 27 khz mode is a very powerful mode (maximum excursion at cone tip is about 600 μ-inch peak-to-peak) and it is noiseless because it is operated in the non-audible (ultrasonic) range. Therefore, this experimental transducer is the first squeeze-film transducer operated at an ultrasonic frequency.

The reasonances at 11 and 18 khz were very sensitive to damping. When the cone wall is touched or pinched, the amplitude at 11 khz would drop 50%, and at 18 khz it would drop 90%. This is an undesirable characteristic. The amplitude at 27 khz was quite insensitive to damping of the cone surface. To evaluate briefly the damping due to dissipation in the squeeze film, a float was made. It consisted of two solid cones on a shaft. Both the cones and the transducer were hard-coat anodized and lapped to fit. One of the cones was press fitted on to the shaft and the other was locked on the shaft by an expander (tapered threaded plug) inside the slit shaft end. This permitted setting of the bearing clearance.

This assembly of transducer and float was operated and worked well at 27 khz with a total axial gap of 1-2 mils. Two types of electrical drive were used. One was the oscillator and amplifier mentioned before. The other was the amplifier alone, connecting to only two of the driver; the third driver was used as input source for the amplifier. By adjusting the gain, resonant amplification at 27 khz would occur quite readily, and for increased gain, resonance at the 11 khz frequency would result.

The effect of inserting the float in the transducer, when operating at 27 khz (3 holes vacant) was a slight reduction in amplitude due to film losses. The load capacity of the cone shaped bearing was 10-20 lbs. The load capacity is not high because of the inaccuracy of the bearing surfaces. The out-of-roundness of the cone surfaces after grinding was in the order of 200-300 μ-in. Lapping of cones onto each other does not necessarily improve surface geometry and surface finish. The results after lapping were judged adequate for the intended experiment (film damping evaluation). The load capacity of the bearing however, was not representative of what can be achieved with nearly perfect surfaces under the same conditions.

In Fig. 2, a ½" wide circumferential groove is shown in the plane of the flexure. This groove was originally intended to be used for nesting ½" wide x 1/8" thick piezoelectric plates. This was never tried because of the much improved design with shrunk-in tubes conceived after the first experimental frame was machined.

In summary, the results obtained with the first one-piece transducer-bearing frame are:

1. Only a small volume of piezoelectric material is needed for squeeze-film transducers.

2. It has been achieved to excite a higher shell mode with sufficient amplitude for squeeze film operation at an ultrasonic frequency (27 khz).

3. Power dissipation in the transducer is in the 10-20 watt range; most of it is dissipated in electrical and mechanical connections.

IV. DESIGN CALCULATIONS

A. Shell Structures

Since the function of the transducer is to provide oscillatory motion at the squeeze-film bearing surfaces, it is necessary to drive the structure at its natural frequencies. The mode functions of the respective natural frequency are also of importance, because in order for the squeeze-film bearing to be effective, it is desirable to have relatively large amplitude in the bearing surface area rather than in the rest of the structure. Therefore, an analysis of free vibrations of a composite shell is in order. A survey of the literature shows that a shell vibration analysis was performed by Kalnins (Ref. 6). A computer program was then obtained from Kalnins. The computer program is applicable to axially symmetric shells. Axisymmetric branches may also be attached to the main shell structure consisting of spherical, conical, cylindrical and other arbitrary-shaped axisymmetrical shells. The program automatically finds either all natural frequencies within a prescribed frequency interval or a specified number of consecutive natural frequencies above a given frequency. The output prints out the mode shapes of all displacements and stresses at any desired number of points.

It is seen from Fig. 2 that there are 6 holes in the central plane of the structure. Some of the holes are shrink-fitted with crystals while the rest is left empty. Since the shrink fit is a force fit, we can as a reasonable approximation, consider that the holes are really filled, although the crystal has different Young's modilus from the structure material (in this case, aluminum). On the other hand, the empty holes have to be treated differently.

In an axisymmetrical shell, a radial displacement would obviously result in hoop stresses. Now, if there are empty holes along a circumferential line, the hoop stress will clearly be relieved. We can, therefore, simplify the analysis by considering the portion of the shell with empty holes as mechanical springs. We shall illustrate the computation of the spring constant as follows:

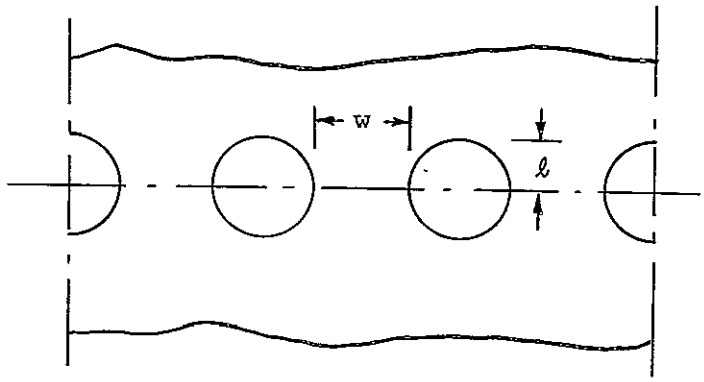

The developed view of the shell with holes is shown in the above sketch.

Denote

ℓ = length of the stub
w = average width of stub
t = thickness of shell
A = area = $w\,t$
E = Young's modulus
d = diameter of hole
D = diameter of shell
n = number of holes
P = force on each stub
δ = deflection

The stiffness of each stub in the axial direction is given by

$$\frac{P}{\delta} = \frac{AE}{\ell}$$

Then, the structure spring constant k expressed in units of lb. per in. per unit circumferential length is

$$k = \frac{n(P/\delta)}{D}$$

Now we replace the portion of shell with holes by a distributed spring whose spring constant is formulated above. The computer program has been modified accordingly.

The structure configuration of Fig. 2 is fed into the modified computer program as input data. The natural frequencies are found to be 9.6 khz and 18.2 khz with all six holes filled, and 9.6, 14.5, 18.0 and 30.0 khz with 3 holes filled and 3 holes empty. Some of the mode shapes are plotted in Figures 5, 6 and 7 and compared with experimental results. In Figure 5 and 6 the two modes of the transducer with all six holes filled are shown. It is seen that the analytical results agree very well with the experimental results. The higher shell mode of the transducer with 3 holes filled is shown in Fig. 7. The mode shapes agree only in a qualitative manner. Both the analytical and experimental mode shapes have a nodal line in the conical section and a nodal line in the center part of the transducer just above the driving crystals.

The shell vibration program is therefore a useful design tool for the development of high-frequency transducers of the type considered here. A new transducer configuration is shown in Fig. 10. This new design has a shorter center section and a spherical section at both ends. Note that there is no flexure in this new design. In Fig. 8, the higher shell mode at 25.2 khz is shown. Again, there is a nodal line in the spherical section. The amplitude of the dynamic bending stress and hoop stress are shown in Fig. 9; the maximum stress occurs at the root of the spherical section.

B. Prestressing of Piezoelectric Drivers

The piezoelectric ceramics used to drive the bearing are a polarized lead zirconate-titanate. The material chosen was Clevite PZT-4, because of its superior performance relative to similar ceramics in high power and high load applications and because of its low internal mechanical losses.

The piezo electric material converts electrical energy to mechanical energy. To do so efficiently, requires a suitable method of coupling the piezoelectric element to the structure to be driven. The mechanical output of a piezoelectric ceramic is a certain strain for a given voltage gradient. For PZT-4, this output is about 12 μ strain/volt/mil, both measured in the direction of poling. A practical maximum operating voltage is 500 volts p-p ($\sim$ 200 V RMS). Suppose that thickness of the ceramic is .100". The voltage gradient is then 5 volts per mil, and the cyclic strain

(at constant stress) associated with this is 60 μ strain. The cyclic change in thickness of the .100" thick ceramic is in the order of 6 μ inch.

The coupling then must be of sufficient stiffness to transmit this small amount of motion without loss of contact in the interface. According to previous experience, an interface stress of 1500-2500 psi would be sufficient to "harden up" the interface to the level of the elastic modulus of the two materials at the interface.

In the design chosen, the electrode inside the tubular ceramic serves also as transducer support. To assure that no slip occurs at the center electrode with respect to the bearing shell, the highest permissible shrink fit stress must be chosen.

The shrink fit stress is limited by

1. Compressible strength of the ceramic
2. The stress at which the piezoelectric performance degrades
3. The temperature differential needed for the shrinking operation as compared to Curie temperature of ceramic
4. The permissible material stress in the bearing shell.

When using aluminum and PZT-4, Items 2 and 4 impose about the same limit, which was conservatively set at 60,000 psi. The compressive strength of PZT-4 is over 75,000 psi and in no way limits the prestress.

To calculate the shrink-fit stress, assume that a pressure p_o is induced by the shrink fit. Let u_1 be the radial deformation of the aluminum pin. Then, from Ref. 7,

$$u_1 = p_o r \frac{1-\mu}{E_{A\ell}}$$

where μ, $E_{A\ell}$ = Poisson's ratio and Young's modulus of aluminum

r = radius of pin

Next, we can calculate the radial deformation of the hole. Assume that the structure near the hole can be approximated by a hollow disk illustrated by the following sketch.

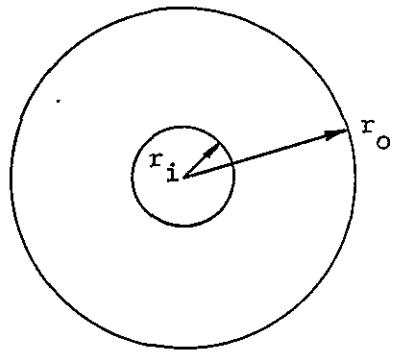

Here, r_i is the radius of the hole and r_o is a fictitious outer radius of the disk. The radial deformation of the hole, u_2, due to an internal pressure p_o, is [Ref. 7],

$$u_2 = p_o \frac{r_i}{E_{A\ell}} \frac{2 r_o^2}{r_o^2 - r_i^2}$$

Since r_o is typically much greater than r_i, we can simplify the above expression to

$$u_2 = p_o \frac{2 r_i}{E_{A\ell}}$$

Let u_3 be the deformation of the slitted ceramic tube whose thickness is obviously $r_i - r$.

$$u_3 = \frac{p_o}{E_c} (r_i - r)$$

The total deformation δ should be equal to the shrink fit.

$$\delta = u_1 + u_2 + u_3$$

$$= p_o \left\{ \frac{1}{E_{A\ell}} [r(1-u) + 2r_i] + \frac{1}{E_c} (r_i - r) \right\}$$

Since $E_{A\ell} \approx E_c \approx E = 10 \times 10^6$ psi

$\mu = 0.3$

and $r \approx 0.7\, r_i$ in this design

$$\delta = 2.8 \frac{p_o}{E} r_i$$

Note that p_o should be equal to the normal compressive stress on the piezoceramic tube. For p_o = 10,000 psi and E = 10 x 10^6 psi,

$$\frac{\delta}{r_i} = 2.8 \times 10^{-3}$$

Therefore, a shrink fit of 2.8 x 10^{-3} inch per inch of hole radius would produce a stress of 10,000 psi.

The maximum temperature differential needed for shrinking of the piezoceramics and center electrode assembly, is 200-250°C which is compatible with the curie temperature of PZT-4 (328°C).

V. DESIGN OF PROTOTYPE BEARING ACCOMMODATING A LIVE AB-5 GYRO FLOAT

Based on results reported in the preceding section the design shown in Fig. 10 was made. Computer analysis of the transducer shell indicated a resonant frequency in the 22-25 khz range for a mode suitable for squeeze film operation. The main difference between the design in Fig. 10 and the design in Fig. 2 is the absence of a flexure section in Fig. 10. The transducer is essentially a shell with a heavy center section and end pieces of reduced wall thickness. To minimize the bearing weight, the axial length of the heavy center section was made shorter. This made it necessary to use ceramic drivers of smaller diameter. To make up for the smaller driver size, four instead of three drivers were used. The total number of radial holes is eight, four of which are vacant, and four occupied by drivers.

The float consists of a shaft and two spherical bearings. One bearing is pinned to the float, and the other is clamped to the shaft by an expander (tapered ring).

Before entering in the details of the design, manufacture and assembly of the bearing, its performance is discussed in the next section.

VI. PROTOTYPE BEARING PERFORMANCE

The transducer of Fig. 10 was either powered by using an oscillator plus a power amplifier or by using only the amplifier with feedback from one of the piezoceramic elements.

Using the first type of drive, various resonant frequencies were excited. Some of the resonances appeared only when powering just one of the ceramics. The resonances that can be excited using all four driving elements are the most desirable electrically because they result in the lowest drive voltage. Fortunately, these resonances appeared to be also excellent for squeeze film operation. For those resonances, the strains at the four driver locations are in phase. This makes it convenient to use one of the ceramic elements for motion feedback to the amplifier when operating closed loop. The mode requiring the lowest loop gain will then be excited first.

When operating open loop (i.e. with oscillator); four modes of vibration were found that resulted in squeeze film lubrication. They were at approximately 10.8, 14.5, 24.6 and 35.8 khz. The motion of the bearing surface was visually evaluated by using alcohol spray. Results are sketched in Figure 11 and are summarized below:

at 10.8 khz. *base of sphere little motion
*edge of sphere large motion
*motion rotationally symmetric

at 14.5 khz	*base of sphere large motion *edge of sphere little motion *motion rotationally symmetric
at 24.6 khz	*motion peaks in the planes of the piezoceramic elements and in the planes of the vacant holes. Maximum aplitude slightly above mid-chord in planes 1-1 and 2-2 (See Fig. 11)
at 35.8khz	*motion peaks at 12 equispaced locations on the bearing surface at about mid-chord

In addition to inspection of the four modes by alcohol spray, a measurement was made of amplitude and phase of input and output voltage vs frequency, when driving three piezoceramic elements and monitoring the output of the fourth piezoceramic element.

The results are shown in Fig. 12. The dotted lines are curves fitted to the test data. The shape of these curves is based on the response to a forced vibration of a single degree-of-freedom, viscously damped, spring-mass system. See reference [8], for the applicable equations. The calculation of the Q for these four modes is also based on the same equations. Although, the formulas for a single degree-of-freedom, lumped-parameter system [8] cannot be applied directly to a continuous system such as the transducer body, they are used here only to provide a convenient basis for comparison between modes.

The phase angle between input voltage and output voltage as measured can be understood as follows. Since displacement and voltage would be in phase in a lossless system and that input-output voltages phase relation would undergo a reversal at resonance, the resonant condition of a system with a slight amount of dissipation would be accurately determined by the 90 degree phase shift point.

In closed loop operation, three driving crystals are connected to the amplifier output through a matching transformer, and the remaining crystal is used for feedback to the amplifier input. The first resonance appears at 24.6 khz. For increased gain the 14.5 khz resonance appears. With the float in place, the loop gain required to start is higher than that needed to run. Therefore, momentarily the 14.5 khz mode will appear, but after reducing gain, the 24.6 khz mode will prevail.

For the 24.6 khz mode this ratio is 1.4 and for the 14.5 khz mode it is only 1.0. Since the phase between V_{in} and V_{out} is about the same for both modes at resonance (See Fig. 12), reducing gain after the float is free, will leave the 24.6 khz mode predominant. In the electronics package described in section IX, an automatic gain control is provided to reduce gain as power increases. If the 14.5 khz mode is desired it can be obtained by tuning the output circuit of the amplifier. This feature has been incorporated in the circuit shown in Fig. 18.

The 24.6 khz mode is attractive because it is beyond human audible range and because of the relatively large V_{out}/V_{in} ratio.

At the 24.6 khz resonant frequency the bearing load vs. deflection characteristics were measured. Before presenting the results, the method of measurement is discussed. The stiffness measurement of a squeeze film bearing is complicated by the fact that the vibrating member is not available for the attachment of instrumentation. In the past, in some instances the stiffness measurement was accomplished by measuring the absolute displacement of the float and the bearing housing independently, both with power on and power off.

By subtracting the absolute displacements and making corrections for housing distortion, the relative displacement between the two bearing members was then calculated. This method was not used here because the stiffness of the bearing was expected to be much higher than that of previous units. The greater stiffness results in smaller relative displacements and less accurate measurements. The absolute accuracy of the method used previously is also limited by the displacement range of the probes, their inherent noise level and the structural stiffness.

Therefore, a new method using the system shown in Fig. 13 was employed. It consists of the bearing assembly without the top cover but otherwise complete. Two proximity sensors (Fotonic Sensors) are mounted on the float. They are used to measure directly the change in position of the float relative to the housing in axial and radial direction. The loads are applied through flexible cables to eliminate moments. The directions of the loads are radial and axial through the center line of the bearing.

The Fotonic Sensor is read out on a digital voltmeter to obtain maximum resolution. This system is free from errors due to bearing housing distortion and support frame distortion.

The axial displacement is measured with reference to the bearing edge. The edge is at 70° with the axial direction. To convert the measurements to axial displacement, the results are divided by the sine of 70° ($\simeq .94$).

Tests were run with only one type of loading, either axial or radial, except for the effect of the float weight ($\simeq$ 6 lbs.). All tests were run with the bearing center line vertical.

Figures 14 and 15 show plots of the results of load vs deflection measurements for either axial or radial loading, at the 24.6 khz resonant frequency. The stiffness in axial and radial direction are about equal for zero loading. The radial load capacity is less than one half of the axial load capacity. Based on a float mass of 6 lbs, the maximum lateral acceleration the bearing could sustain is 3g and the axial acceleration limit is about 8g.

Some additional performance data were taken with the transducer operated at 14.5 khz. The radial load capacity and stiffness are plotted against radial displacement in Fig. 16. From Figures 15 and 16, it can be seen that for the same radial load the radial stiffnesses of the two modes are about equal. For the same radial displacement, the 24.7 khz mode has higher radial load capacity and stiffness than the 14.5 khz mode. It is pointed out here that the input voltage for the 14.5 khz mode is about 20% higher than the 24.7 khz mode. The excursion amplitude at the center plane (plane "KK" in Fig. 10) is 170 μ-in and 520 μ-in peak-to-peak for the 24.7 khz mode and the 14.5 khz mode respectively.

Attempts were made to measure the power used to drive the bearing. The power level is very low, judging by the amount of heat generated in the bearing. After about ½ hour of operation the bearing temperature is increased by 3-5°C. Based upon a bearing mass of about 15 lbs, this is equivalent to an average power dissipation of 5-7 watts. At this power level the phase angle between voltage and current, at a voltage of 250 V rms and current of 1A rms is 90°-89°, consequently it is not possible to extract an accurate estimation of the power dissipation from the voltage and current signals. Therefore, a calorimetric power measurement is more practical.

The data given in Fig. 12 on relative amplitude of the feedback voltage vs frequency can be used to calculate the Q of the transducer without float. The value of Q for the four modes of vibration in Fig. 12 is 2100-2700. The Q with the float in place was not measured.

The tabulation on the following page compares the performance of the present bearing at 24.6 khz with the unit shown in Figure 1, for the same squeeze amplitude and axial clearance.

The interesting items in this list are 9, 10, 12, 13, 17, 18 and 20. These are discussed in the following:

Item 9

The maximum stiffness per unit bearing area is increased by a factor of four. This stiffness increase is probably due in part to the better sphericity of both bearing surfaces. This allows closer average proximity before contact occurs.

Item 10

The average film pressure over ambient has doubled at maximum load. The same comment applies as under 9 above.

Item 12

The power consumption per unit film pressure at maximum load is down by a factor of 5 to 10 for the new unit. The high Q of the transducer (Q=2400) - a result of one piece construction - is one reason for the reduced power.

ITEM NO.	ITEM	PRESENT UNIT (SEE FIG. 10 & FIG. 13)	PREVIOUS UNIT (SEE FIG. 1)	RATIO NEW VS OLD DESIGN
1	Operating frequency	24.6 khz	5.75 khz	4.3
2	Driving voltage	540 v p-p	400 v p-p	1.35
3	Maximum squeeze amplitude	350μ in. p-p	350μ in. p-p	1.0
4	Axial clearance	.0021 in.	.0021 in.	1.0
5	Bearing area of single bearing	23 in^2	10 in^2	2.3
6	Maximum axial load	50 lbs.	12.6 lbs.	4.0
7	Axial stiffness at zero load (one bearing only)	12,000 lbs/in	10,000 lbs/in.	1.2
8	Maximum axial stiffness (one bearing only)	200,000 lbs/in	22,000 lbs/in.	9.0
9	Axial stiffness at maximum load per unit bearing area	8,700 lbs/in/in^2	2,200 lbs/in/in^2	4.0
10	Average film pressure over ambient at maximum load	3.4 psi	1.8 psi	1.9
11	Input power	3-6 watt	15 watt	.2-.4
12	Specific power consumption	.9-1.8 watt/psi	8 watt/psi	.1-.2
13	Power per unit bearing area (both bearings)	.065-.13 watt/in^2	.75 watt/in^2	.1-.2
14	Transducer weight (all vibrating parts except ceramic) approx.	4 lbs.	3 lbs.	1.3
15	Ceramic dimensions Length x O.D. x wall	1 1/8" x 3/4" x 1/8"	1 3/4" x 3 3/8" x 5/16	
16	Total ceramic weight	.3 lbs.	1.7 lbs.	.18
17	Mass ratio ceramic/transducer	.075	.57	.13
18	Ratio of input power to transducer mass	.75-1.5 watt/lb	5 watt/lb	.15-.30
19	Ceramic power density	10-20 watt/lb	9 watt/lb	1-2
20	Ceramic voltage gradient	4300 v/in.	1300 v/in.	3.3

Item 13

Power per unit bearing area is down by a factor of 5 to 10.

Item 18

Power per unit transducer mass is down by a factor of 3 to 6. In comment on items 12, 13 and 18, it should be noted that the 4X higher operating frequency should cause proportionally higher losses. But contrary to this, power is reduced. The actual reduction of mechanical losses is therefore not 5 to 10 times but 20 to 40 times, when also including the effect of the squeeze frequency on power.

Item 17

The ceramic volume per unit transducer volume is reduced by a factor of 8. This was one of the basic objectives of the new design. The actual power density (Item 19) in the ceramic is up by a factor of less than 2. Within the limit set by the maximum permissible voltage gradient (25,000 v/inch) the relative ceramic volume can be decreased by an estimated factor of 2 to 5.

In summary, it can be concluded that the new design is an order of magnitude more efficient in converting power to squeeze film support. The primary objective of the new design was to obtain a very stable structure, by eliminating bolted and cemented joints. A second objective was ultrasonic operation, without an increase in input power. These objectives were attained by the introduction of shrink-fitted piezoceramic drivers. The stability of the structure has not been tested yet, but elimination of the many joints that could directly influence the stability should be a major improvement.

The 14.5 khz mode is also a strong mode suitable for squeeze-film application. It has a peak-to-peak amplitude of 300 μ-in at the inner edge (near pole) of the sphere. The driving efficiency of this mode is about the same as the 24.6 khz mode. The power input is approximately 5 watts which is comparable to that of the 24.6 khz mode. The radial load capacity and stiffness of the 14.5 khz mode are respectively 12.4 lbs. and 4.6×10^5 lb/in at a radial displacement of 0.5×10^{-3} in. as compared to 17.5 lb and 6.7×10^5 lb/in of the 24.6 khz. Although this 14.5 khz mode has somewhat lower load capacity and stiffness, it has no "friction problem" as will be discussed in the next section.

VII. EXPERIENCE OF OPERATION WITH TORQUER

After complete assembly of the bearing and the AB5 gyro with pick-off and torquer, the unit was delivered to the Astrionics Laboratory, MSFC, NASA.

The bearing was operated with a Mackintosh power amplifier and a matching transformer using one crystal for feedback and three for excitation. The frequency of operation was 24.6 khz, the mode of vibration was shown in Fig. 11C.

It appeared that (with the gyroscope motor off) when using the pick-off and torquer to position the float, the torquer voltage needed to move the float was 10 to 20 times greater than normal. In this test the bearing was positioned with its center line vertical. This excessively high voltage indicated presence of friction. During subsequent tests with the bearing axis horizontal, using unbalance weights to move the float (torquer disconnected), the minimum moment needed to rotate the float was about 40 dyne cm.

Typically, a properly functioning float can be disturbed by a moment as low as .01 dyne cm. The 40 dyne cm "friction torque" appeared to be present when operating the bearing at 24.6 khz or 35.8 khz (see Fig. 11C and 11D for mode shape). However, when operating at 14.5 khz (see Fig. 11B for mode shape), the "friction" was reduced by approximately 2 orders of magnitude. The most notable difference between the 14.5 khz mode and the higher modes is that the 14.5 khz mode is rotationally symmetric.

For the time being, no satisfactory explanation is available for the phenomenon described above. It is believed, however, that the lack of rotational symmetry in the higher modes (24.6 khz and 35.8 khz) combined with the bearing ellipticities could be the main cause of this "friction torque".

The transducer in Fig. 2 has a flexible section, similar to the flexure used in the design in Fig. 1. The flexure in Fig. 2 isolates the driving ceramics from the bearing surface thus eliminating the complex nodal patterns as seen in Fig. 11C and 11D. It is therefore proposed for new designs to use a flexure for the purpose of isolation.

VIII. PROTOTYPE BEARING DESIGN, MANUFACTURE, ASSEMBLY AND ADJUSTMENT

In the following, some of the details of design, manufacture and assembly are discussed. They are reported here because they may provide useful information in operation, maintenance and adjustment of the unit.

The design consists of three separate parts:

A. Transducer, Spherical Bearings and Hollow Shaft

B. Bearing support frame.

C. Gyroscope attachment inside hollow shaft.

A. Transducer, Spherical Bearings and Hollow Shaft

The overall dimension of the bearing system is based on load capacity, float size, balance between axial and radial stiffness and load capacity, operating frequency, total weight and choice of structural material.

The design was aimed at a bearing of minimum weight and size. Because of the experimental nature of the unit, the shell is possibly made heavier than necessary. This benefits dimensional stability of the spherical surfaces, an important aspect of the bearing. The spherical segments are solid to better maintain sphericity.

The spherical bearings and the shaft are lapped to fit. The shaft is anodized, but the bore of the spherical bearing is not anodized. The right hand sphere in Fig. 10 has a heavy sliding fit (50 lb. load will make it slide) on the shaft, and is pinned to the shaft. The left hand sphere is held in place by expanding the shaft elastically near the end. This is done by pulling a clamping gib (pt 12) with an external taper into a tapered bore inside the shaft. This allowed setting any desired bearing

clearance without change in the setting caused by tightening of the clamp.

The bearing surfaces were lapped individually to fit to each other with a radial clearance of .0005 inch. The sphericity of the bearing surfaces is within 20 μ in.

Two balancing rings (pt 16) are provided, one at each end of the shaft.

The ground lead connection to the transducer body is made through a carbon steel spring brazed to a steel set screw. The set screw is bottomed in a threaded hole.

B. Bearing Support Frame

The transducer structure is supported by four flexures (pt 9) as shown in Fig. 10. The center posts of the flexures are shrink-fitted with the ceramic into the holes of the transducer structure.

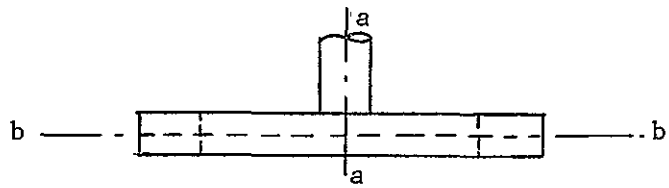

The stiffnesses of the flexure are 10,000 lb/in in the "aa" direction and 600,000 lb/in in the "bb" direction (see above sketch). Note that the stiffness in the "aa" direction is very low. From Fig. 10, it is clear that this "aa" direction is in the radial direction of the transducer center plane. Therefore, this low stiffness in the "aa" direction serves

the purpose of isolating the radial vibratory motion of the transducer at the center plane.

These four flexures would contribute an axial and a lateral stiffness to the transducer frame; they can be readily calculated as follows:

$$\text{Axial Stiffness} = 4 \times 600{,}000 = 2.4 \times 10^6 \text{ lb/in}$$

$$\text{Lateral Stiffness} = 2 \times 600{,}000 + 2 \times 10{,}000$$

$$= 1.22 \times 10^6 \text{ lb/in}$$

The top cover supports the AB5 torquer assembly. A plexiglass dust cover (pt 2) surrounds the bearing assembly.

The center posts in the ceramic serve as a radial support for the ceramic, a point of attachment for the frame (through a flexure) and the electrical connection. Insulation is provided as shown in Section N-N, by a shim (pt 15) and a bushing (pt 33).

No special mounting surfaces are provided. The unit can be held down to a test fixture by e.g. removing four of the bolts (pt 37) in the bottom plate (pt 1), and by using the vacant holes to bolt the unit down.

C. Gyroscope Attachment

The shaft was designed to have the existing AB-5 float mounted in the mid-plane of the bearing. Subsequently it was decided to move the gyro to one end, to eliminate the need for extension posts on the three motor connections. Therefore, the extension (pts 10 and 11) was inserted.

The gyro is bolted to the extension by bolts (pt 43), and the extension is bolted to the shaft by bolts, (pt. 42). Manufacturing tolerances of the shaft, the extension piece (pts 10 and 11) and the spherical ends (pts 3 and 5) were held such that the angular misalignment between the actual bearing center line and the gyro centerline would be minimal. To adjust the remaining small misalignment, if necessary, requires shaft disassembly and removal of very small amounts of material of various mating surfaces followed by reassembly. It was judged impractical to obtain the required accuracy of alignment in this way due to the effects of repeated disassembly and assembly. Instead, adjustment by elastic deformation of the extension piece end surface was chosen. The elastic deformation is obtained by tightening the four bolts (pt 42) to different torques and possibly also by using jacking screws (pt 41), which are incorporated specifically for the purpose of alignment. If alignment can be obtained by only manipulating the bolt tension in pts 42 that seems to be the preferred method. Bolts (pt 42) can be reached with a wrench by removing the plug (pt 38) in the bottom plate.

A photograph of the complete assembly under test is shown in Fig. 17. It shows the bearing, the matching transformer, the power amplifier and the monitoring oscilloscope. Fig. 17A shows a close up of the bearing without plexi-glass dust cover. The power amplifier as a drive is to be replaced by a bearing power supply unit custom made for the demonstrator unit. A description of the special power package is given in the next section. It features automatic gain control to adjust gain to provide a reduced driving voltage at the moment the float is free.

IX. ELECTRONIC SQUEEZE FILM TRANSDUCER POWER PACKAGE

The Squeeze Film Bearing Driver is a variable gain amplifier capable of supplying up to 25 watts at 14.5 khz. The output circuit is especially adapted to match a load of .015 mfd in shunt with a resistive component. Automatic gain control is provided so that a constant output current can be maintained. The power input required is 115V, 60 hz, 1 ampere (approximately).

Automatic gain control is needed to insure that the transducer will select the desired mode of operation when going through the process of lifting the float. During the lifting transient, the gain needed to keep the float lifted becomes smaller. The automatic gain control provides the proper amount of gain to stabilize the amplitude of vibration.

Referring to schematic diagram in Fig. 18, the voltage generated by the pick-up (or feed-back) element on the bearing is applied to the input terminals of the amplifier. The voltage across the secondary winding of the input transformer (T_1) is attenuated by a voltage divider consisting of R_1 and a light sensitive resistor R_{11}. The voltage across R_{11} is applied to the base of transistor Q_1 operating as an emitter follower to provide high input impedance. The collector current of Q_1 flows through the primary of T_1 and the center-taped secondary of T_2 drives the bases of Q_2 and Q_3. The output transformer is tapped so that various output voltages may be obtained by changing the lead on the transformer terminal board. The inductance of T_3 is adjusted by shims in the air gap to tune out the capacitive current drawn by the load and compensating capacitors C5, C6, C7.

The output current from T_3 flows through R_{10}, the voltage across which lights a lamp, P_2, which illuminates the light sensitive resistor R_{11}. An increase in output current increases the brilliance of the lamp and decreases the resistance of the light sensitive resistor thus decreasing the input to transistor Q_1 and stabilizing the output. The current through R_9 caused by the shunt capacitance of the load (approximately .015 mfd) is balanced out by the current through C_5, C_6, C_7, C_x in parallel which if fed by a voltage

of reverse polarity. Trimmer capacitors C_5 and C_6 are available through openings on the rear panel. The voltage across output terminals 2 and 3 with 3 as ground as compared to voltage 1 to 3 can be observed to see that the compensating adjustment is properly made. The voltage 2 to 3 should be 180^{o} in phase from voltage 3 to 1. The watts drawn by the load can then be calculated by

$$W_{out} = \text{current} \times \text{voltage} = V_{2-3} \times V_{1-3}$$

V_{2-3} and V_{1-3} are rms voltages.

Varying R_{10} will vary the output current at which regulation occurs, and hence the amplitude of vibration.

Once the proper setting of R_{10} is found, the bearing is operated simply by turning on line power.

X. SUMMARY AND CONCLUSIONS

The concept of integral-design squeeze-film transducer has been demonstrated. The key to the success of this new concept is to install the piezoelectric drivers into the transducer structure by shrink fit. This eliminates the bolt and screw joints in the previous design, and greatly reduces the power input to the transducer.

Two transducers, one experimental transducer and one prototype transducer accommodating a live AB-5 gyro have been designed and fabricated using the integral-design concept. Both transducers were successfully operated at ultrasonic frequencies with ample amplitude for squeeze-film application. The power required to drive the transducer is considerably lower than that of previous designs.

The radial and axial load capacities and stiffnesses of the prototype squeeze-film bearing were evaluated experimentally both at the 14.5 khz mode and at the 24.6 khz mode, and they were found to be adequate for the present application. The 24.6 khz mode being at an ultrasonic frequency is not audible, but its mode shape is not rotationally symmetric and there is a large "friction torque" associated with this mode. For this reason, the 14.5 khz mode is preferred.

XI. RECOMMENDATIONS

Operation of the prototype squeeze-film bearing at ultrasonic frequencies results in adequate load capacity and stiffness, but unusually large "friction torque". The "friction torque" appears to be associated with rotationally non-symmetric modes. It is therefore recommended to add in the transducer design a flexible section between the driving center section and the bearing section (similar to the flexures in Fig. 1 and Fig. 2). The purpose of the flexible section is to attain ultrasonic modes with rotational symmetry. Since weight and size are important considerations for space applications, we also recommend to redesign the gyro float to be an integral part of the shaft.

ACKNOWLEDGMENT

The authors wish to express their gratitude to Messrs. Ken Streifert, Myron Swidersky and Frank Bartnicki of the M.T.I. Design Room for their assistance in the design of the hardware, to Mr. Bill Atkinson of the M.T.I. Machine Shop for providing the hardware and to Athbro Corporation, Sturbridge, Mass. for manufacturing the spherical bearing and transducer structure.

REFERENCES

1. Pan, C.H.T., Editor, "Analysis, Design and Prototype Development of Squeeze-Film Bearings for AB5 Gyro - Phase I Final Report, Bearing Analysis and Preliminary Design Studies", MTI-64TR66, Contract NAS8-11678, 1964.

2. Pan, C.H.T., Orcutt, F.K., and Teitelbaum, B., "Analysis, Design and Prototype Development of Squeeze-Film Bearings for AB5 Gyro Phase II Final Report, Fabrication and Evaluation of Floating-Transducer Squeeze-Film Bearing Prototype", MTI-67TR17, Contract NAS8-11678, 1967.

3. Orcutt, F.K. and Pan, C.H.T., "Analysis, Design, and Prototype Development of Squeeze-Film Bearings for AB-5 Gyro - Phase IV Final Report, Development of a Conical Bearing, Axial Excursion Prototype", MTI-67TR30, Contract NAS8-11678, 1967.

4. Chiang, T., and Pan, C.H.T., "Analysis and Design Data for the Axial Excursion Transducer of Squeeze-Film Bearings", MTI-65TR25, Contract NAS8-11678, 1965.

5. Orcutt, F.K., Kissinger, C., and Pan, C.H.T., "Investigation of an Axial Excursion Transducer for Squeeze-Film Bearings", MTI-65TR63, Contract NAS8-11678, 1965.

6. Kalnins, A., "Free Vibration of Rotationally Symmetric Shells", Journal of Acoustical Society of America, Vol. 37, No. 7, P. 1355, July 1964.

7. Den Hartog, J.P., "Advanced Strength of Materials" p.52 and 54, McGraw-Hill Book Company, 1952.

8. Den Hartog, J.P., "Mechanical Vibrations" pp. 61-62, McGraw-Hill Book Company, 194.

LIST OF FIGURES

Fig. 17 Gyro Squeeze Film Bearing under Test at Marshall Space Flight Center, NASA

Fig. 17-A Gyro Squeeze Film Bearing - Close Up

Fig. 18 Schematic Squeeze-Film Bearing Driver

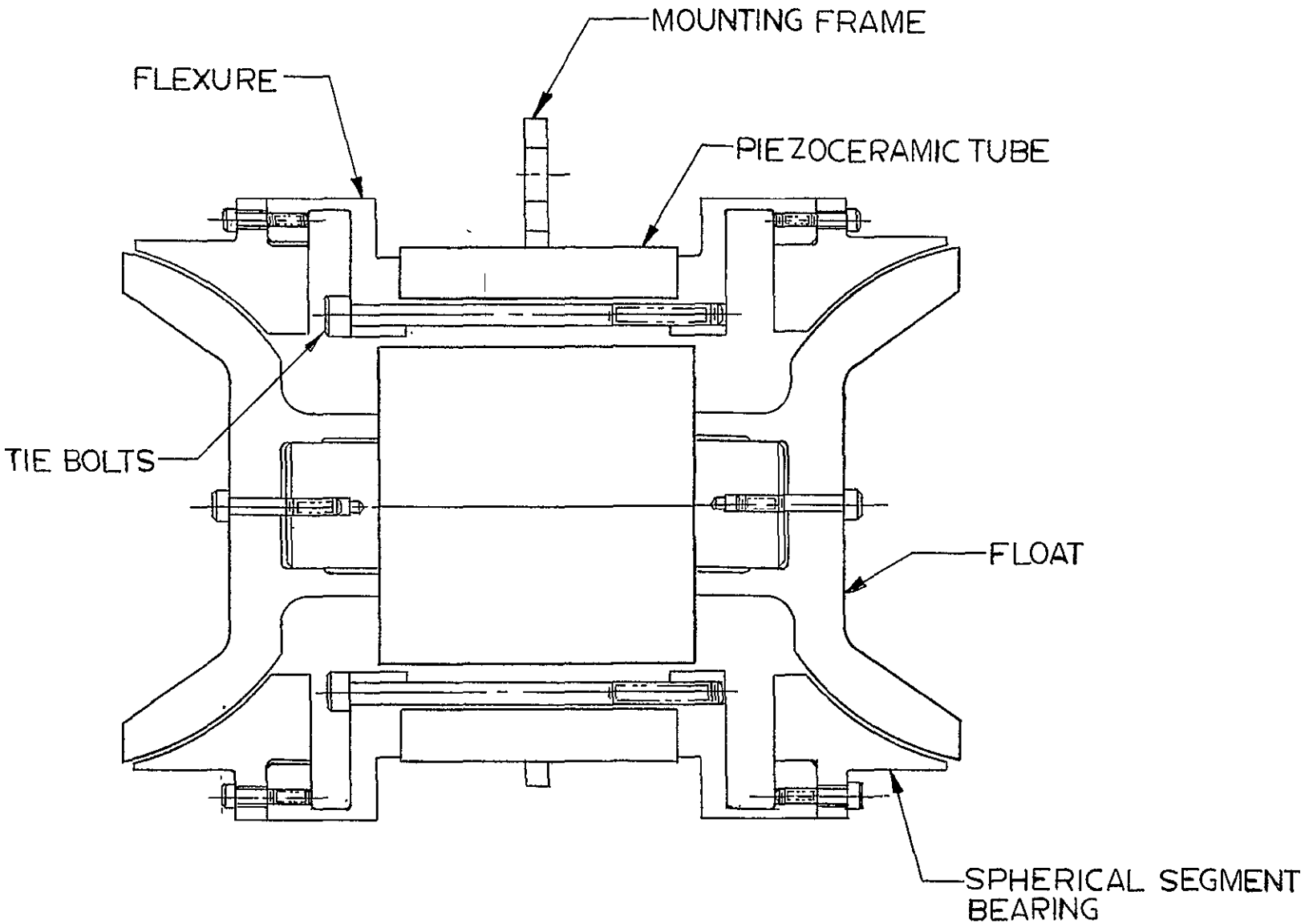

Fig. 1 Cross Sectional View of Modified Spherical-Bearing, Axial-Excursion Squeeze-Film Tranducer

MTI-3044

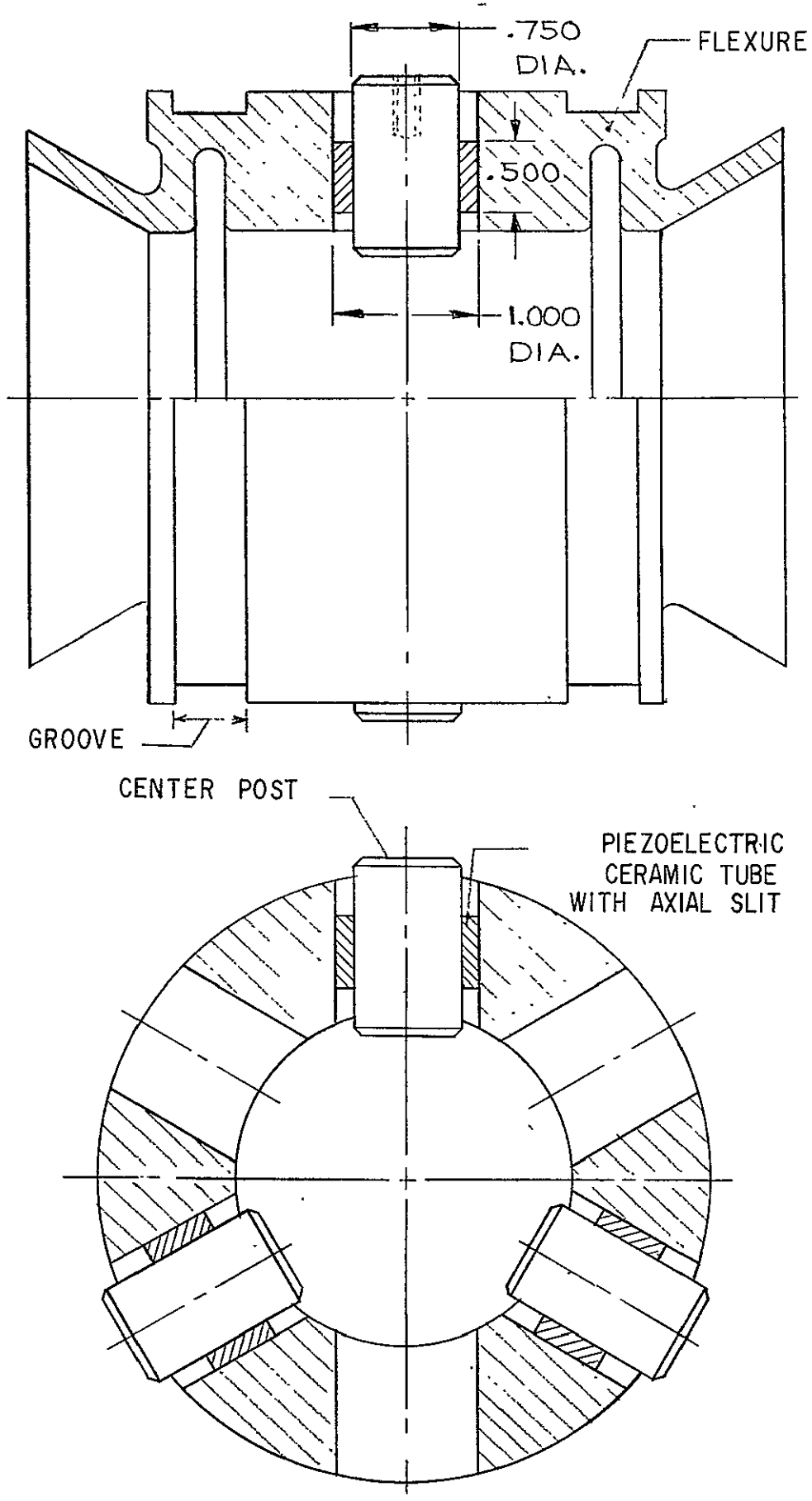

Fig. 2 Experimental Transducer Frame

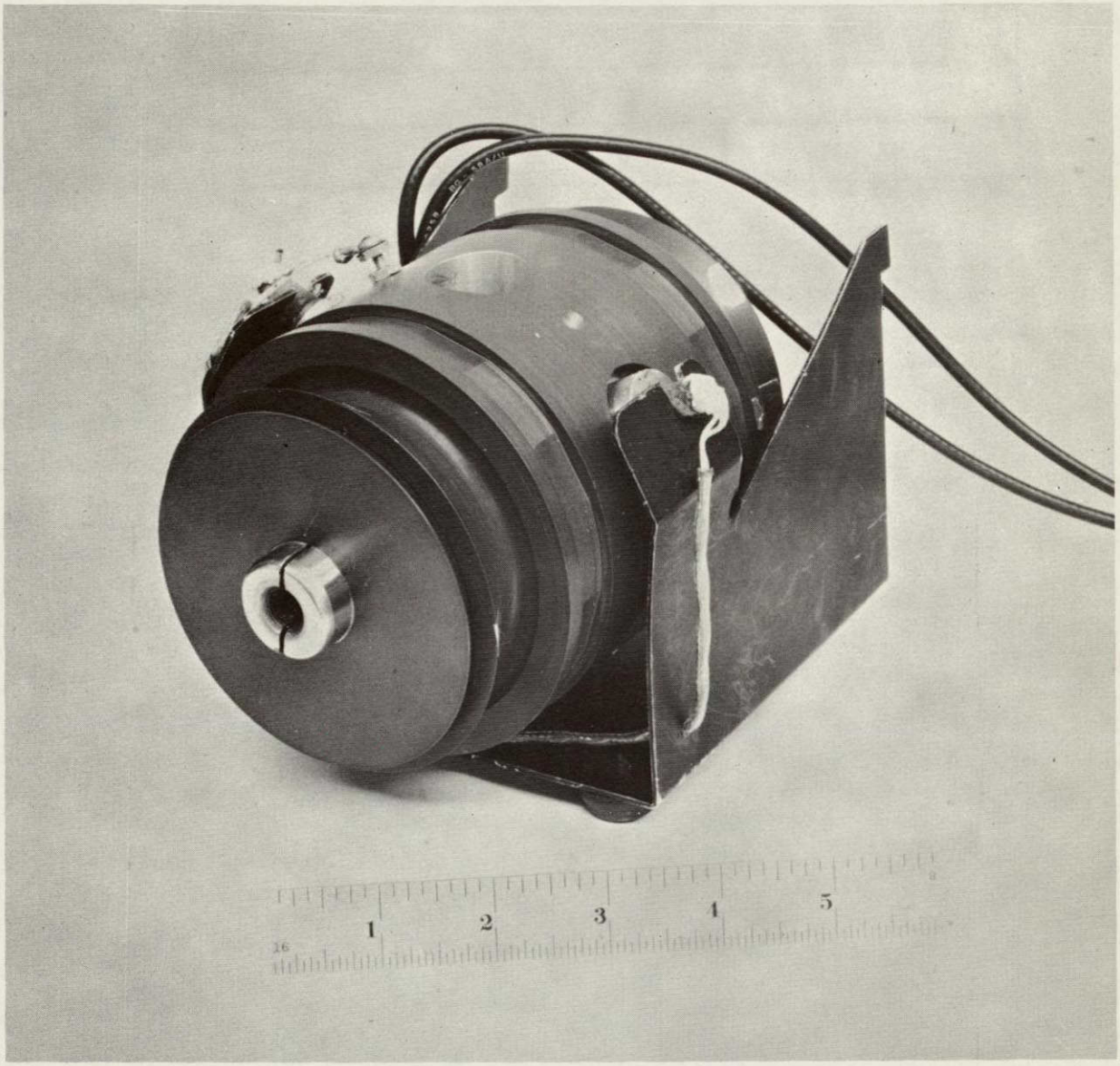

Fig. 2-A Experimental Transducer with Float Installed. See Fig. 2 for section of frame.

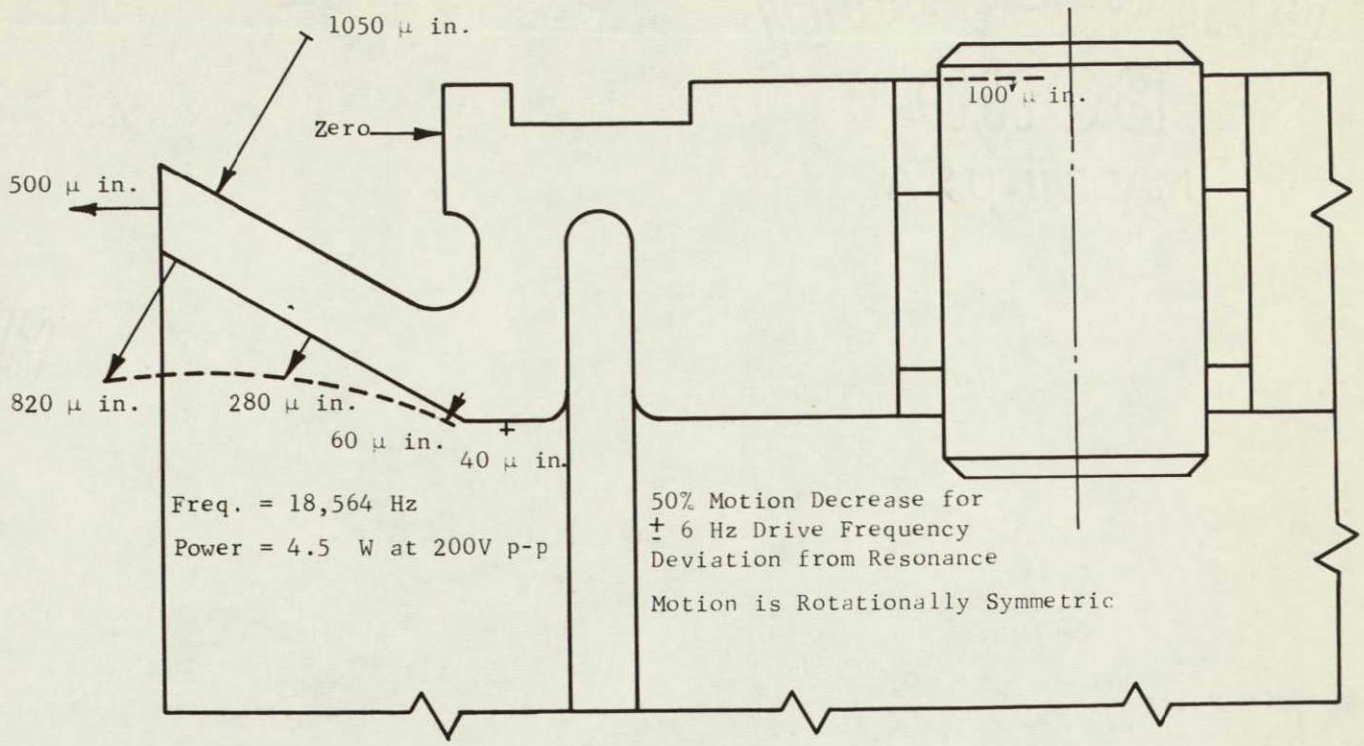

(a)

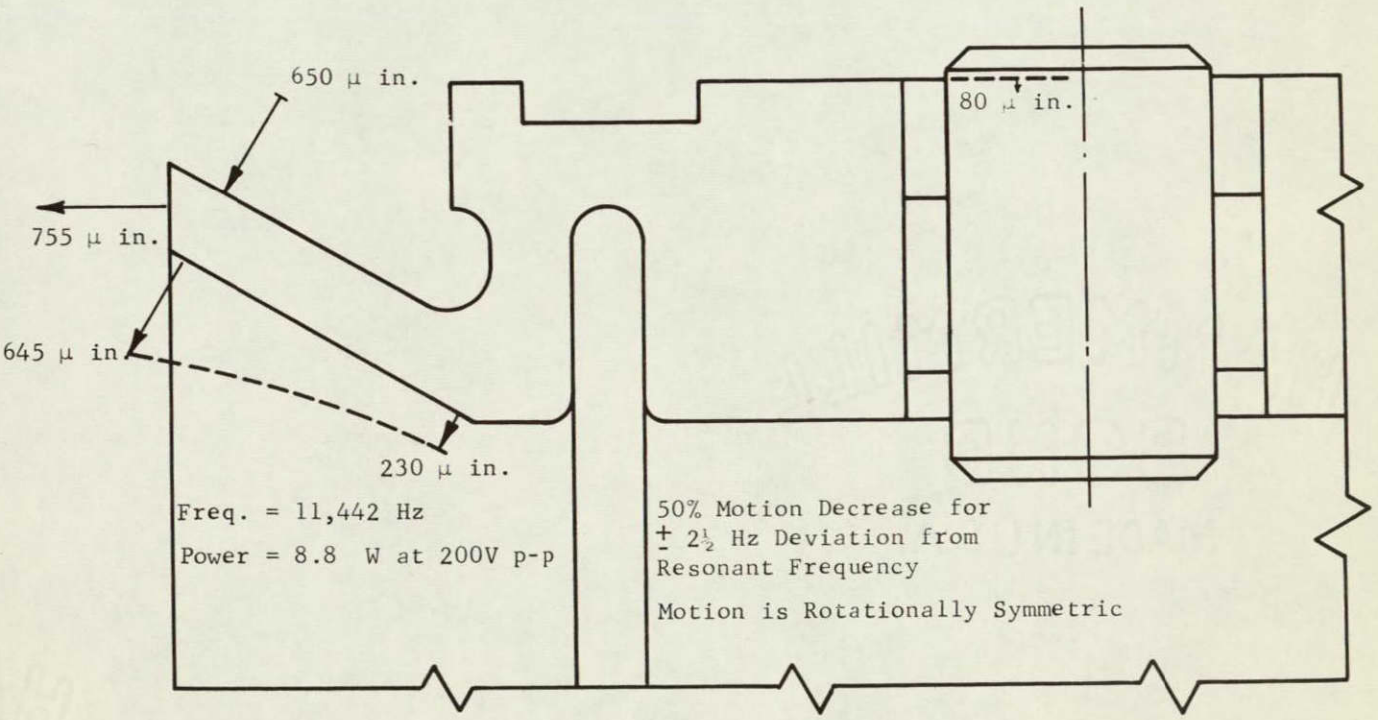

(b)

Fig. 3 Two Resonant Modes of Vibration with Six Drivers Used in Parallel

MTI-7275

Freq. = 27,035 Hz

3 Holes with Driver

3 Holes Vacant

Motion is Rotationally Symmetric

X = NODE

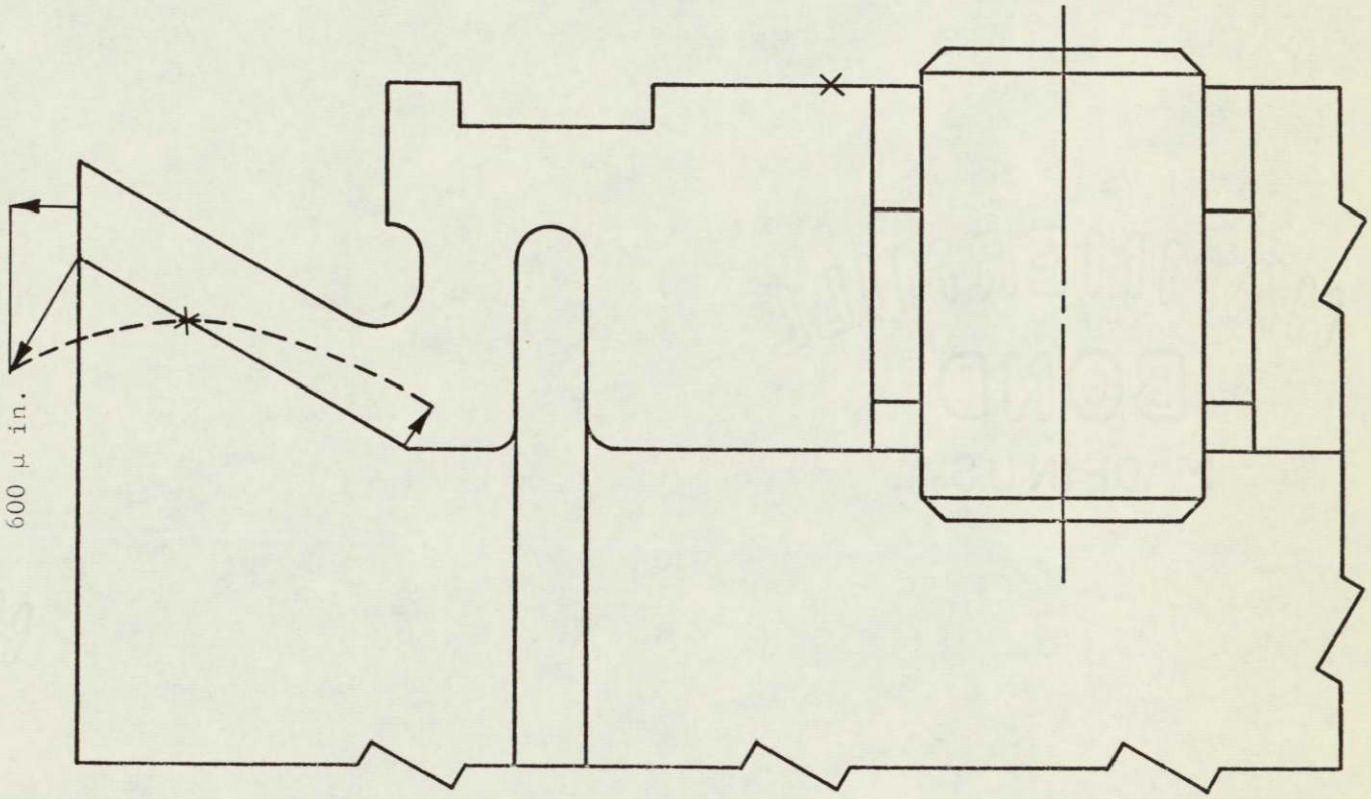

FIG. 4 Resonant Mode with 3 Drivers Used in Parallel

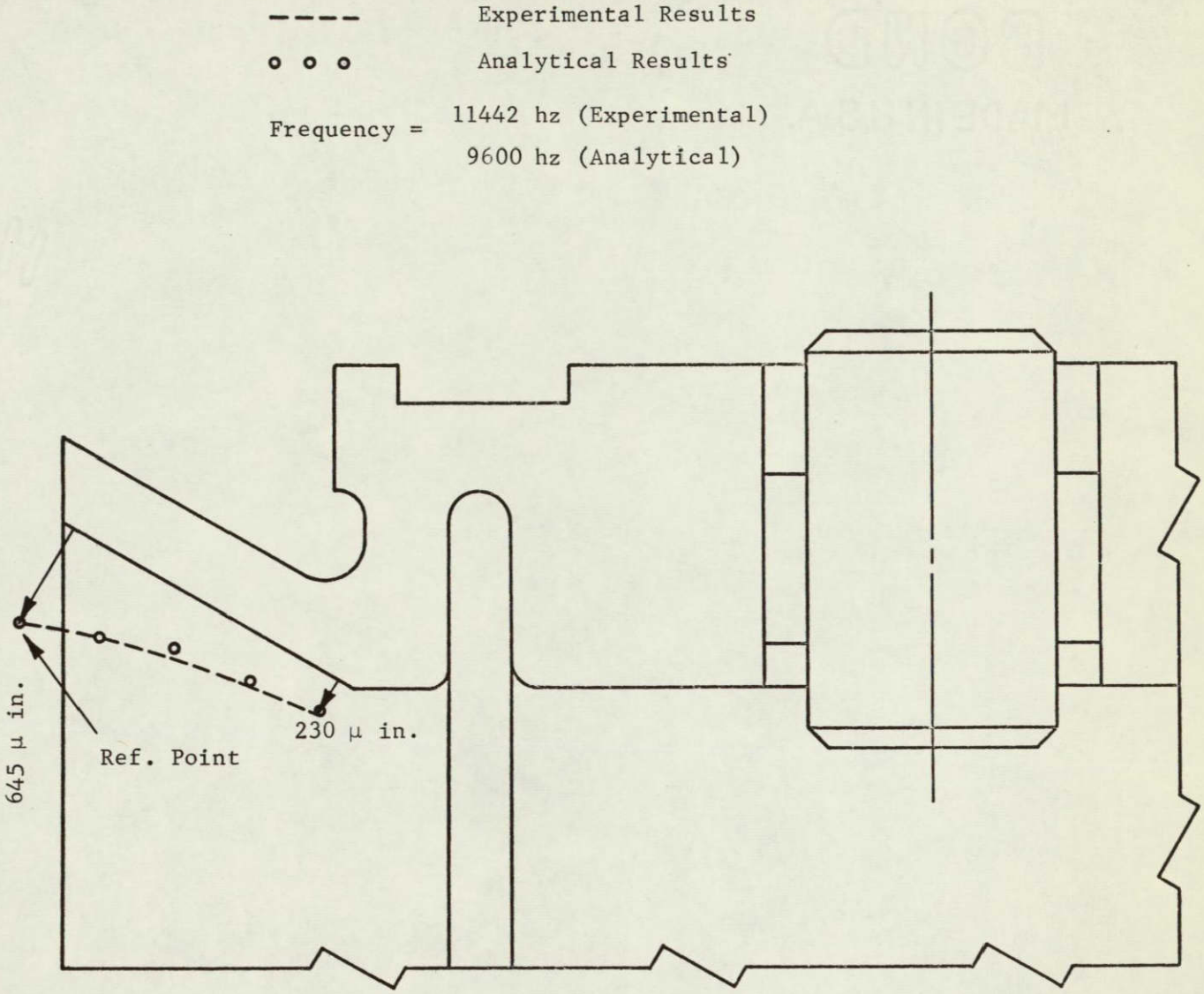

Fig. 5 Comparison of Experimental and Analytical Results of the 11 khz Mode with All Six Holes Filled

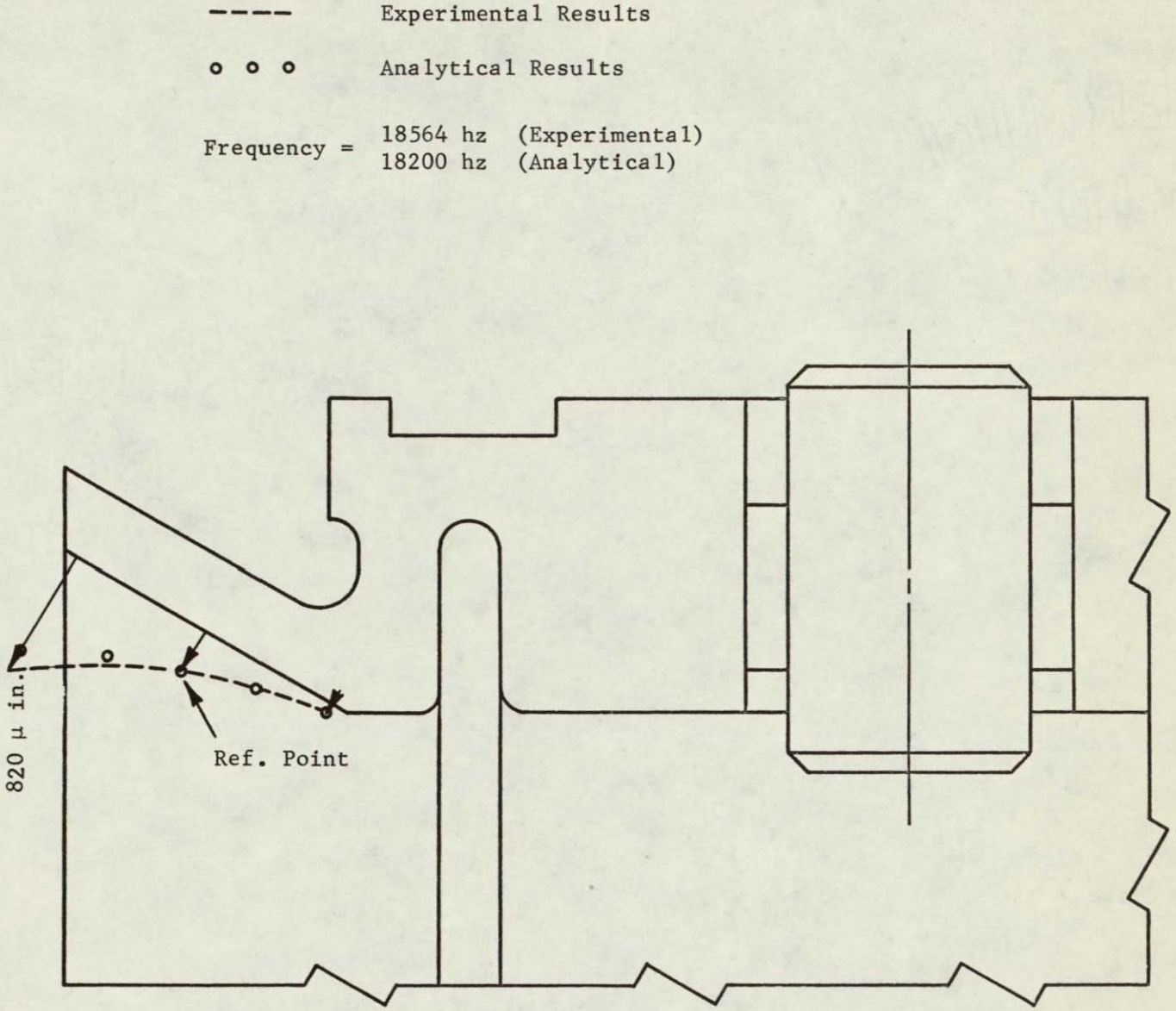

Fig. 6 Comparison of Experimentl and Analytical Results of the 18 khz Mode with all Six Holes Filled

———— Experimental Results

o o o Analytical Results

Frequency = 27035 hz (Experimental)
30000 hz (Analytical)

X = Node

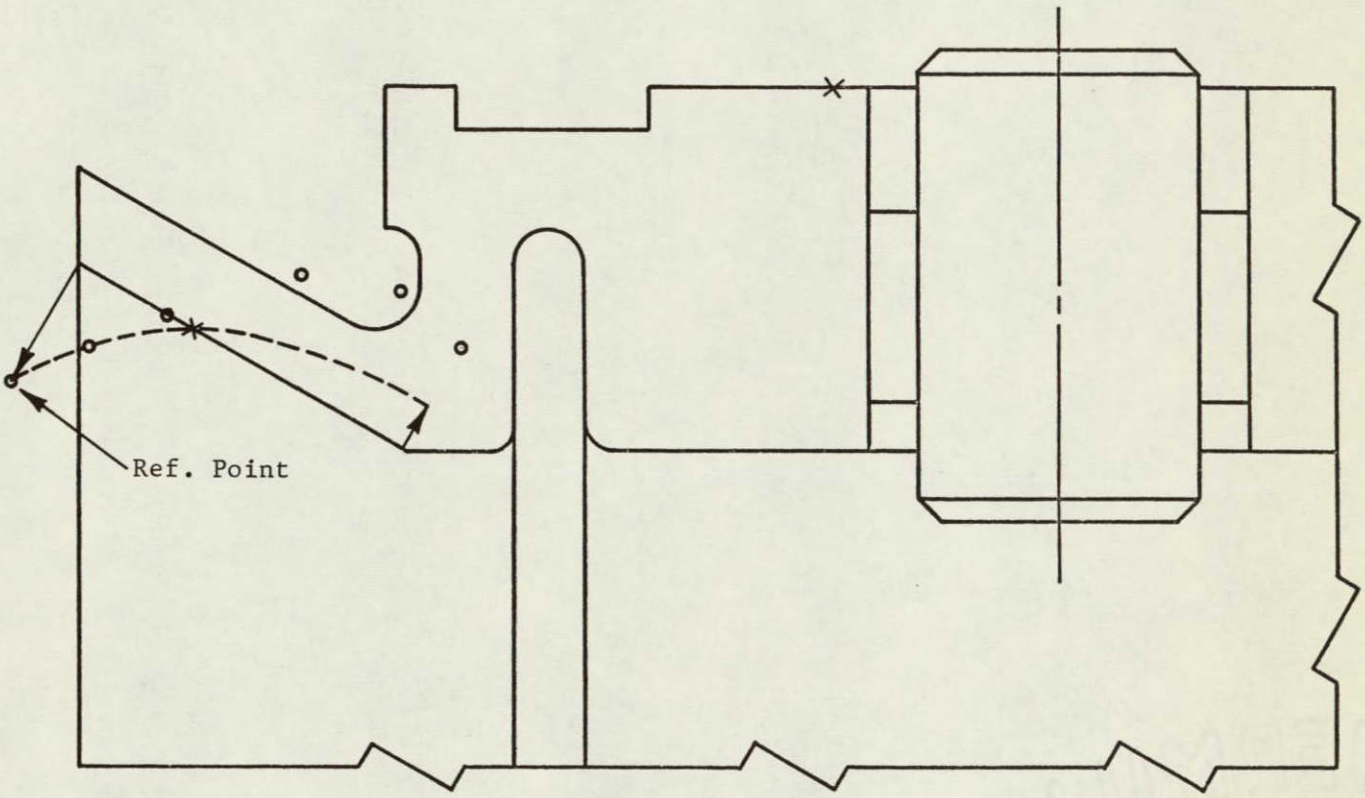

Fig. 7 Comparison of Experimental and Analytical Results of the 27 khz Mode with 3 Holes Filled with Drivers Used in Parallel

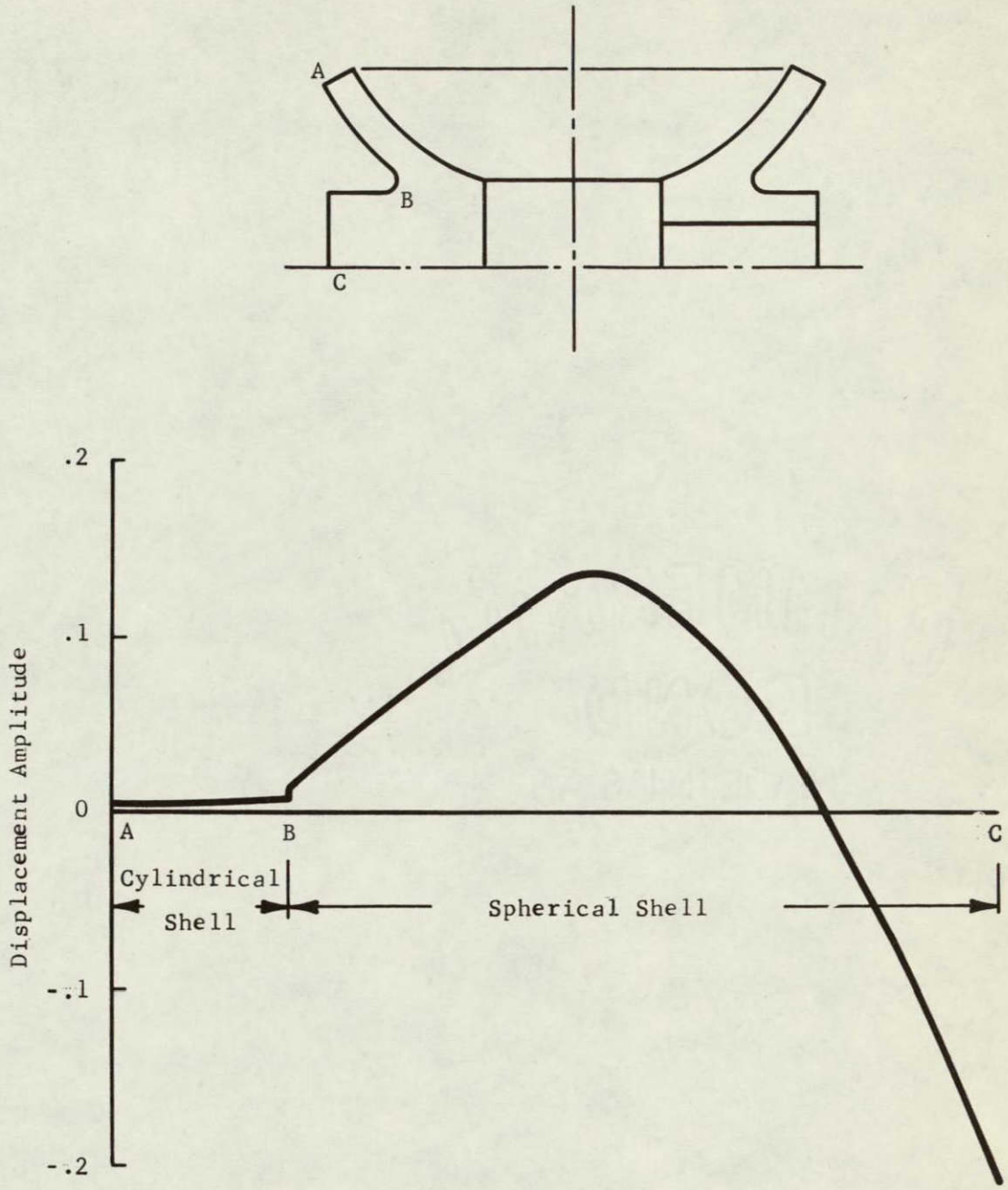

Fig. 8 Mode Shape at 25.2 khz; Transducer has 4 Holes Empty, 4 Holes Filled with Drivers

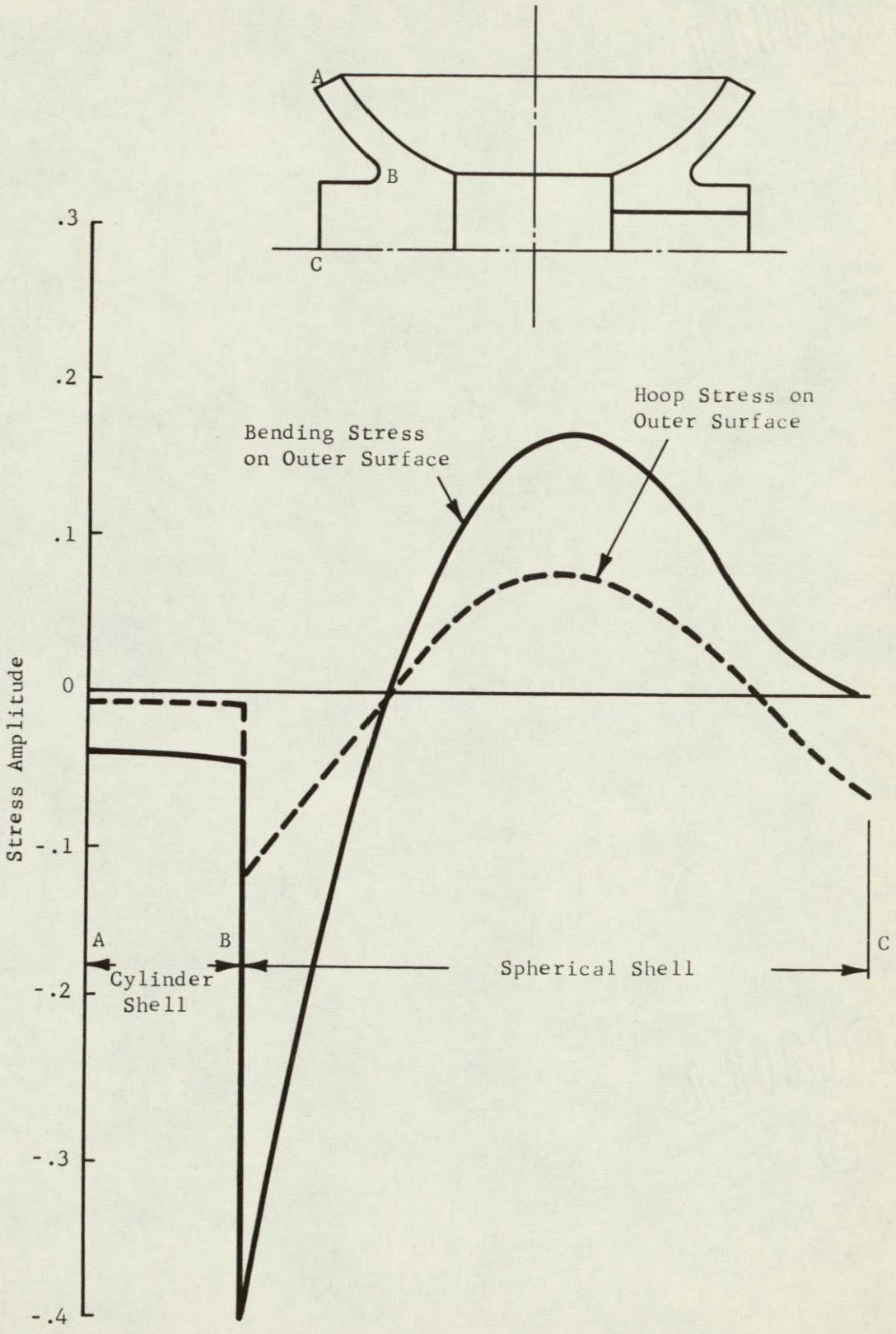

Fig. 9 Dynamic Stress Distribution Corresponding to the Mode Shape Shown in Fig. 8

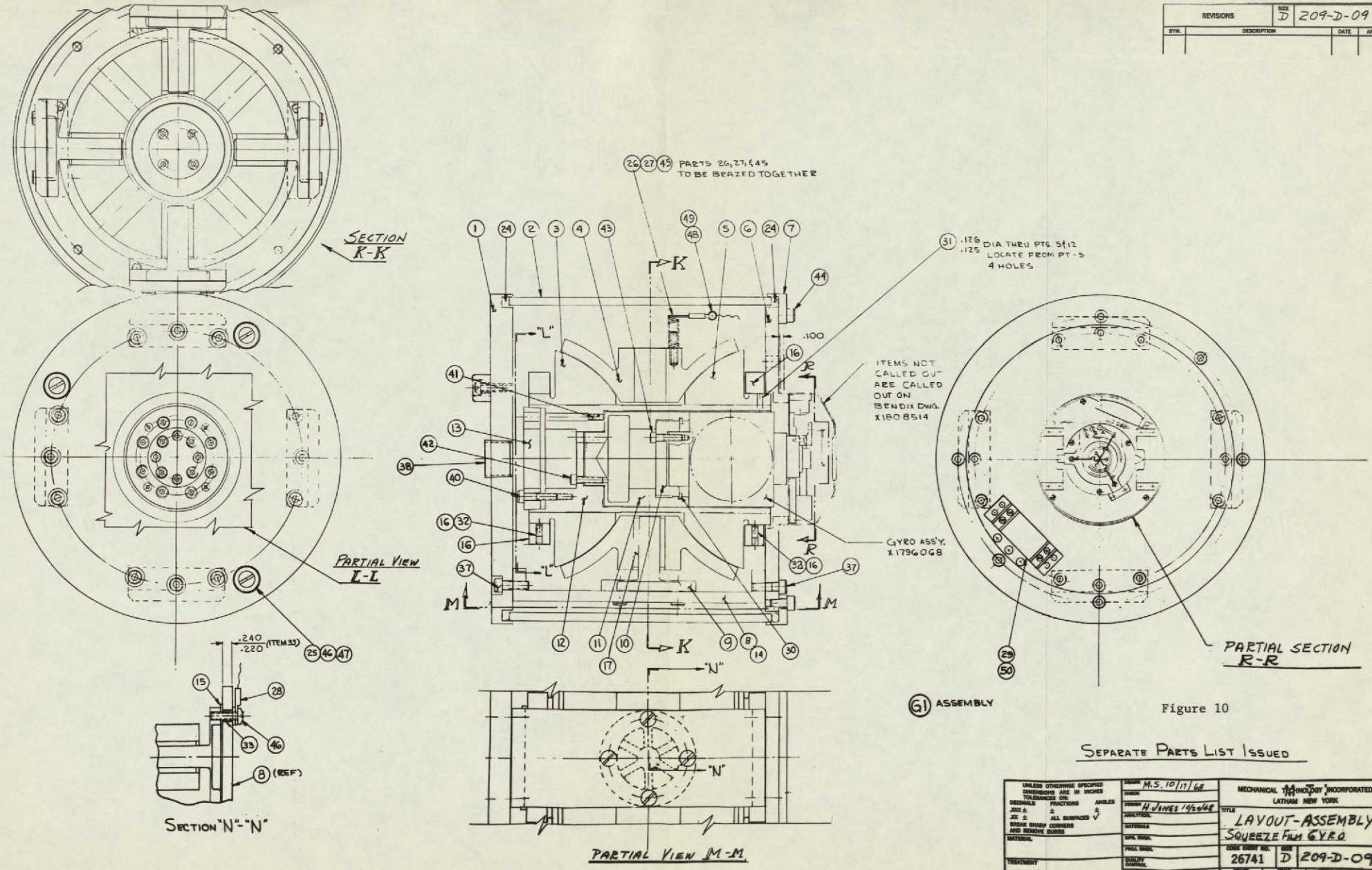

Figure 10

SEPARATE PARTS LIST ISSUED

UNLESS OTHERWISE SPECIFIED DIMENSIONS ARE IN INCHES TOLERANCES ON: DECIMALS FRACTIONS ANGLES .XXX ± ± .XX ± ALL SURFACES BREAK SHARP CORNERS AND REMOVE BURRS	DRAWN M.S. 10/17/68	MECHANICAL TECHNOLOGY INCORPORATED LATHAM NEW YORK	
MATERIAL	CHECK		
	DESIGN H. JONES 10/24/68	TITLE LAYOUT-ASSEMBLY SQUEEZE FILM GYRO	
TREATMENT	ANALYTICAL		
	MATERIALS		
	MFG. ENGR.		
	PROJ. ENGR.	CODE IDENT NO. 26741	SIZE D 209-D-09
	QUALITY CONTROL	SHEET	

MTI-7309

FOLDOUT FRAME 1

FOLDOUT FRAME

MECHANICAL TECHNOLOGY INCORPORATED

PL209D09
sheet 1 of 3

Title PARTS LIST FOR
ASSEMBLY
SQUEEZE FILM GYRO

Quantity Per Group						Item No.	Part No.	Description
6	5	4	3	2	1			
					X		209D09G1	ASSEMBLY
					1	1	209C11P1	BOTTOM PLATE
					1	2	209C14P1	CYLINDER
					1	3	209C03P2	SPHERICAL SEAT
					1	4	209C21G1	SPHERICAL BRG. ASSEMBLY
					1	5	209C02P1	SPHERICAL SEAT
					1	6	209C10P1	TOP COVER
					1	7	209C12P1	RING-RETAINING
					4	8	209C13P1	SUPPORT
					4	9	209B05P2	FLEXURE
					1	10	209B16P1	ADAPTER
					1	11	209B15P1	SPACER
					1	12	209C04P1	SHAFT
					1	13	209B06P1	CLAMPING GIB
					AR	14	209B17	SHIM (PLASTIC)
					AR	15	209B18	SHIM (PLASTIC)
					2	16	209B19P1	BALANCING RING
					4	17	209B20P1	CYLINDER

Approved H. Jones 2/5/69
Checked
Drawn F. Bartnicki 5 FEB 69

Rev. No.

PL209D09
sheet 1 of 3

MTI-72 (11-67)

MTI-7304

MECHANICAL TECHNOLOGY INCORPORATED

PL 209 D 09
sheet 2 of 3

Title PARTS LIST FOR
ASSEMBLY
SQUEEZE FILM GYRO

Quantity Per Group						Item No.	Part No.	Description
6	5	4	3	2	1			
					2	24	CAT. # 2-367	"O" RING BUNA N (45-50 DUR.)
								PARKER OR EQUIV.
					3	25	CAT. # 680	RUBBER GROMMET
								ATLANTIC INDIA RUBBER OR EQUIV.
					1	26	CAT. #	SPRING (MUSIC WIRE)
							LC-020B-9	LEE SPRING CO. OR EQUIV.
					1	27	CAT. # 31878	TERMINAL
								AIRCRAFT MARINE PRODUCT INC.
								OR EQUIV.
					4	28	CAT. # 31884	TERMINAL
								AIRCRAFT MARINE PRODUCTS INC.
								OR EQUIV.
					1	29	CAT. # 410-C-	TERMINAL STRIP
							3/4ST-G-S1-F	KULKA ELECTRIC CORP OR EQUIV.
					1	30	CAT. #	RETAINING RING
							N5002-175	WALDES TRUARC OR EQUIV.
					2	31	CAT. # 52-	ROLLPIN ESNA OR EQUIV.
							028-125-0375	
					8	32	CAT. # CS-15	NO-MAR SET SCREW
								PIC DESIGN CORP OR EQUIV.
					16	33	CAT. # 2537	BUSHING (MODIFIED AS
								SHOWN) ARROW ELECTRONICS
								OR EQUIV.

Approved H. Jones 2/5/69
Checked
Drawn J. Bartick 5 FEB 69

Rev. No.

PL 209 D 09
sheet 2 of 3

MTI-12 (11-67)

MTI-7302

MECHANICAL TECHNOLOGY INCORPORATED

PL209D09
sheet 3 of 3

Title PARTS LIST FOR

ASSEMBLY SQUEEZE FILM GYRO

Quantity Per Group						Item No.	Part No.	Description
6	5	4	3	2	1			
					24	37		HEX. SOCKET HD. CAP SCREW
								#10-32 X 5/8 LG. ALLENOY
					1	38		1/2 NPT PIPE PLUG
								STEEL
					16	39		HEX. SOCKET SET SCREW (FLAT PT.)
								#8-32 X 1/2 LONG ALLENOY
					8	40		HEX. SOCKET HD. CAP SCREW
								#8-32 X 3/4 LONG. ALLENOY
					4	41		HEX. SOCKET SET SCR. (NYLOK) (FLAT PT.)
								#6-40 X 3/8 LONG ALLENOY
					4	42		HEX. SOCKET HD. CAP SCREW
								#6-32 X 5/8 LONG ALLENOY
					4	43		HEX. SOCKET HD. CAP SCREW
								#6-40 X 5/8 LONG ALLENOY
					8	44		HEX. SOCKET HD. CAP SCREW
								#10-32 X 3/8 LONG ALLENOY
					1	45		HEX. SOCKET SET SCR. (FLAT PT.)
								#10-32 X 3/4 LONG ALLENOY
					19	46		ROUND HEAD MACHINE SCR
								#10-32 X 5/8 LONG. STL. CAD PL.
					3	47		WASHER FOR #10 SCREW
								(MEDIUM) STL. CAD. PL.
					1	48		ROUND HEAD MACHINE SCREW
								#4-40 X 1/4 LG STL. CAD. PL.
					1	49		HEX. NUT #4-40 STL. CAD. PL.
					4	50		ROUND HEAD MACHINE SCREW
								#2-56 X 3/8 LG. STL. CAD. PL.
					16	51		

Approved H. JONES 2/5/69
Checked
Drawn J. Bartruski 5 FEB '69

Rev. No.

PL209D09
sheet 3 of 3

MTI-12 (11-67)

MTI-7303

Patterns Obtained by Driving Three Piezo Electric Elements

V_{in} = Driving Voltage, V_{out} = Voltage from Fourth Element

Note: 4 Drivers Total in Planes 1-1 and 2-2

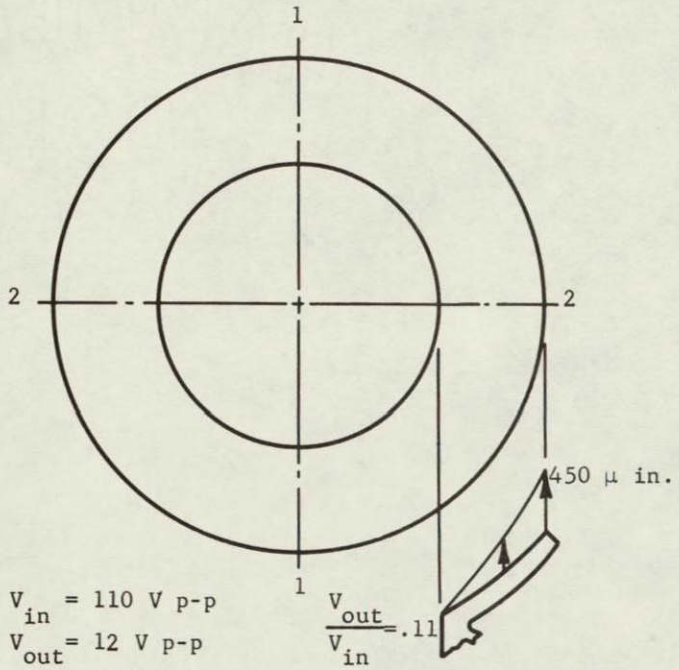

V_{in} = 110 V p-p
V_{out} = 12 V p-p
f = 10.864 KHz
$\frac{V_{out}}{V_{in}}$ = .11

Fig. 11A

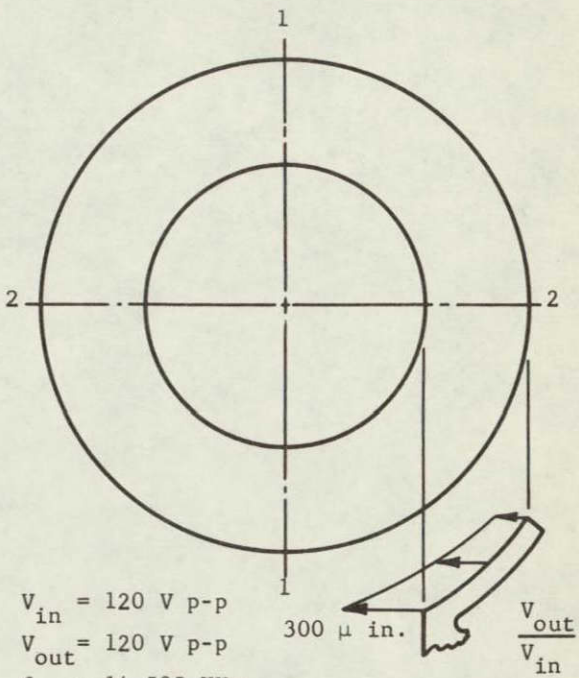

V_{in} = 120 V p-p
V_{out} = 120 V p-p
f = 14.505 KHz
$\frac{V_{out}}{V_{in}}$ = 1.0

Fig. 11B

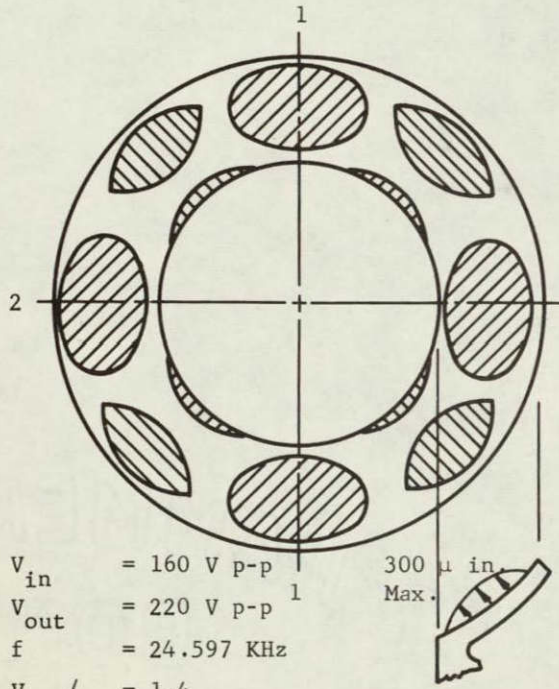

V_{in} = 160 V p-p
V_{out} = 220 V p-p
f = 24.597 KHz
V_{out}/V_{in} = 1.4

Fig. 11C

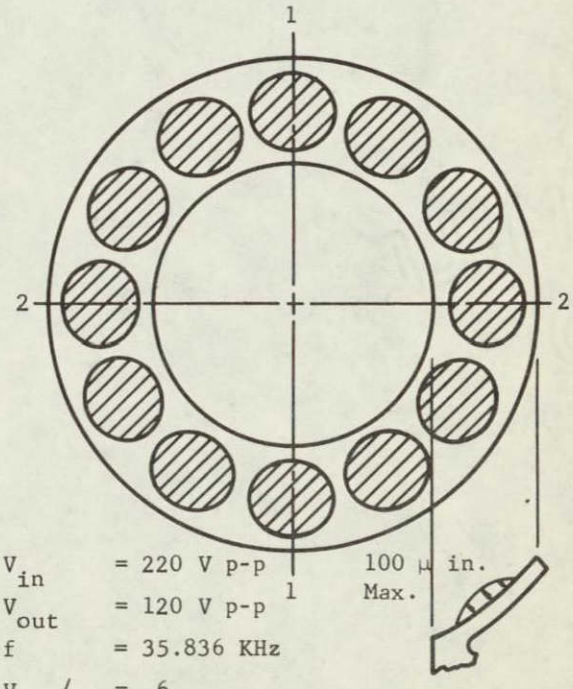

V_{in} = 220 V p-p
V_{out} = 120 V p-p
f = 35.836 KHz
V_{out}/V_{in} = .6

Fig. 11D

Fig. 11 Alcohol Patterns of Bearing Surface
(See Fig.10 for Transducer Section)

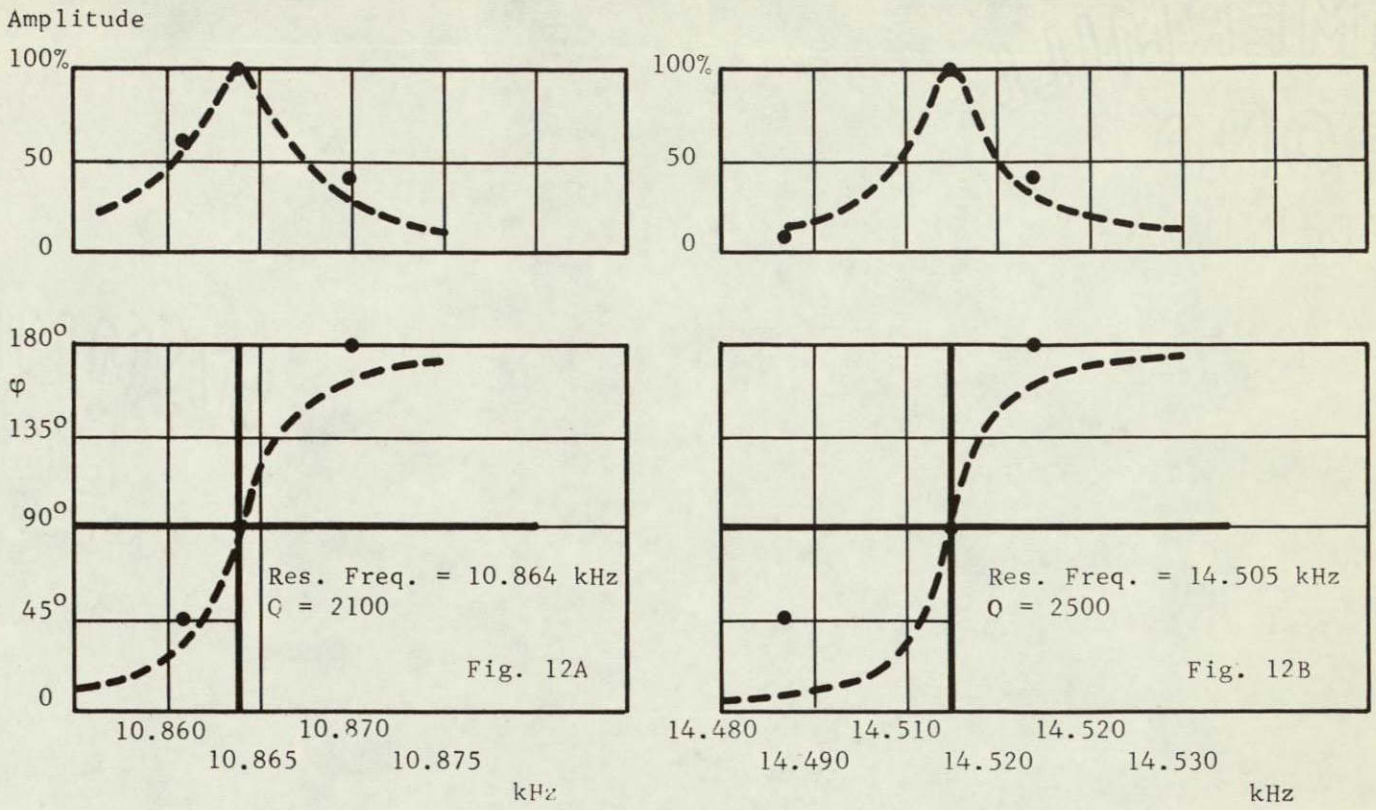

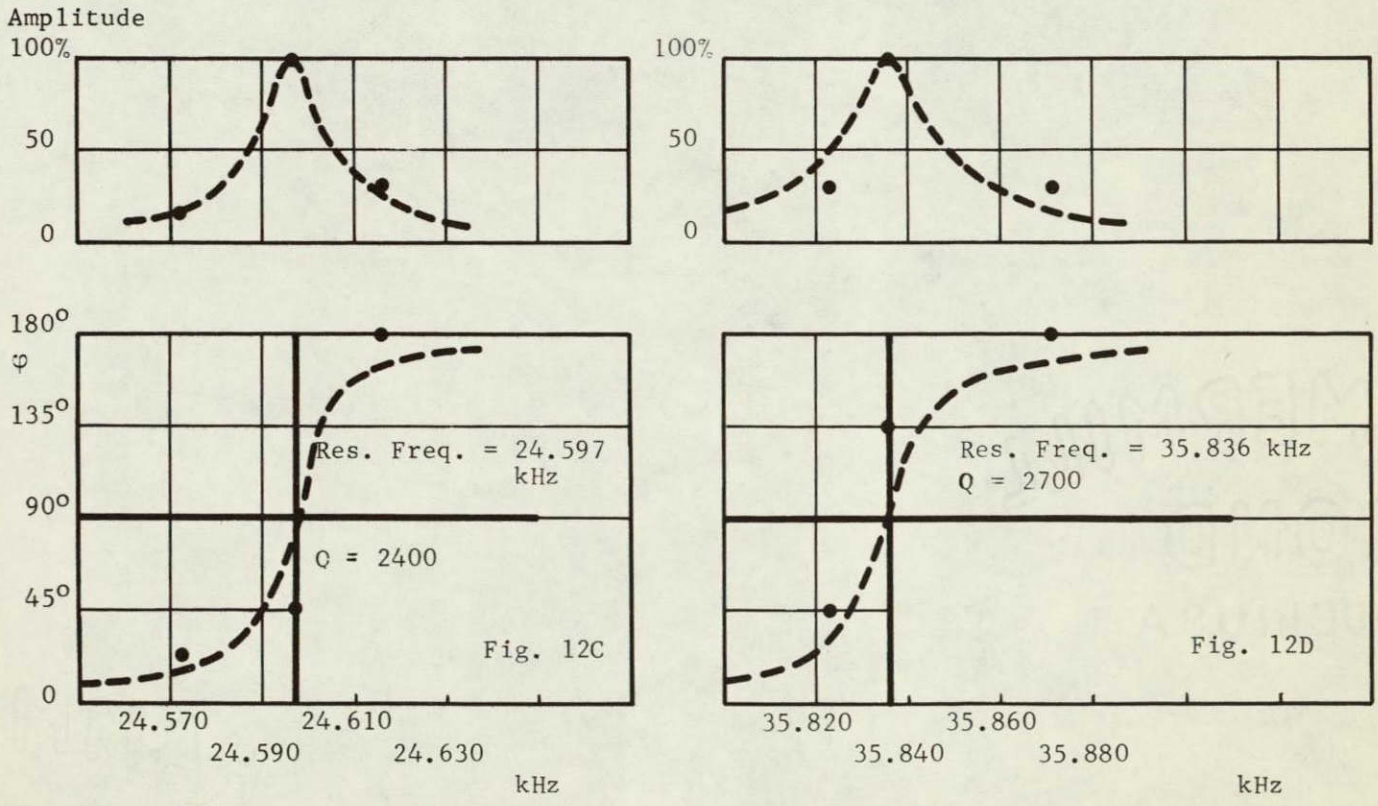

Fig. 12 Phase Between V_{in} and V_{out} vs. Frequency, and Relative Output Voltage $V_{out} / (V_{out})_{max}$ vs. Frequency, At and Near Resonance With Constant Drive Voltage. For Test Conditions, See Fig. 11

MTI-7280

REVISIONS		SIZE C	SK-C-3366	REV.
SYM.	DESCRIPTION		DATE	APPROVAL

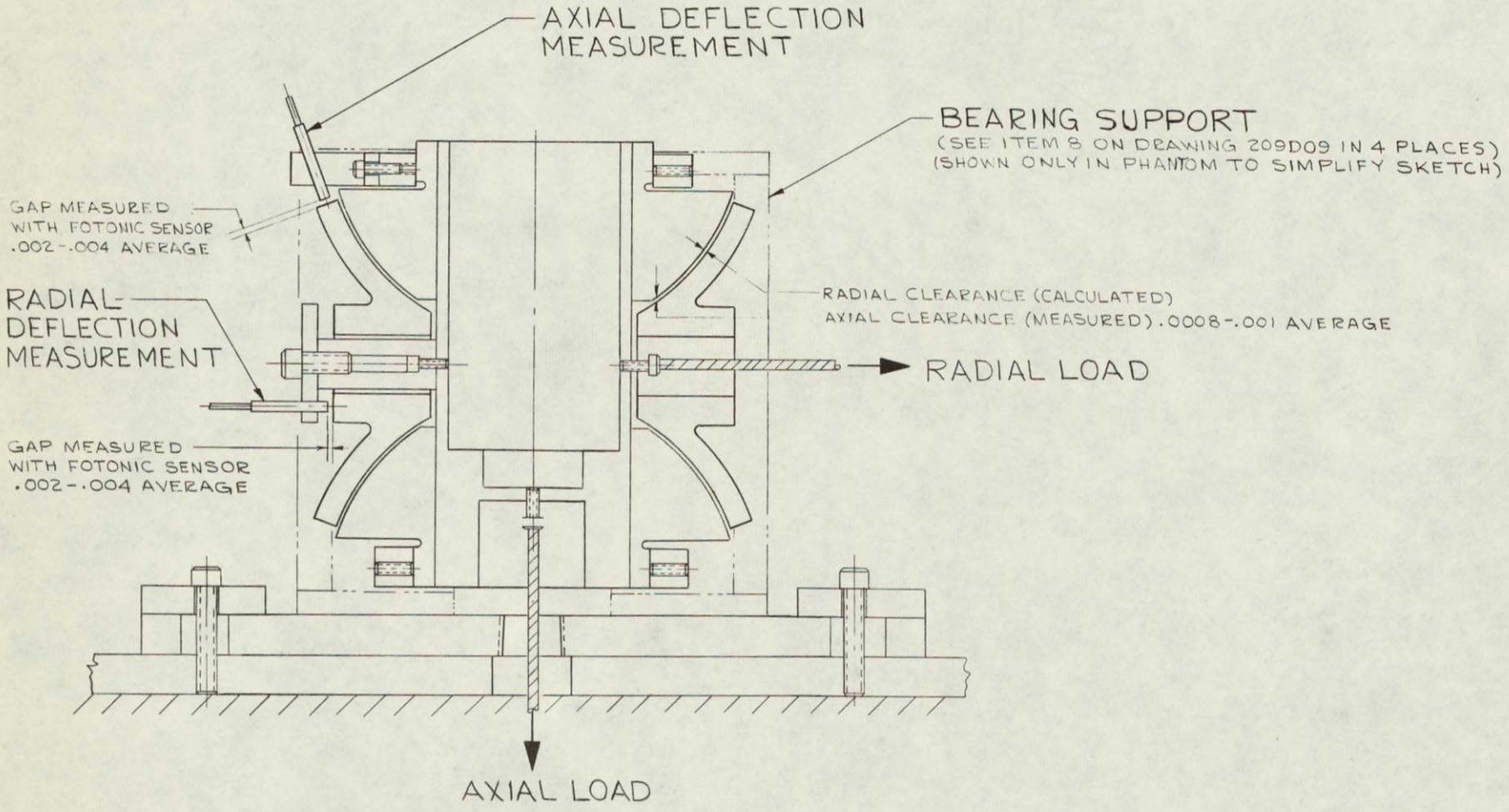

Figure 13

UNLESS OTHERWISE SPECIFIED DIMENSIONS ARE IN INCHES TOLERANCES ON: DECIMALS FRACTIONS ANGLES .XXX ± ± ± .XX ± ALL SURFACES √ BREAK SHARP CORNERS AND REMOVE BURRS	DRAWN L. Bartnicki 6 FEB '69	MECHANICAL TECHNOLOGY INCORPORATED LATHAM NEW YORK	
MATERIAL	CHECK	TITLE BEARING LOAD DEFLECTION MEASUREMENT	
	DESIGN		
	ANALYTICAL		
	MATERIALS		
	MFG. ENGR.		
	PROJ. ENGR.		
TREATMENT	QUALITY CONTROL	CODE IDENT NO. 26741	SIZE C SK-C-3366
		ISSUED	SCALE WT. ACT. CALC.

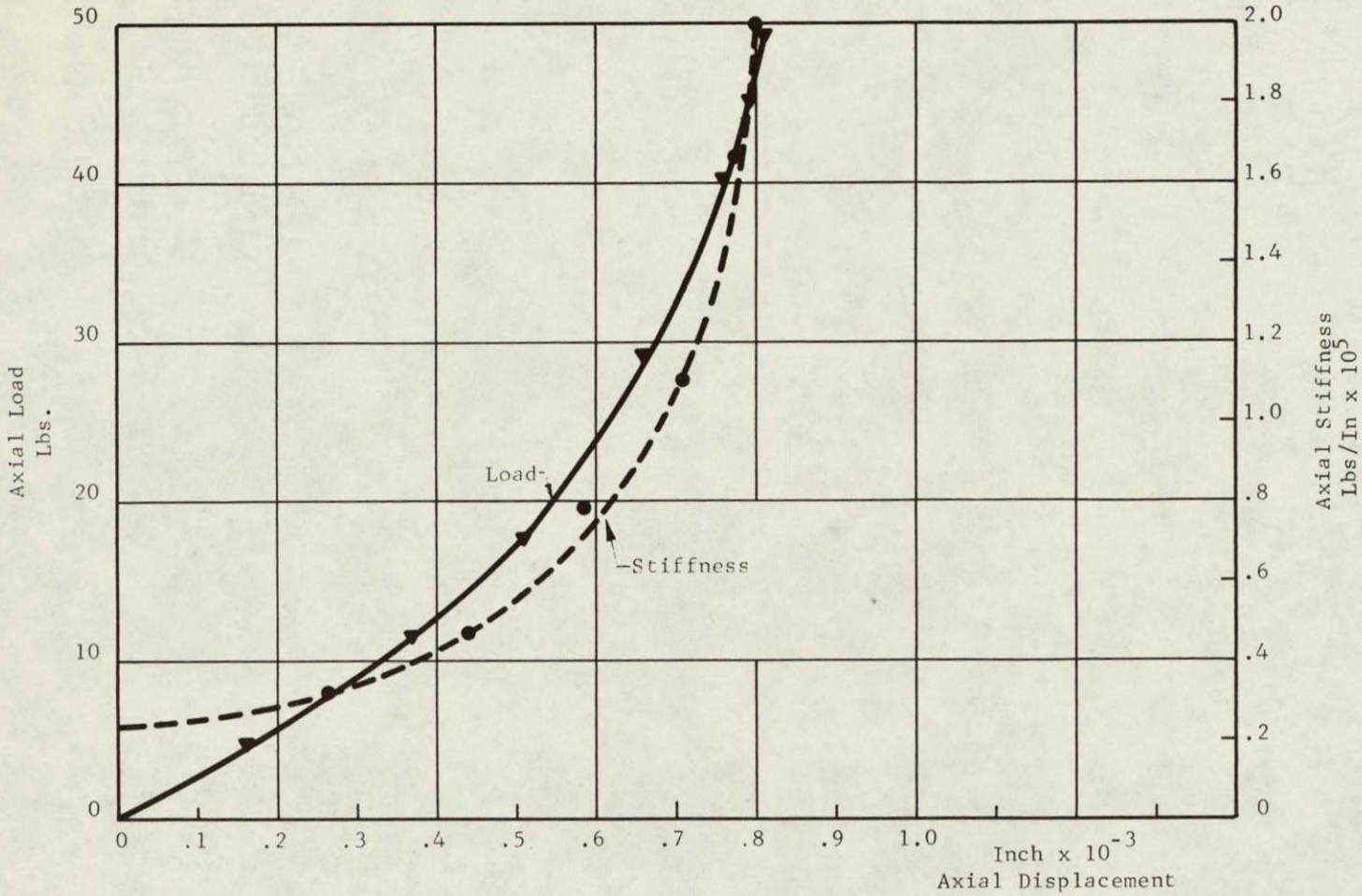

Fig. 14 Experimental Data on Squeeze Film Bearings,
Axial Load and Axial Stiffness vs. Axial Deflection

Axial load capacity = 50 lbs.
Operating frequency 24.661 - 24.747 khz, increasing linearly from no load - full load
Radial load is zero
Three piezo electric drivers are powered and one piezo electric element used as feedback
Input voltage 540 V p-p and feedback voltage 140 V p-p
Maximum radial bearing surface motion 350 in. p-p
(see Fig.11C for mode)
Total axial clearance 2.1×10^{-3} in.

MTI-7281

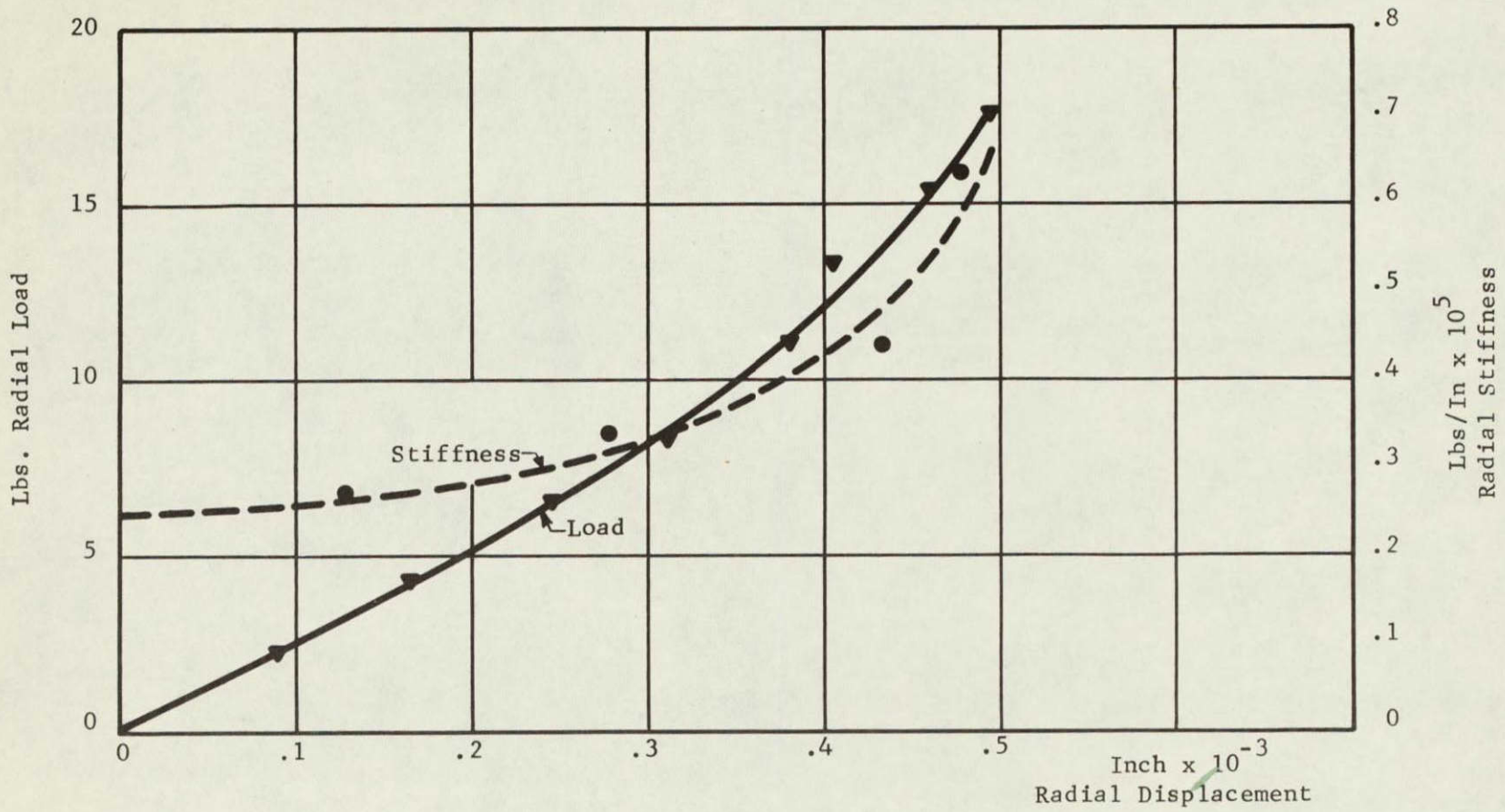

Fig. 15 Experimental Data on Squeeze Film Bearing,
Radial Load and Radial Stiffness vs. Radial Deflection

Maximum radial load capacity = 18 lbs.
Radial vibratory motion superimposed on static deflection = 170 μ in. p-p
Operating frequency 24.665 - 24.677 khz
Axial load is 5 lbs (= float weight)
Three piezo electric drivers are powered and one piezo electric element used for feedback
Input voltage 540 V p-p and feedback voltage 140 V p-p
Maximum radial bearing surface motion 350 μ in. p-p (see Fig.11C for mode)
Total axial clearance 2.1 x 10^{-3} in.

MTI-7282

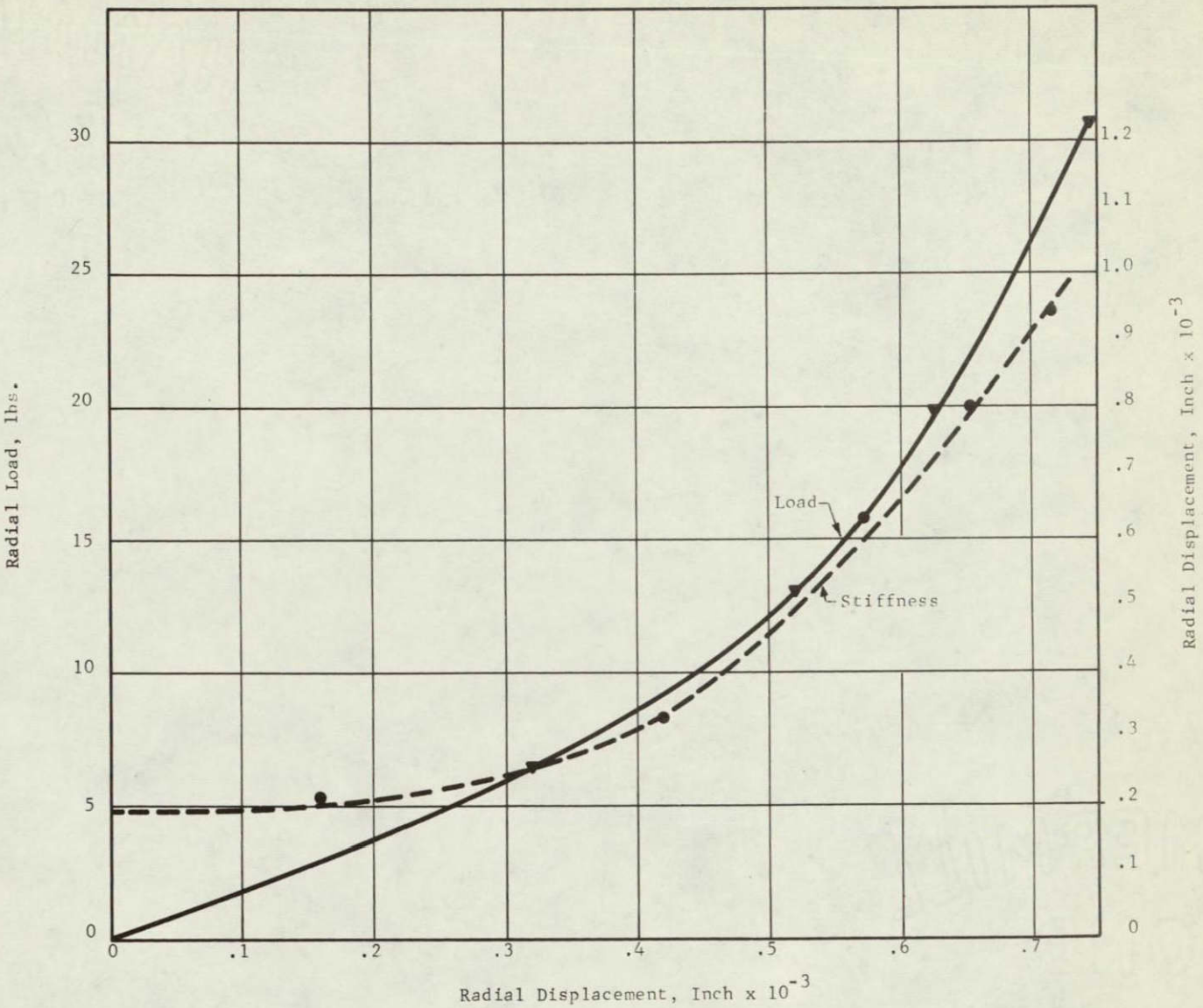

Fig. 16 Experimental Data on Squeeze Film Bearing,
Radial Load and Radial Stiffness vs. Radial Deflection

Maximum radial load capacity > 30 lbs.
Radial vibratory motion superimposed on static deflection = 520 μ in. p-p
Operating frequency 14.534 khz, independent of radial load
(see Fig. 11B for mode)
Axial load is 5 lbs. (= float weight)
Three piezo electric drivers are powered and
one piezo electric element used as feedback
Input voltage 680 V p-p and feedback voltage 240 V p-p
Total axial clearance 2.1 x 10^{-3} in.

Fig. 17 Gyro Squeeze Film Bearing under Test at Marshall Space Flight Center, NASA

MTI-7307

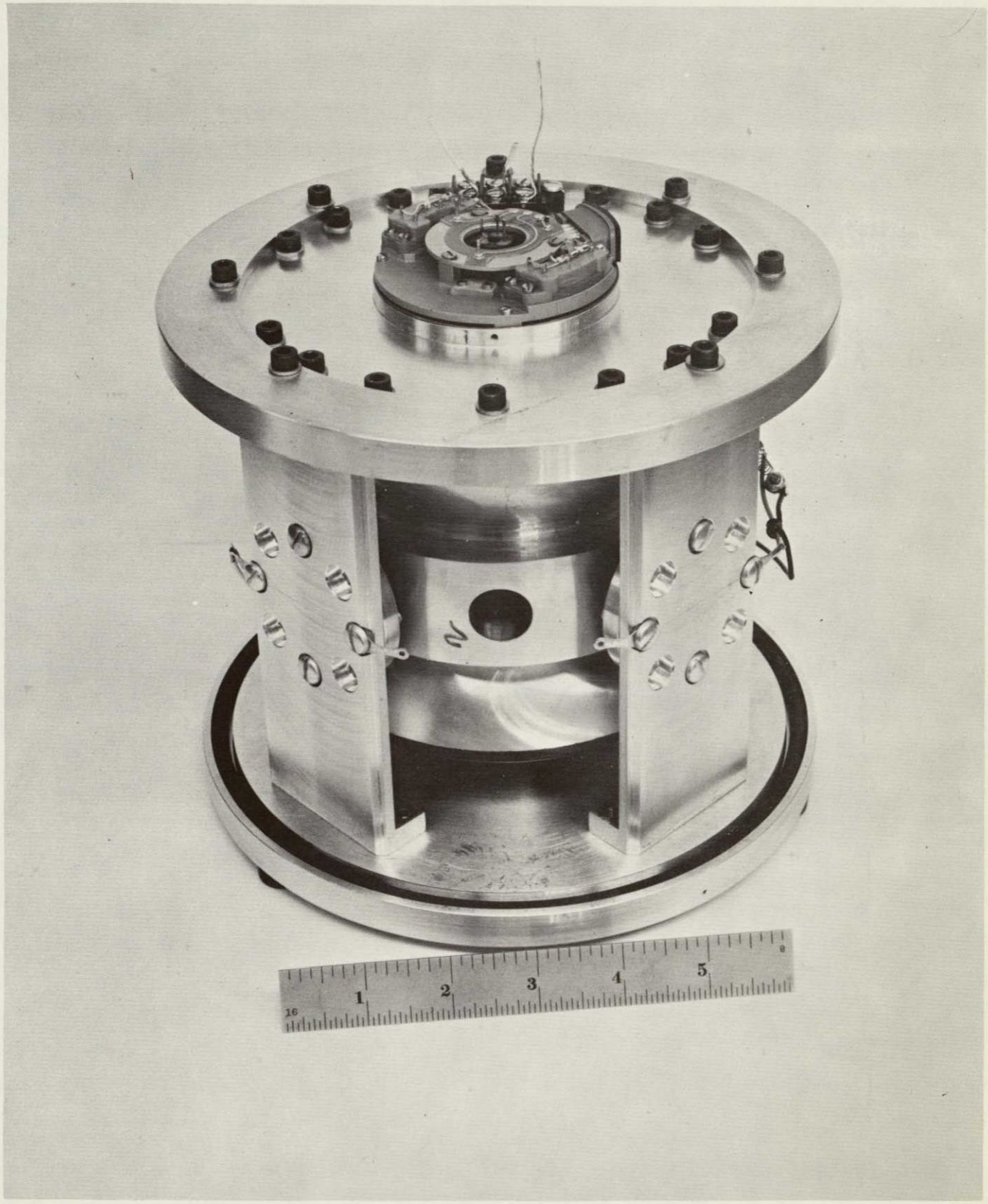

Fig. 17-A Gyro Squeeze Film Bearing - Close Up

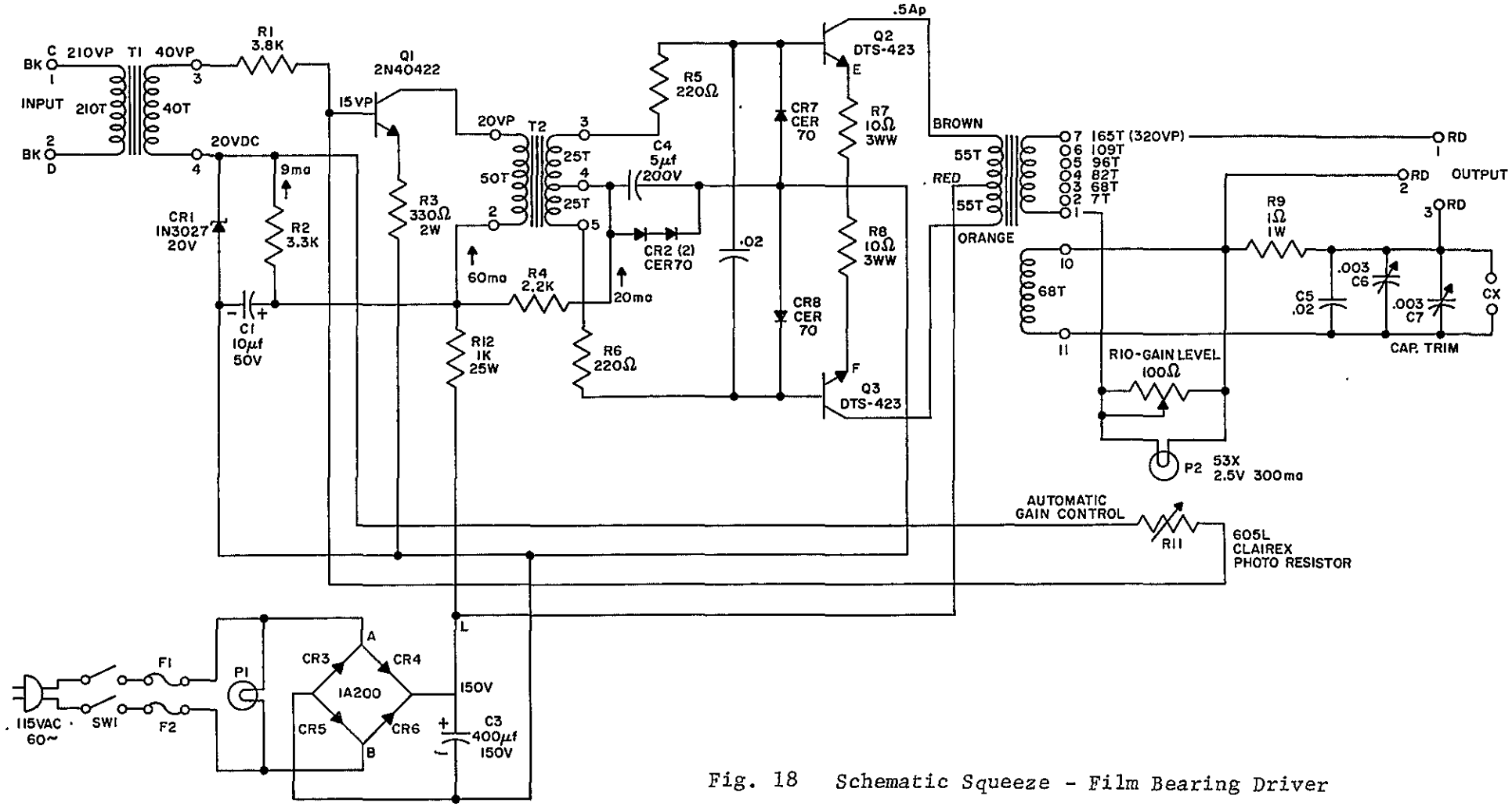

Fig. 18 Schematic Squeeze - Film Bearing Driver

MTI-7283

APPENDIX A

DIMENSIONAL STABILITY OF FERROELECTRIC CERAMICS

Final Report

Mechanical Technology Incorporated
Purchase Order No. 17-3070

by

H. H. A. Krueger
S. R. Burlage

Approved: _____

Don Berlincourt, Head
Electromechanical
Research Department

Clevite Corporation
ELECTRONIC RESEARCH DIVISION
Cleveland, Ohio 44108

DIMENSIONAL STABILITY OF FERROELECTRIC CERAMICS

This report summarizes the results of measurements of strain aging under maintained stress made on PZT-7A, PZT-8 and temperature-stabilized PZT-4 and PZT-8. The strain parallel to the polar axis (S_3) versus stress parallel to the polar axis (T_3) was measured for all these compositions, and in addition, the lateral strain (S_1) was measured versus lateral stress (T_1) on PZT-8. The specimens were tubes of about 1.1" length, 1.5" diameter and .125" wall thickness with the exception of the specimen of PZT-7A which was a tube of 0,9" length, 1,0" diameter and .25" wall thickness. Strains were measured with foil gages, and stress was applied with a Dillon Universal Tester. An effort was made to calibrate the strain gages by absolute length measurements using gage blocks. This was not successful apparently due to permanent deformation of the fired-on silver electrodes.

It was initially planned to make these measurements on PZT-7A and PZT-8, the former because of its outstandingly low aging and satisfactory high drive characteristics, the latter because of its outstanding high-drive characteristics. Studies quickly showed that PZT-7A depoles rapidly with 10,000 psi parallel compressive stress, and therefore PZT-4 was substituted for further tests.

PZT-7A

There were no previous data for PZT-7A on the effects of high static stress. The parallel strain (S_3) versus maintained parallel stress (T_3) is shown in Figs. 1-3. The excessively large strains during application of stress and the lack of recovery after removal of stress indicate severe depoling. This was confirmed by the decrease of the piezoelectric constant d_{33} to 53×10^{-12} C/N after the stress cycle from a value of 152×10^{-12} C/N before. No further measurements were made on this composition; it was decided instead to determine the strain aging on PZT-4.

PZT-8

A set of aged, radially poled tubes of PZT-8 was obtained from Clevite Piezoelectric Division. The dimensions were 1.5" O.D., 1.1" long and 0.125" wall thickness. Strain gages were applied on the O.D. parallel to the tube axis. Measurements were made of strain vs. stress (T_1) to slightly over 9 kpsi, creep at this stress for 100 hours, strain during stress release, and recovery creep for 100 hours after stress release. The entire curve is shown on a log time plot in Fig. 4. As indicated in Fig. 4, the stress strain portions of the curve were taken

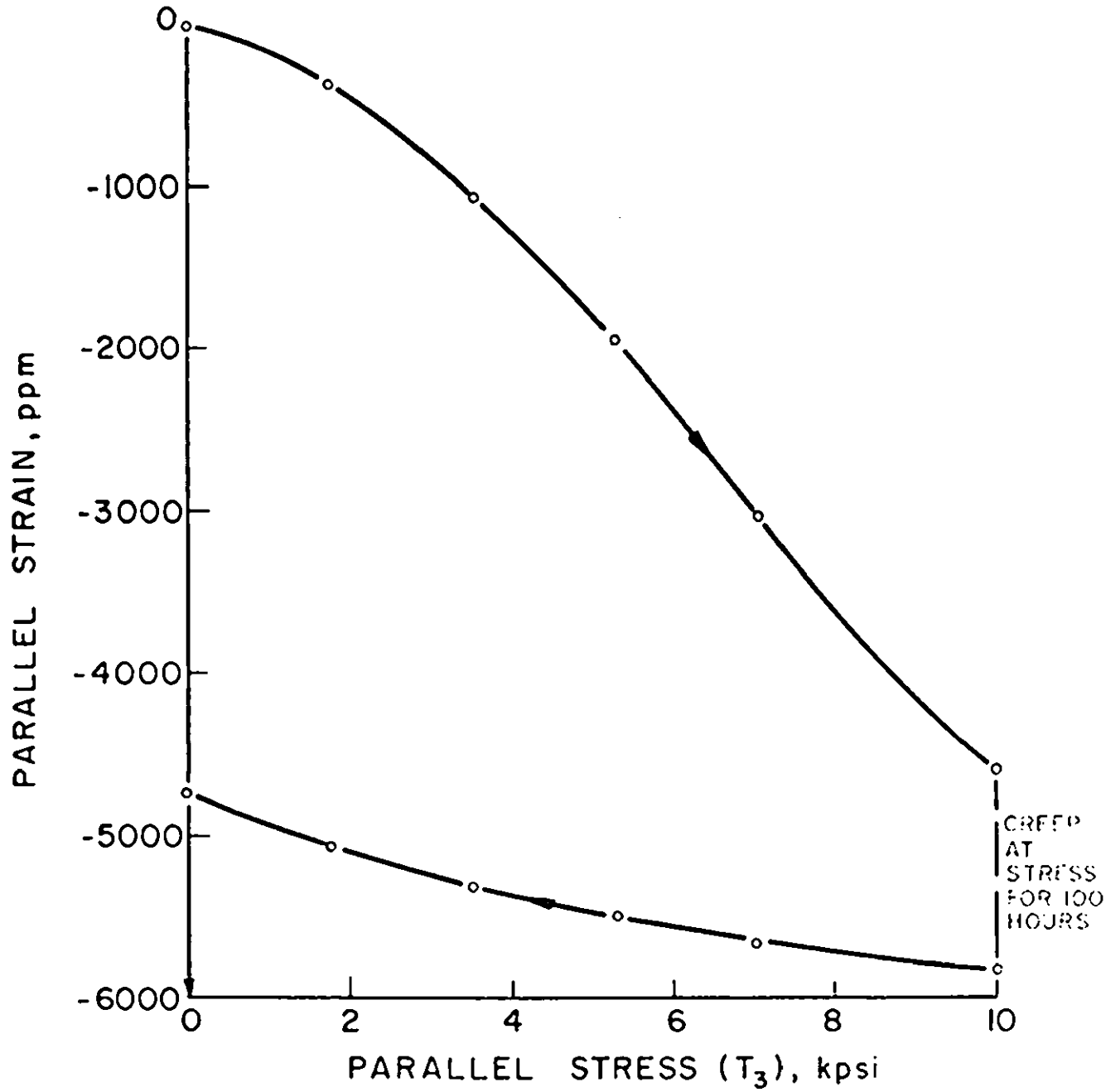

FIG. 1. STRESS-STRAIN CURVE, PZT-7A (T_3)
ONE MINUTE BETWEEN DATA POINTS.

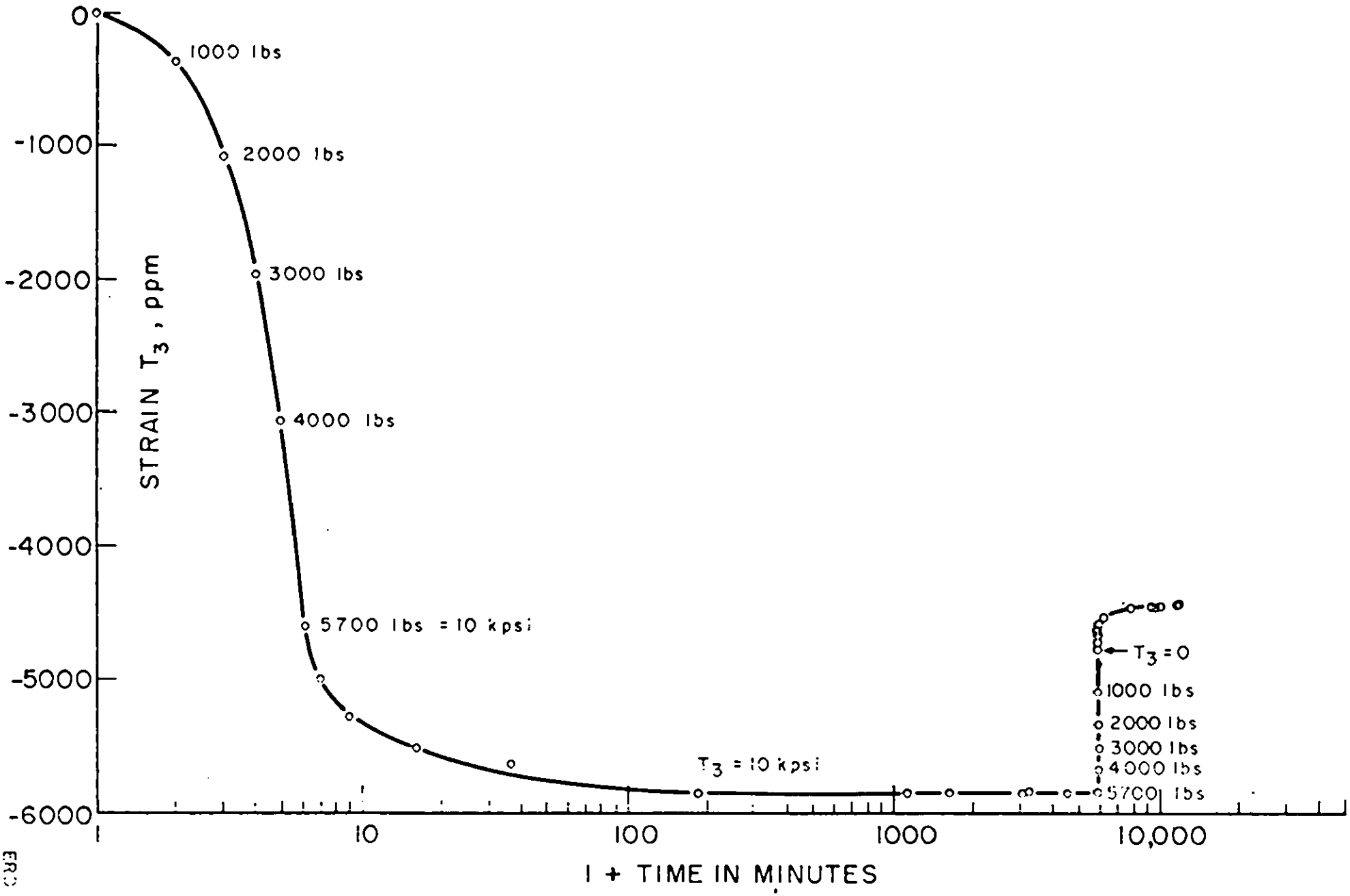

FIG. 2. STRESS-STRAIN AND STRAIN AGING, PZT-7A, 100 HOURS AT 10 kpsi PARALLEL STRESS

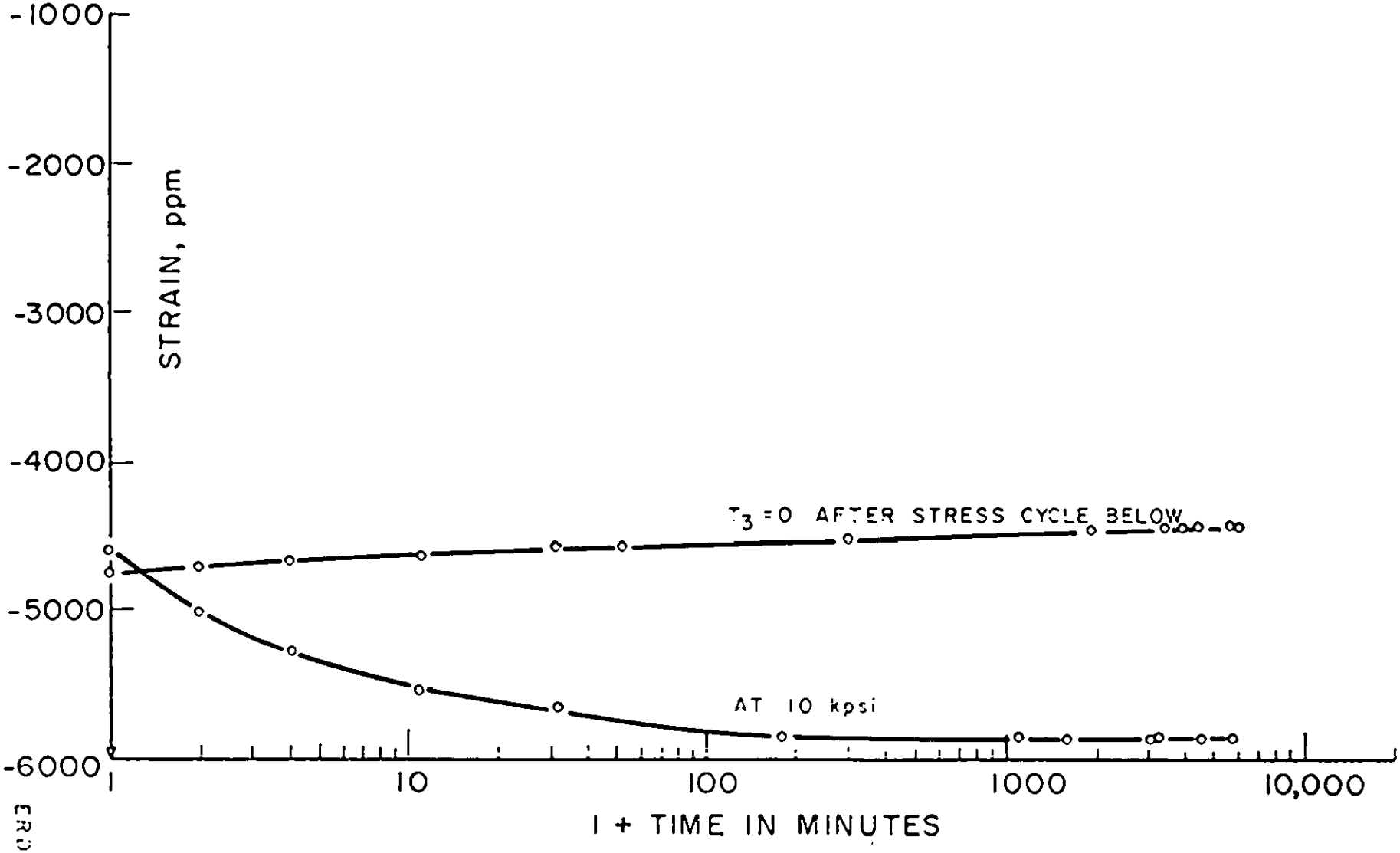

FIG. 3. STRAIN AGING AT PARALLEL STRESS OF 10 kpsi AND STRAIN AGING AFTER 100 HOURS AT 10 kpsi. PZT-7A.

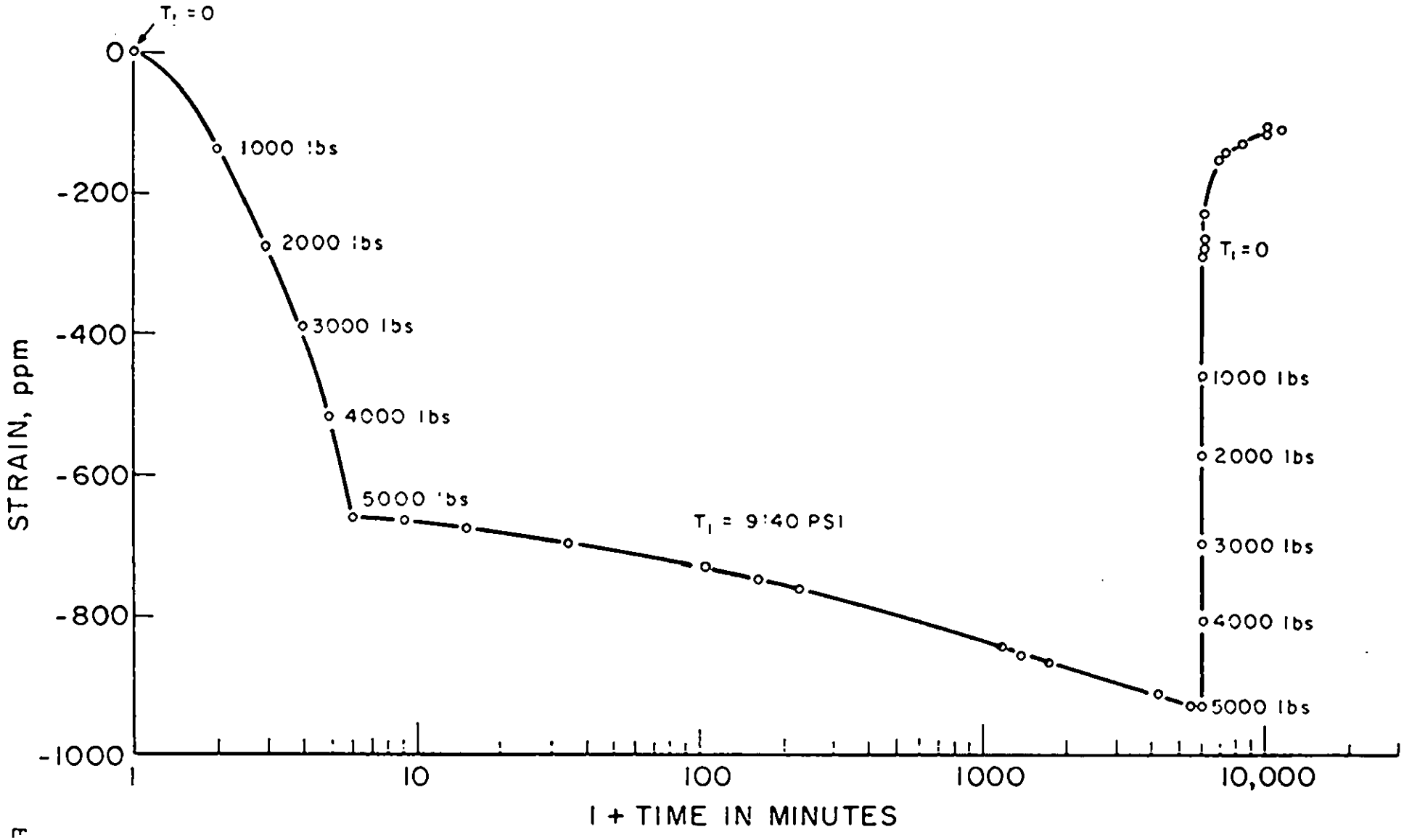

FIG. 4. STRESS-STRAIN AND STRAIN AGING, T_1 = 9140 PSI, PZT-8

ERD 7714

A-5

after close to one minute wait at stress. Changing the stress required approximately 10 seconds; the remaining 50 seconds were allowed for temperature stabilization, and then the readings were taken. Resonant and antiresonant frequencies were measured before and after the stress cycle at the second resonance (a high coupling mode associated with length vibration, but not dissociated completely from the lowest frequency hoop mode; the coupling is therefore higher than k_{31} and lower than k_p). As a result of the stress cycle, this dynamic coupling factor dropped from 0.36 to 0.31. The creep under stress was -270 ppm; the recovery creep was 180 ppm 100 hours after stress removal. The creep portions of Fig. 4 are replotted in Fig. 5 with zero times readjusted to be time of attainment of stress and time of removal of stress for the stressed and unstressed portions of the curve respectively. One would expect good correlation between coupling loss and unrecovered creep. Figure 6 shows the strain vs. stress portions without time as a variable, and both are seen to be nearly linear.

It appears from these results that a PZT-8 specimen operated in a lateral mode with bias stress would not maintain close dimensional tolerance; total creep for a 1" specimen was almost 0.0003" in 100 hours with no sign of leveling off on a log time plot. Also, the drop in coupling factor is appreciable, indicating higher than normal aging under 9,000 psi compressive lateral stress.

Strain under maintained stress parallel to the polar axis (T_3) was measured on temperature-stabilized PZT-8 and an unstabilized PZT-8. Specimen dimensions and strain gage orientation were the same as for the measurements of lateral stress; however, in this case the polarization was paralle to the tube axis. The stabilization procedure consisted of exposure of the specimen to 200°C for one hour followed by a room temperature quench.

Figures 7-9 show the strain data for the temperature-stabilized material; these may be compared with Figs. 10-12 which show the results for the unstabilized material. The elastic strain (Fig. 7) is slightly less for the stabilized material, and is more nearly linear and in better agreement with the standard value Young's Modulus for PZT-8 of 7.2×10^{10} N/m^2, which predicts an elastic strain of 880 ppm at 9200 psi. Figures 8 and 9 show the strain with stress maintained; creep is substantially lower for the stabilized material (compare Figs. 9 to 12). At 5000 minutes the strain beyond the elastic strain is -400 ppm for stabilized PZT-8 versus -580 ppm for the unstabilized material (Fig. 12), and the strains at 10,000 minutes are -460 ppm and -660 ppm respectively.

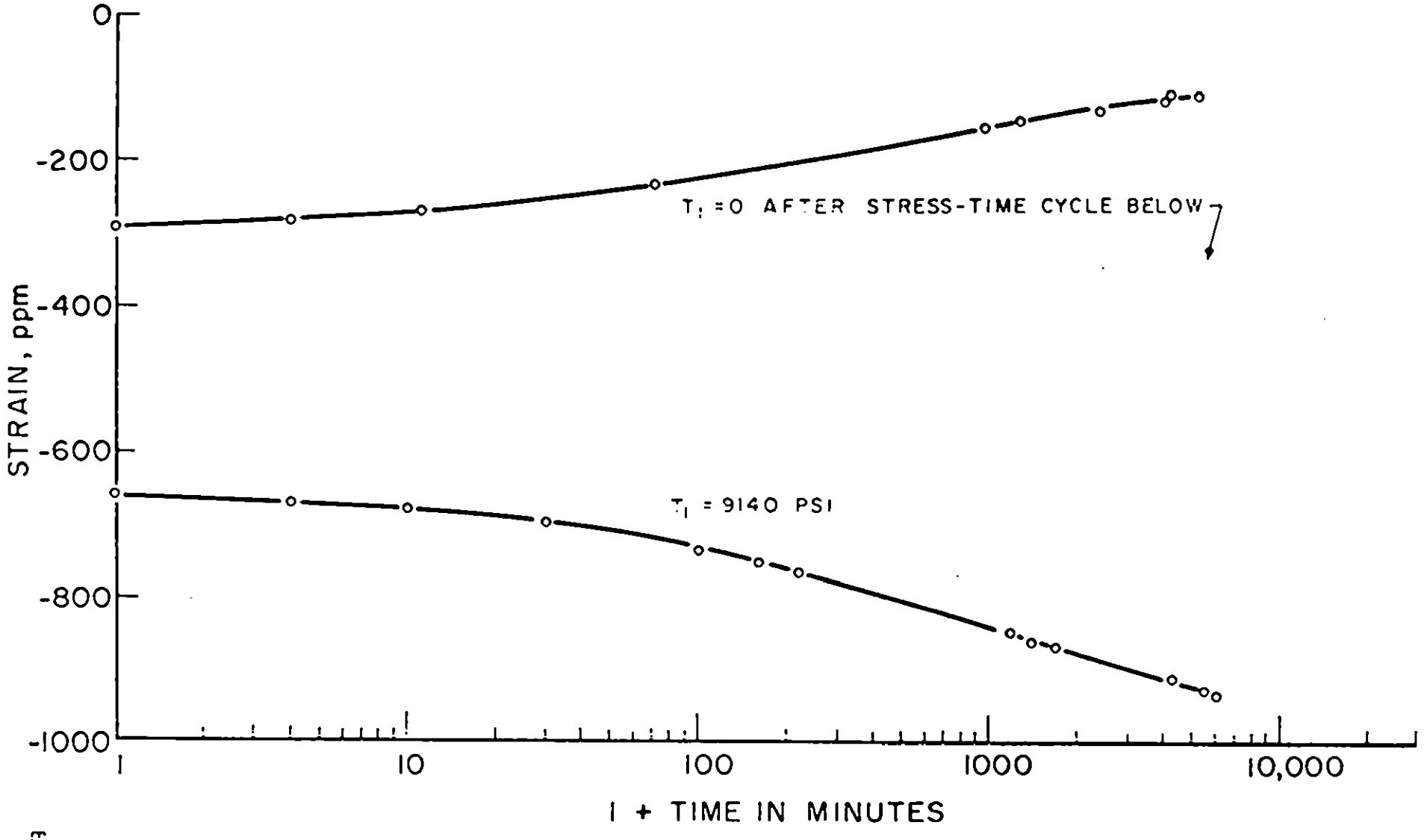

FIG. 5. STRAIN AGING, T_1 = 9140 PSI AND T_1 = 0 AFTER 100 HOURS AT 9140 PSI, PZT-8

ERD 7715

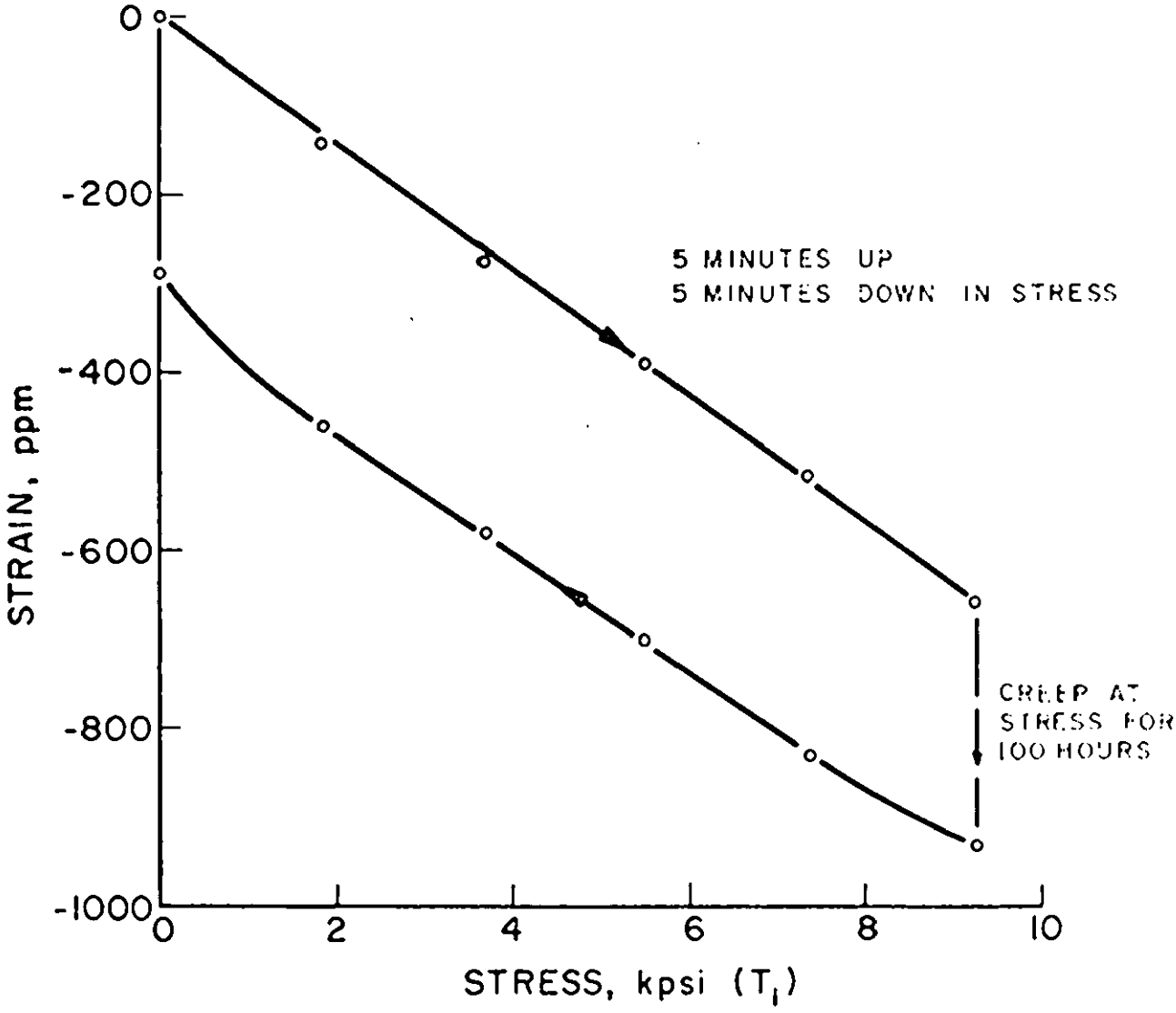

FIG. 6 STRESS-STRAIN CURVE, PZT-8 (T_1)

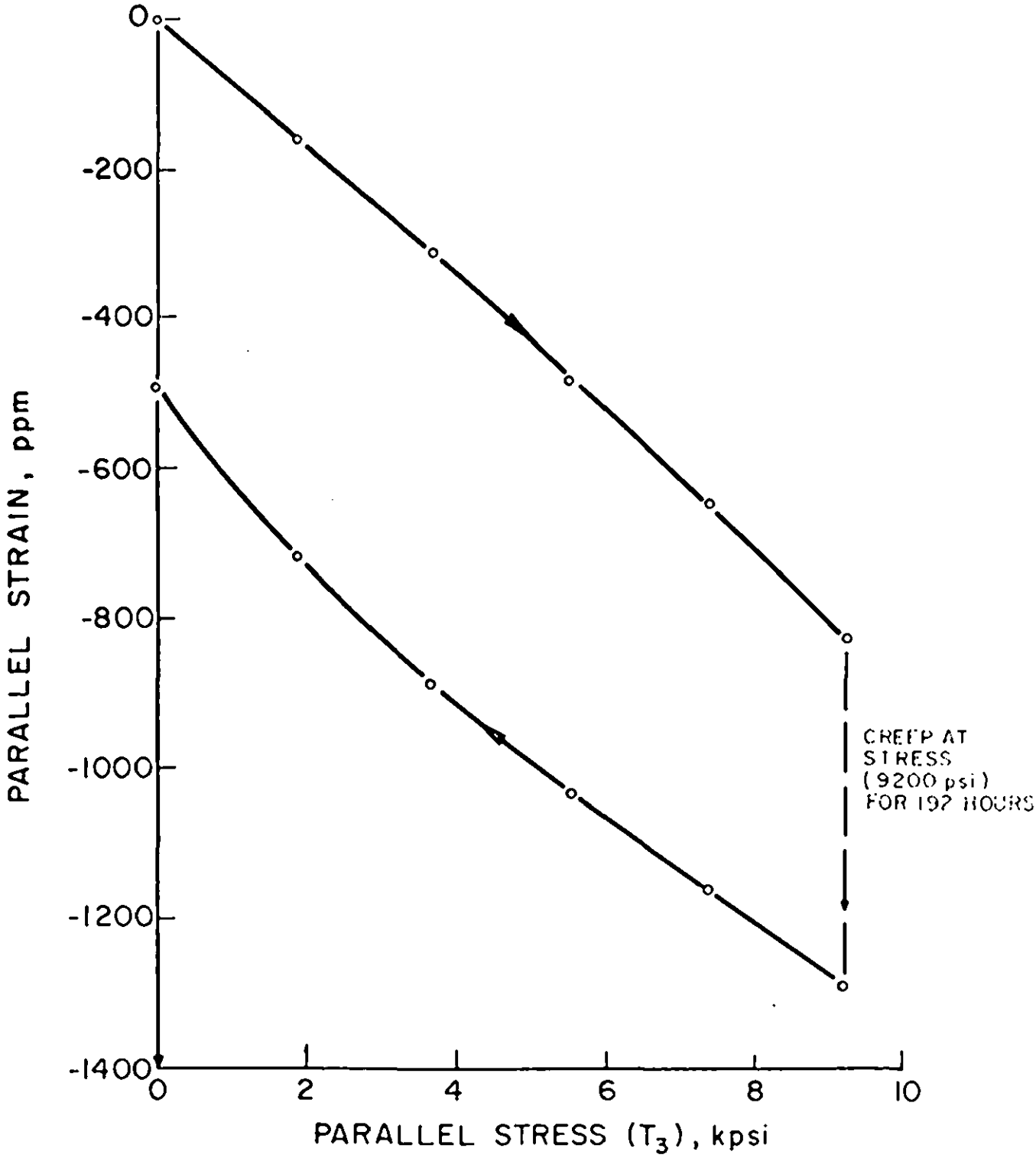

FIG. 7. STRESS-STRAIN CURVE, HEAT-STABILIZED PZT-8.

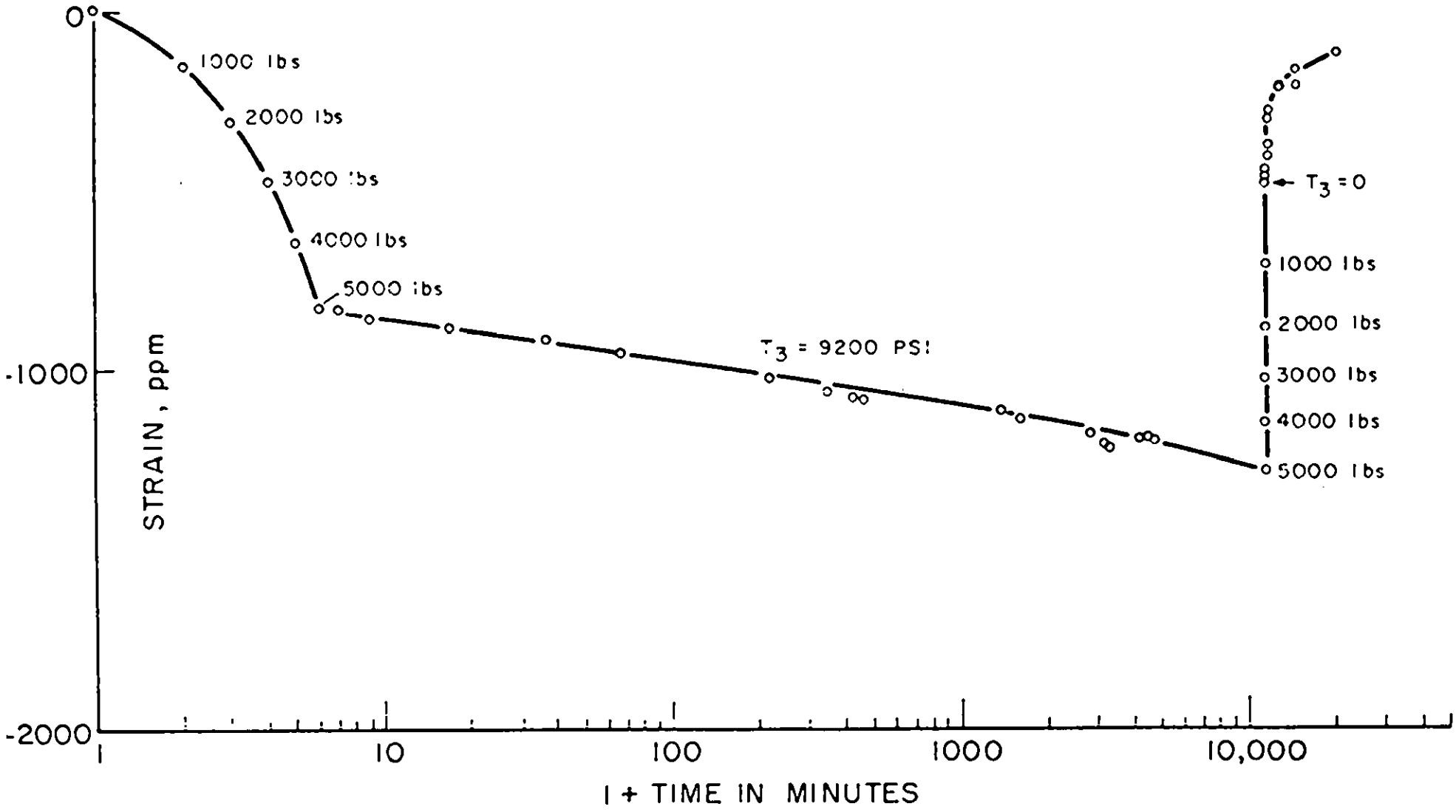

FIG. 8. STRESS-STRAIN AND STRAIN AGING, T_3 = 9200 PSI, PZT-8 HEAT STABILIZED.

ERC 7718

A-13

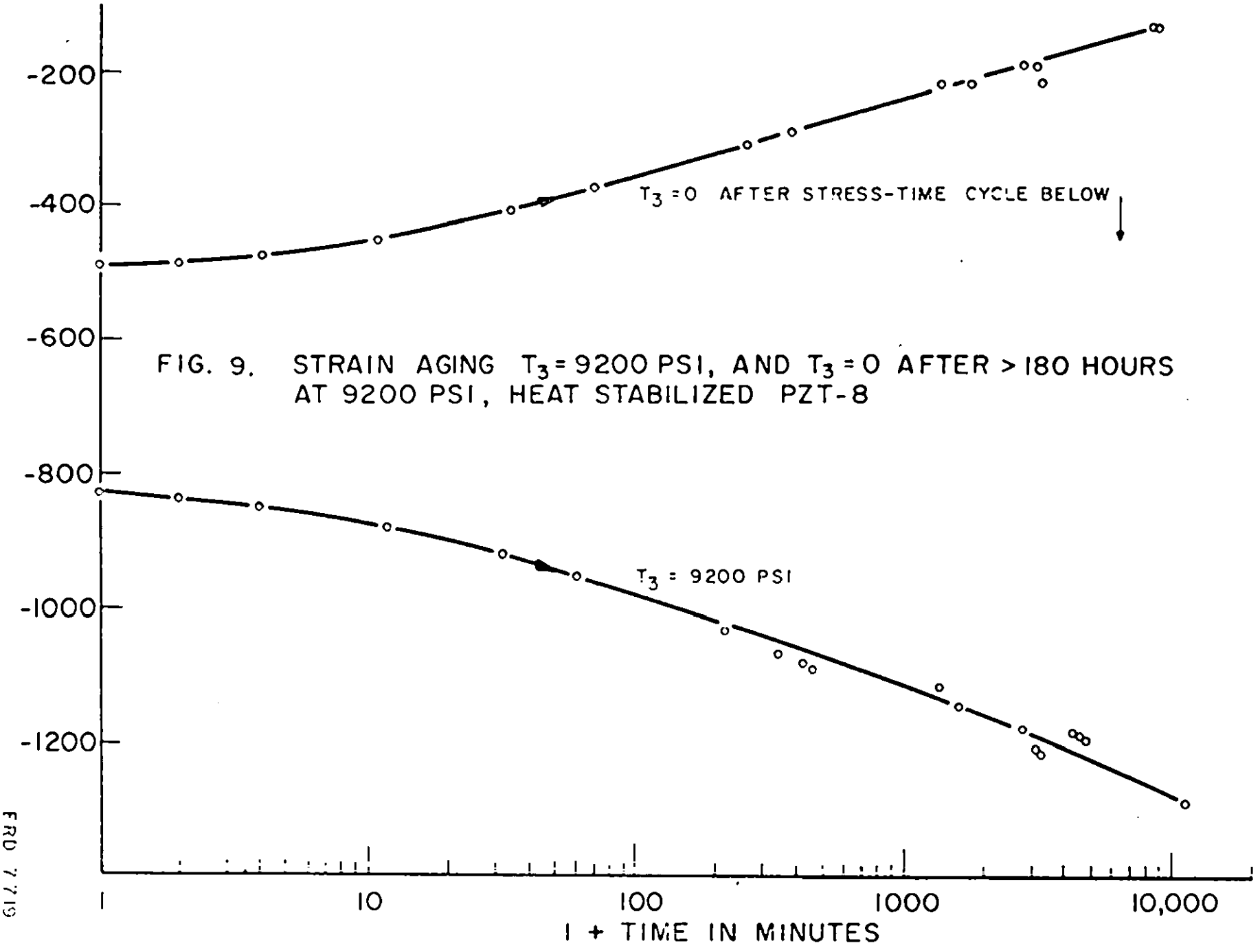

FIG. 9. STRAIN AGING T_3 = 9200 PSI, AND T_3 = 0 AFTER > 180 HOURS AT 9200 PSI, HEAT STABILIZED PZT-8

FRD 7719

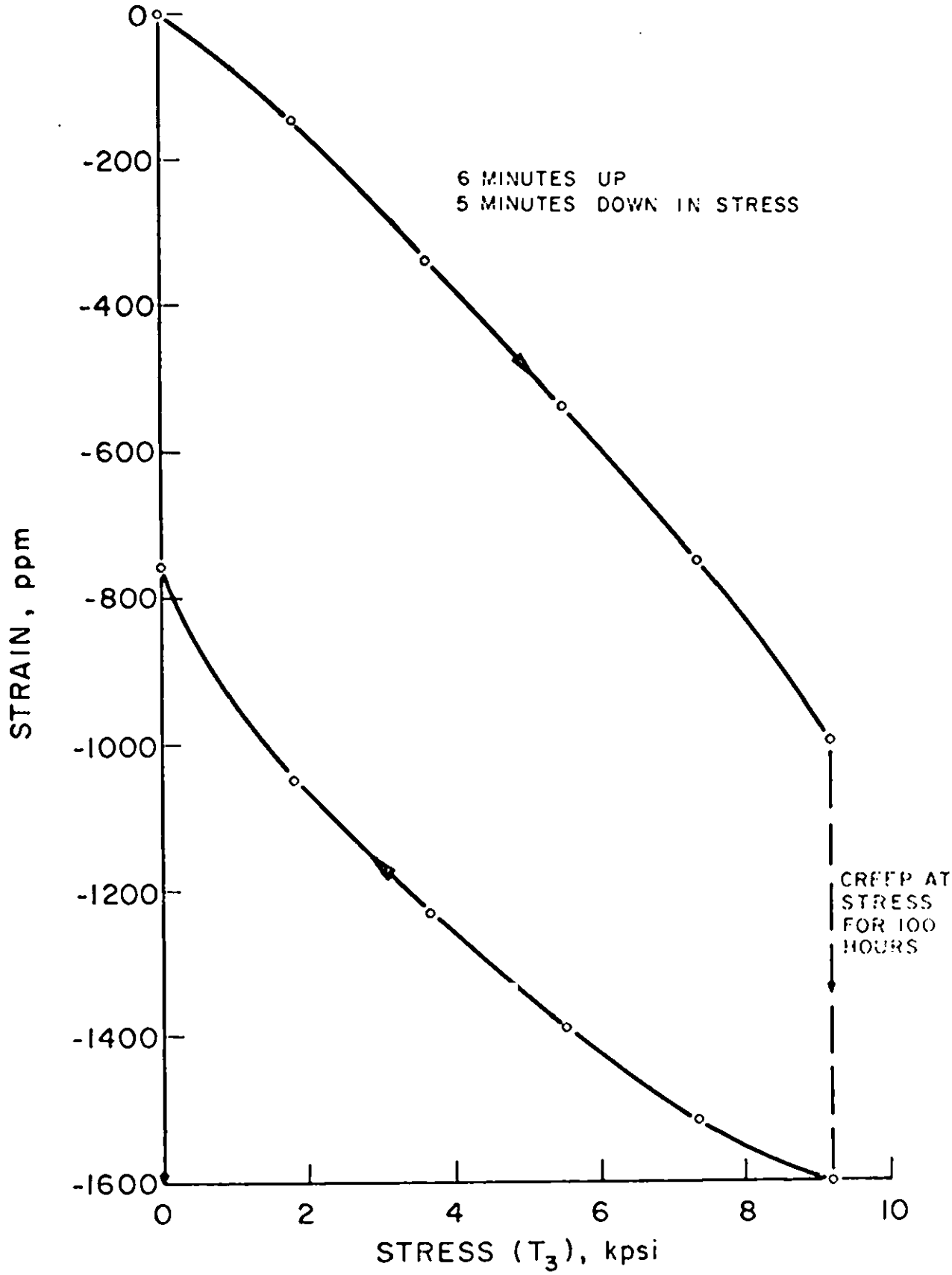

FIG. 10. STRESS-STRAIN CURVE, PZT-8 (T_3)

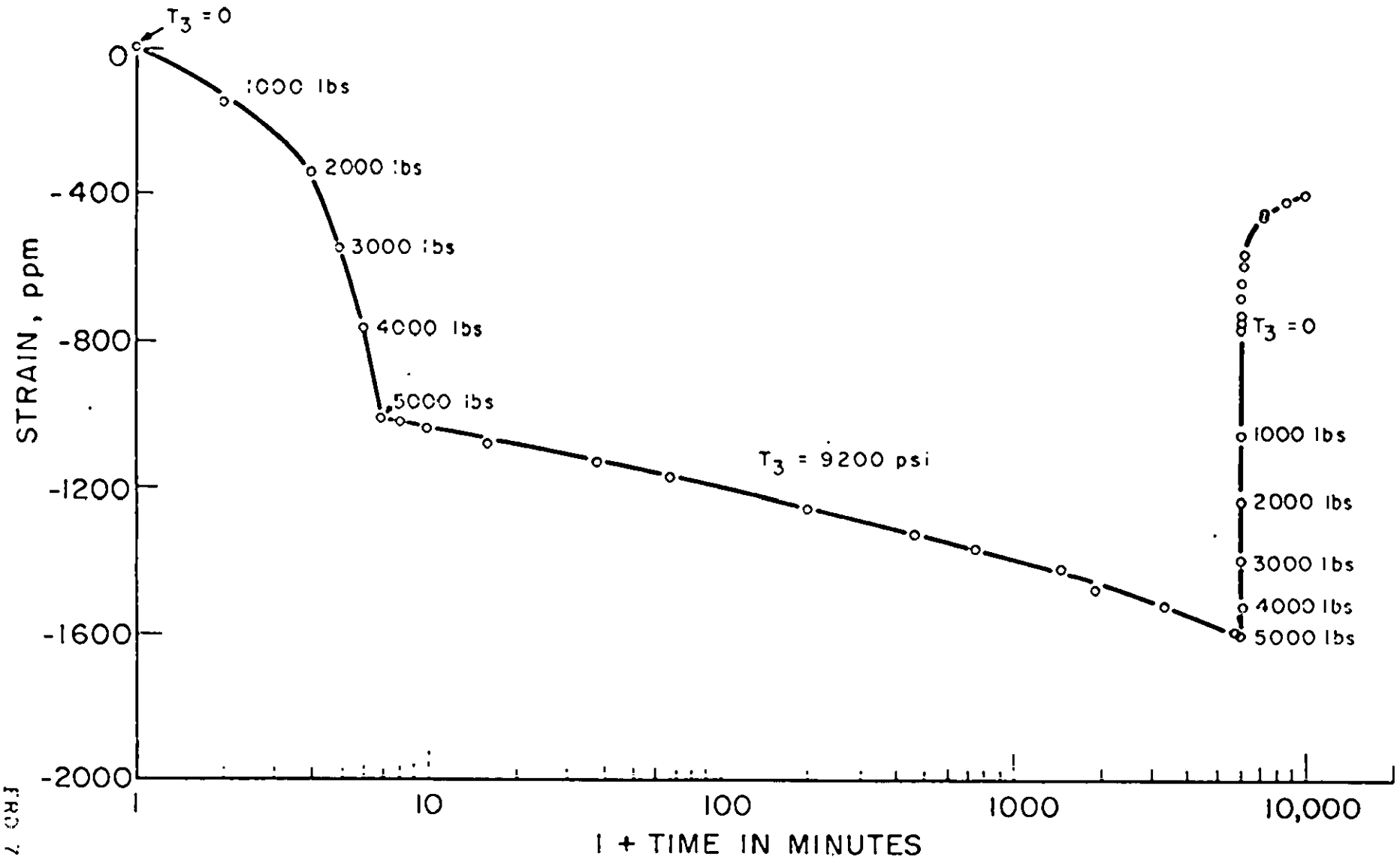

FIG. 11. STRESS-STRAIN AND STRAIN AGING, T_3 = 9200 PSI, PZT-8

FRD 7721

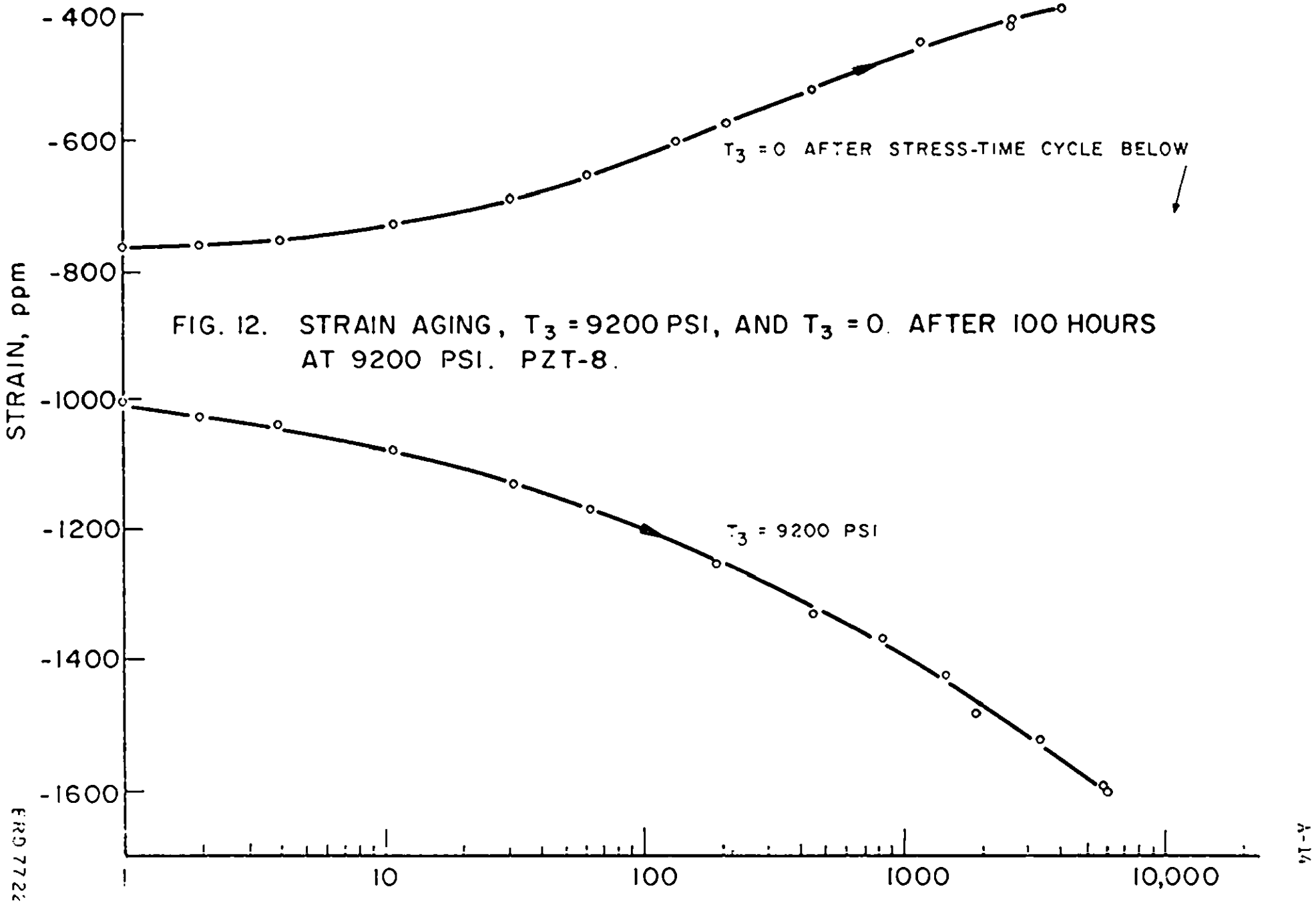

FIG. 12. STRAIN AGING, T_3 = 9200 PSI, AND T_3 = 0. AFTER 100 HOURS AT 9200 PSI. PZT-8.

There was no significant change in the piezoelectric constant d_{33} due to stress in either stabilized or unstabilized PZT-8. The piezoelectric constant d_{33} was 205 x 10^{-12} C/N before and after the stress cycle on the temperature-stabilized PZT-8; for the unstabilized ceramic the value before the first stress cycle was 205, before the second cycle it was 188, and after the second cycle it was 198. The value of 188 was measured some time after the first stress cycle and is somewhat low because the d-constant ages down. It increases with stress, and the final value of 198 was measured shortly after the second stress cycle. Since for a given value of d_{33} the parallel coupling factor is approximately inversely proportional to ε^T_{33}, which increases slightly as a result of the stress cycle, these results indicate a slight decrease in k_{33}.

An attempt was made to measure the strain during a second stress cycle on the unstabilized PZT-8, but the results indicated severe nonuniformity of stress and results were rejected. For the temperature-stabilized specimen of PZT-8, the indicated Young's Modulus at 9200 psi agreed within 8% of the value on the first cycle. It was therefore assumed that the stress was sufficiently uniform. The data for this second stress cycle are shown in Figs. 13-15. Comparing these figures with Figs. 7-9, it may be seen that the results are almost identical except for an apparent remanent strain of -60 to -70 ppm following the first stress cycle. This difference is probably not significant since it could result from either a slight difference in stress distribution or from simply an insufficient measurement period following the first stress cycle. This latter statement follows from the fact that the curve of strain versus log time after removal of stress (the upper curve of Fig. 9) shows no indication of leveling.

Results in Figs. 13-15 show that there is no observed change of strain aging under stress due to stress cycling with temperature stabilized PZT-8. On the other hand, there is a significant reduction in strain aging under stress due to temperature stabilization (compare Figs. 9, 12 and 15).

PZT-4

Because of the similarity of the PZT-4 and PZT-8 compositions, and because of the improved strain aging characteristics of the temperature-stabilized PZT-8, it was decided to measure the strain aging with maintained parallel stress for temperature-stabilized PZT-4 only. The same stabilization procedure was used as with PZT-8. The cross section of the PZT-4 specimen was slightly larger than for the PZT-8, resulting in a somewhat lower stress for a 5000 pound load,

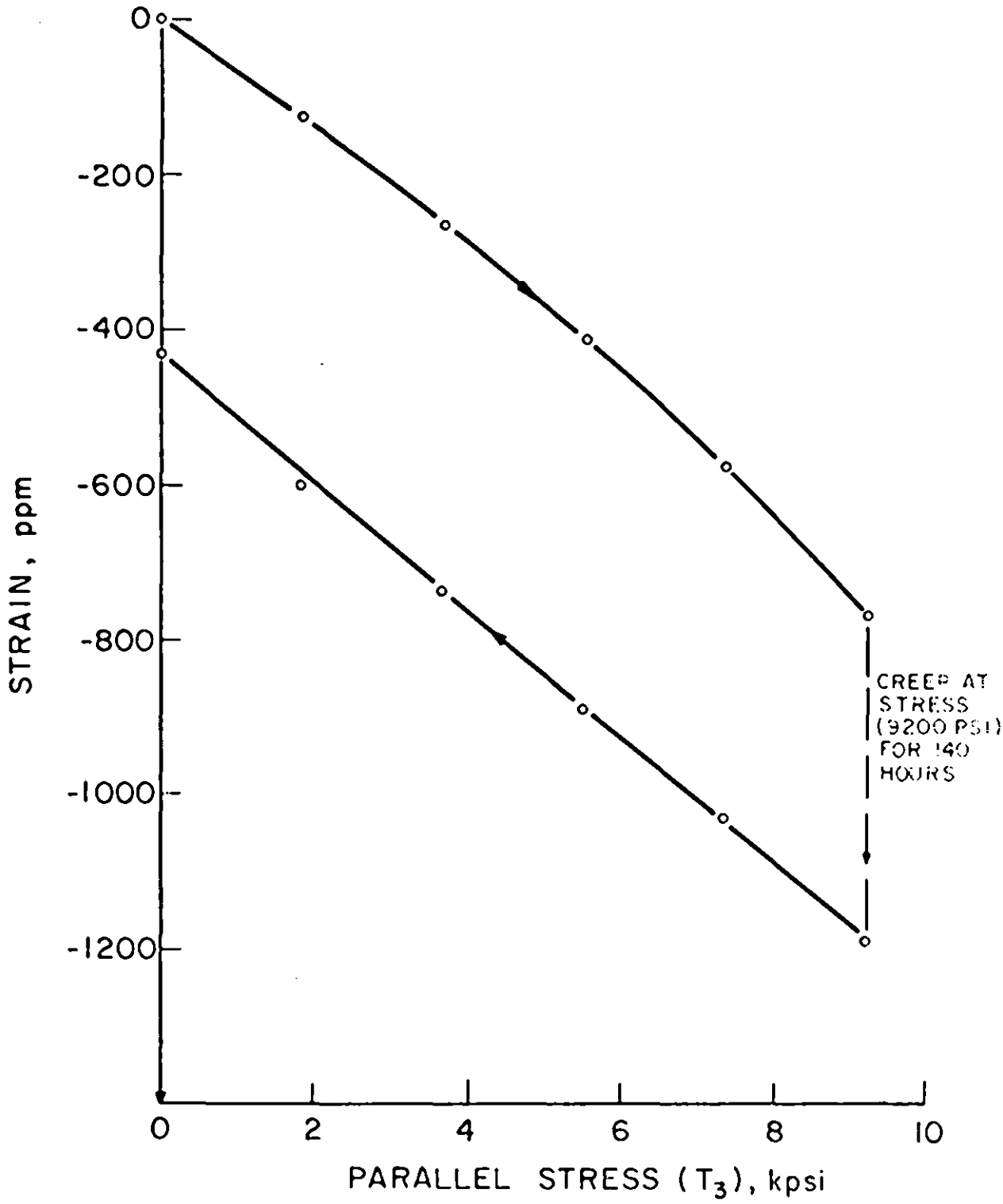

FIG. 13. STRAIN-STRESS CURVE, HEAT-STABILIZED PZT-8, 2nd STRESS CYCLE.

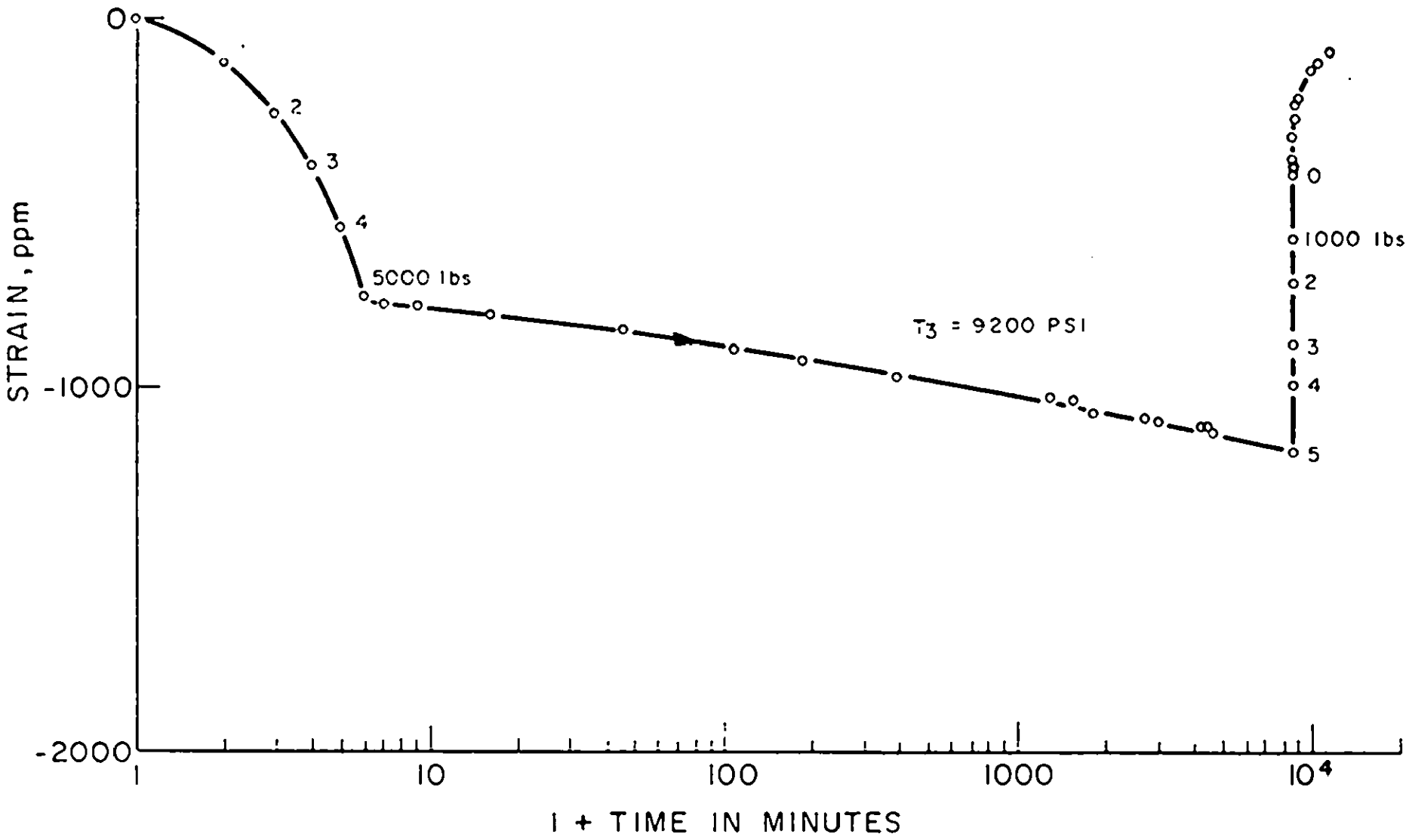

FIG. 14. STRESS-STRAIN AND STRAIN AGING, T_3 = 9200 PSI, HEAT STABILIZED PZT-8, 2nd STRESS CYCLE.

ERC 7724

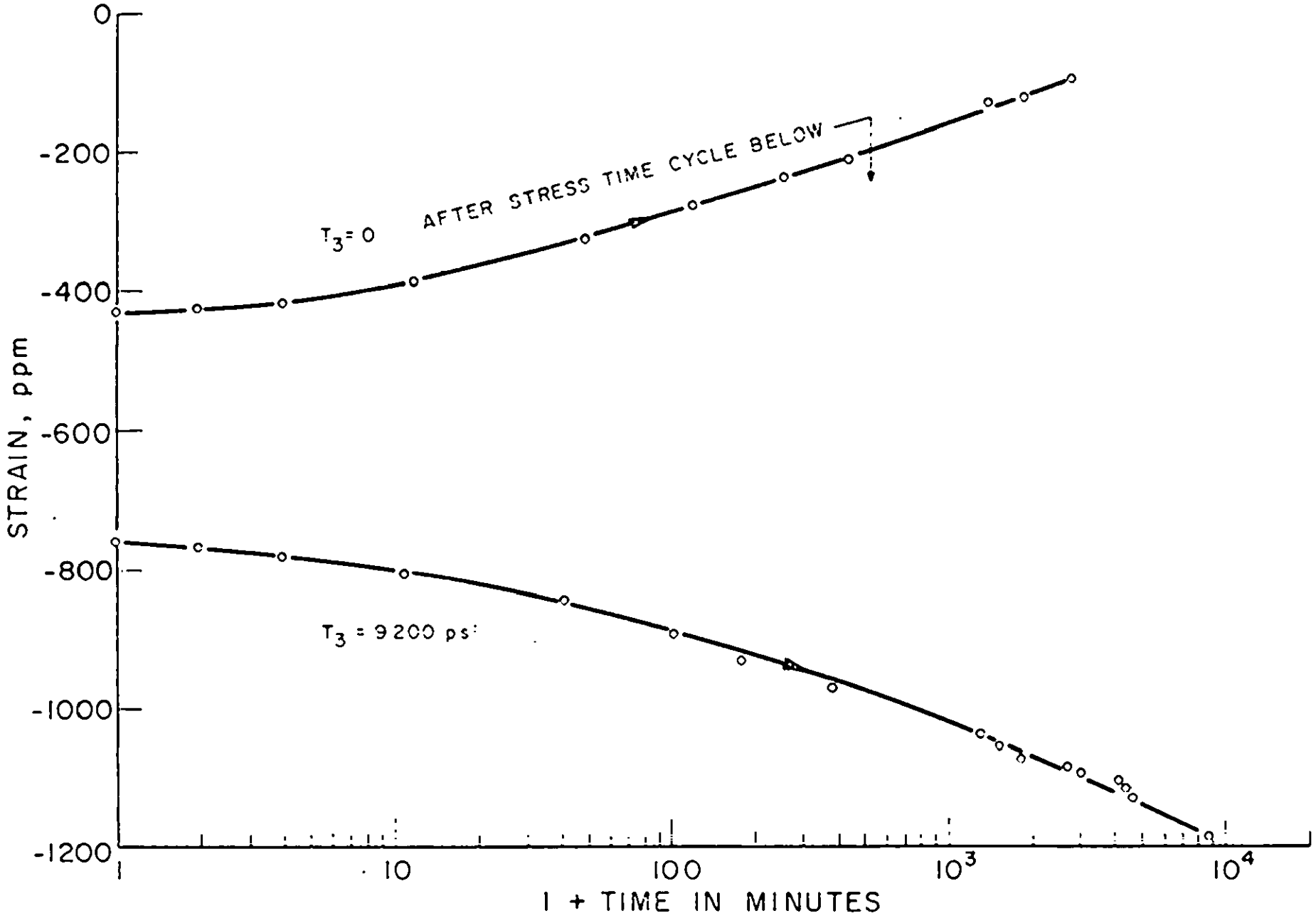

FIG. 15. STRAIN AGING, T_3 = 9200 PSI, AND T_3 = 0 AFTER 140 HOURS AT 9200 PSI HEAT STABILIZED PZT-8, 2nd STRESS CYCLE

i.e., 8660 psi versus 9200 psi for PZT-8. The data for temperature stabilized PZT-4 are shown in Figs. 16-18. The observed elastic strain (Fig. 16) corresponds to a Young's Modulus of 5.65×10^{10} N/m^2. This is about 12% smaller than the nominal value for PZT-4 of 6.45×10^{10} N/m^2 determined from small signal piezoelectric resonance measurements. This discrepancy may be compared with the results for the temperature-stabilized PZT-8. In that case the stress measurements yield a Young's Modulus of 7.7×10^{10} N/m^2. The nominal value for untreated PZT-8 is 7.2×10^{10} N/m^2. Again, stress nonuniformity may be partly responsible for the difference.

The strain aging under stress is appreciably greater for the stabilized PZT-4 than for stabilized PZT-8, -150 ppm/decade time and -115 ppm/decade respectively averaged once for time decades in a one week period. In addition, the residual strain after removal of stress is about -750 ppm compared with -490 ppm for stabilized PZT-8. Of these amounts, 75% is recovered in four decades of time for both materials. The change in d_{33} for the PZT-4 was well within experimental error; 248×10^{-12} C/N before the stress cycle, and 246 after the cycle. This result is the same as that for PZT-8, which showed no change after the stress cycle.

CONCLUSION

It was conclusively demonstrated that a low aging composition with suitable high-drive characteristics (PZT-7A) is subject to extreme depoling with parallel bias stress in the 10,000 psi range. Strain aging at zero stress is much lower for this composition than for the compositions normally used in high-drive applications, PZT-4 and PZT-8. An interesting sidelight is that the PZT-5 donor doped compositions, which have low mechanical Q and extremely poor high-drive characteristics, are not subject to significant depoling at 10,000 psi maintained parallel or lateral stress. Repetitive cycling to 10,000 psi, however, rapidly leads to depolarization.

Results of this study indicate that applications requiring good high-drive characteristics and low mechanical creep are best met by temperature stabilized PZT-8. The strain aging rate at 9,000 psi parallel stress is much lower for stabilized than for unstabilized PZT-8 (compare slopes in Figs. 9 and 12 at 1000 minutes). Nevertheless even after a one week period at 9,000 psi the aging rate is about -165 ppm/time decade. Thus in a period one to ten weeks after stress application additional creep of about -165 would be encountered. With the

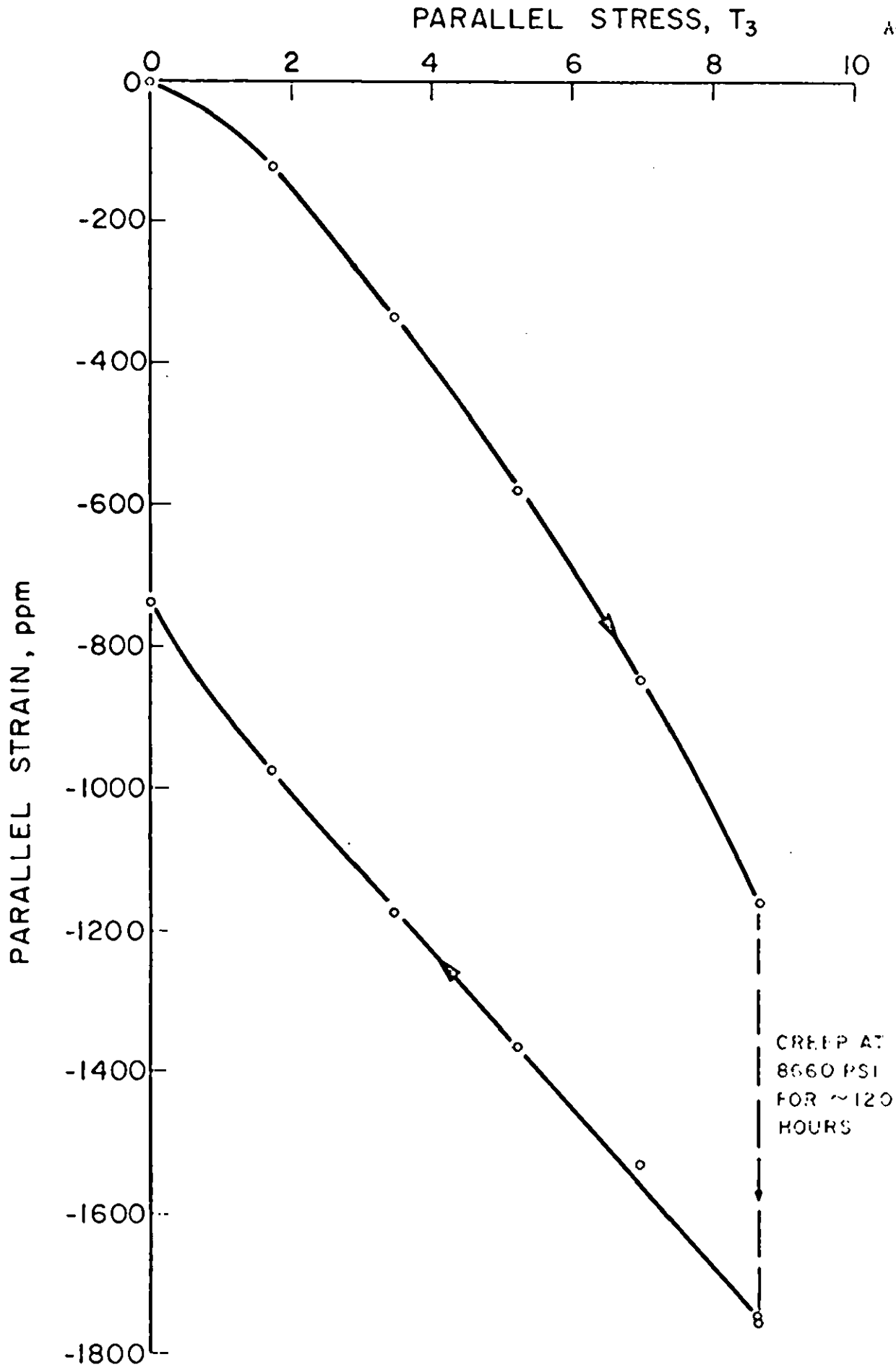

FIG. 16. STRESS-STRAIN CURVE, PZT-4, HEATED TREATED.

ERO 7726

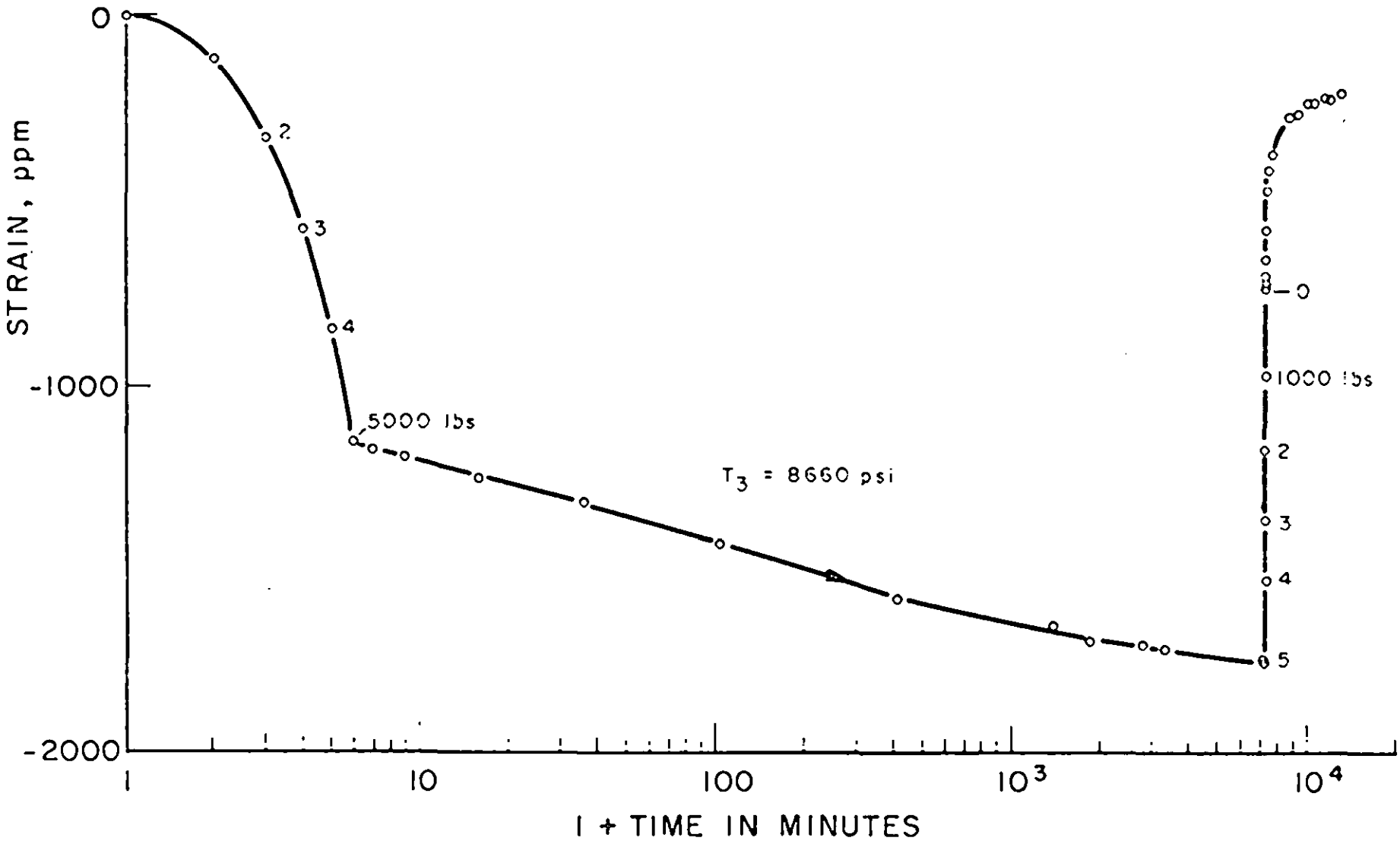

FIG. 17. STRESS-STRAIN AND STRAIN AGING, PZT-4, HEAT-TREATED, PARALLEL STRESS (T_3).

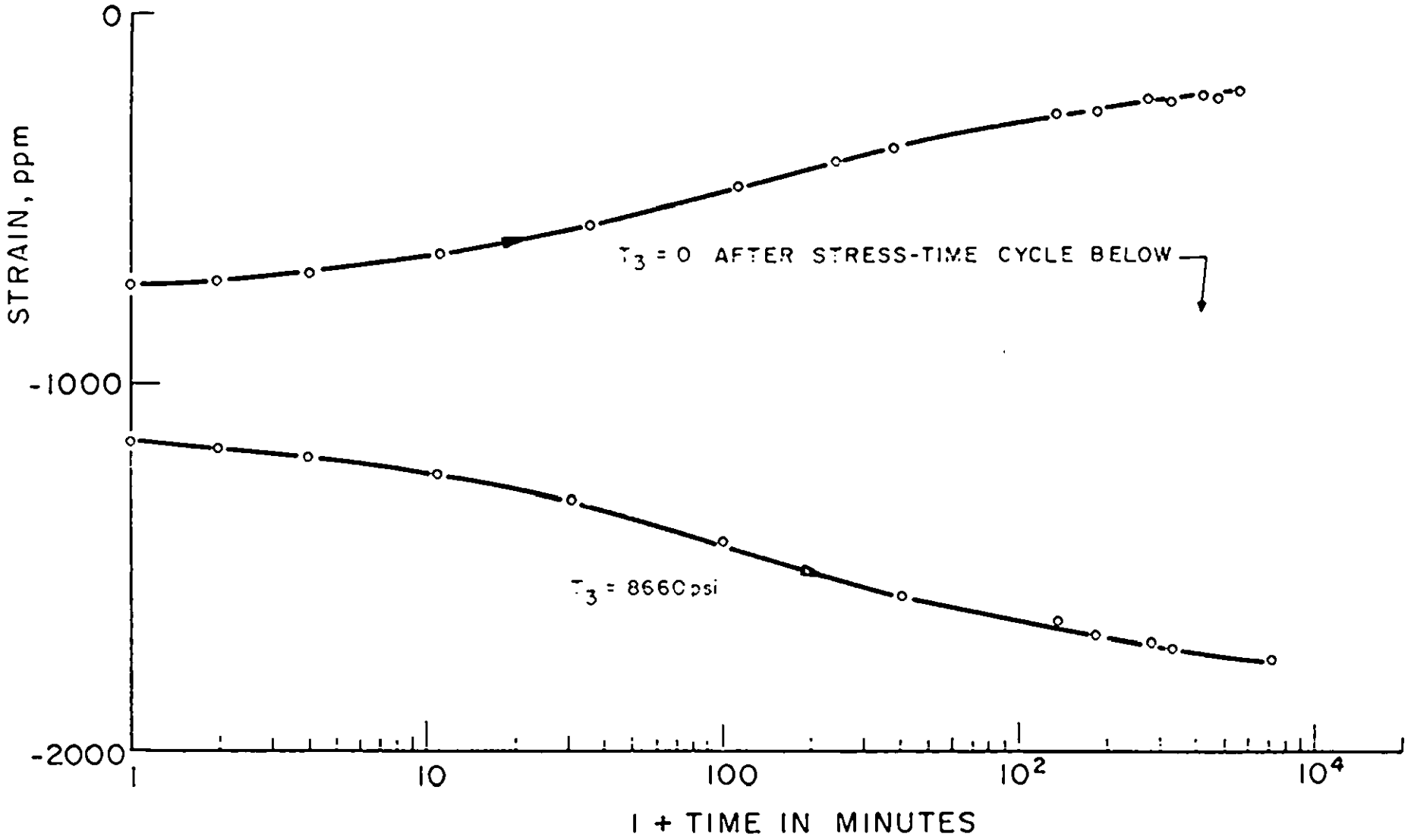

FIG. 18. STRAIN AGING AT PARALLEL STRESS AND WITH STRESS REMOVED, PZT-4, HEAT TREATED.

orientation of the stress lateral a similar figure is ±110 ppm for unstabilized PZT. If the reduction in slope for stabilization is the same in the lateral as for the parallel stress orientation, this figure is reduced to -68 ppm by temperature stabilization. Creep is thus only about 40% as great for the lateral mode, the piezoelectric coupling is also reduced almost this much in a purely lateral mode.